SANDIA REPORT

SAND95–2001 • UC–814
Unlimited Release
Printed September 1996

Yucca Mountain Site Characterization Project

Preliminary Validation of Rock Mass Models by Comparison to Laboratory Frictional Sliding Experiments

Steven R. Sobolik, Joel D. Miller

Prepared by
Sandia National Laboratories
Albuquerque, New Mexico 87185 and Livermore, California 94550
for the United States Department of Energy
under Contract DE-AC04-94AL85000

"Prepared by Yucca Mountain Site Characterization Project (YMSCP) participants as part of the Civilian Radioactive Waste Management Program (CRWM). The YMSCP is managed by the Yucca Mountain Project Office of the U.S. Department of Energy, DOE Field Office, Nevada (DOE/NV). YMSCP work is sponsored by the Office of Geologic Repositories (OGR) of the DOE Office of Civilian Radioactive Waste Management (OCRWM)."

Issued by Sandia National Laboratories, operated for the United States Department of Energy by Sandia Corporation.

Available to DOE and DOE contractors from
Office of Scientific and Technical Information
PO Box 62
Oak Ridge, TN 37831

Prices available from (615) 576-8401, FTS 626-8401

Available to the public from
National Technical Information Service
US Department of Commerce
5285 Port Royal Rd
Springfield, VA 22161

NTIS price codes
Printed copy: A05
Microfiche copy: A01

DISCLAIMER

Portions of this document may be illegible electronic image products. Images are produced from the best available original document.

SAND95-2001
Unlimited Release
Printed September 1996

Distribution
Category UC-814

Preliminary Validation of Rock Mass Models by Comparison to Laboratory Frictional Sliding Experiments

Steven R. Sobolik and Joel D. Miller
Nuclear Waste Management Programs Center
Sandia National Laboratories
Albuquerque, New Mexico 87185

ABSTRACT

The U.S. Department of Energy's (DOE) Yucca Mountain Site Characterization Project (YMP) is studying Yucca Mountain in southwestern Nevada as a potential site for a high-level nuclear waste repository. Site characterization will be facilitated by the construction of an Exploratory Studies Facility (ESF). The ESF and potential repository will be excavated from both nonwelded and welded ashflow tuff with varying rock quality (degree of welding, rock mass strength, etc.) and fault and fracture characteristics. Design concerns for the construction of these facilities include the integrity of the structure during underground testing operations and, if it occurs, the emplacement and storage of high-level nuclear waste which could increase the local temperatures in the underground rock mass to as high as 300°C. Because of the associated issues regarding personnel and long-term environmental safety, sophisticated jointed rock mass models will be required to provide a high degree of confidence for decisions regarding the design, site characterization, and licensing of such facilities.

The objective of the work documented in this report is to perform code validation calculations for three rock-mass computer models. The three rock-mass computer models used for this report are the discrete element code UDEC, Version 1.82; and the finite element continuum joint models JAC2D Version 5.10 and JAS3D Version 1.1. The rock mass behavior predicted by the models are compared to the results of laboratory experiments on layered polycarbonate (Lexan) and granite plate experiments. These experiments examine the rock mass behavior of well-defined jointed rock structures or models of jointed structures under uniaxial and biaxial loading. The laboratory environment allows control over the boundary conditions, material properties, and quality and quantity of the data obtained. Such experiments are ideal for model validation purposes and provide a foundation on which to base future validation efforts using field rock-mass data. A comparison of all of the predicted results to the experimental results points to the necessity of quantifying the joint normal and shear stiffnesses for a given system in order to better estimate frictional slip.

This work was conducted at Sandia National Laboratories for the U.S. Department of Energy, under contract DE-AC04-94AL85000. This work activity was directed and planned using Work Agreement WA-0165, Revision 00 for work description WBS Number 1.2.3.2.7.4 for the Yucca Mountain Site Characterization Project Office. This work activity was performed under the controls of a qualified QA program, and the codes UDEC and JAC2D used for this report are maintained by the Software Configuration Management System controlled by this QA program. The code JAS3D has not yet been submitted to this Configuration Management System; as a result, this report is designated as NQ. The experimental data used in this report is unqualified.

ACKNOWLEDGMENTS

The authors acknowledge the work of fellow coworkers who helped in the preparation of this report. Joe Jung was instrumental in the development of the combined experimental and numerical efforts described herein. Billy Thorne and Mark Blanford were very helpful in getting JAS3D ready to perform calculations for this report. Ray Finley, John Pott, and Larry Costin reviewed the technical content of this document and offered corrections and ideas for improvement.

CONTENTS

1.0 Introduction

The U.S. Department of Energy's (DOE) Yucca Mountain Site Characterization Project (YMP) is studying Yucca Mountain in southwestern Nevada as a potential site for a high-level nuclear waste repository. Site characterization will be facilitated by the construction of an Exploratory Studies Facility (ESF). The ESF and potential repository will be excavated in both nonwelded and welded ashflow tuff with varying rock quality (degree of welding, rock mass strength, etc.) and fault and fracture characteristics. Design concerns for the construction of these facilities include the integrity of the structure during underground testing operations, facility construction, and, if it occurs, the emplacement and storage of high-level nuclear waste which could increase the local temperatures in the underground rock mass to as high as 300°C. Because of the associated issues regarding personnel and long-term environmental safety, sophisticated jointed rock mass models may be required to provide a high degree of confidence for decisions regarding the design, site characterization, and licensing of such facilities.

The design of underground facilities and the predicted long-term performance of an underground nuclear waste repository will be evaluated with complex numerical models. One example of these models is the group of jointed rock mass models which predict the mechanical and thermal-mechanical behavior of underground excavations and the surrounding host rock. These jointed rock mass models include continuum and noncontinuum geomechanical codes. A validation effort is required for all the numerical codes which may be used to support repository design, licensing, and operation decisions. As discussed here, the term "validation" should be understood to mean the evaluation of a numerical model (i.e., code) for its strengths and weaknesses in modeling the type of behavior it is designed to simulate. Therefore, a code may be shown to be easily applicable and physically accurate when modeling some particular set of boundary conditions with well-known material properties. The same code will also produce results highly dependent on the input parameter assumptions which may possess a high degree of uncertainty. Calculations are highly dependent, also, on the experience level and expertise of the modeler. Such validation efforts require laboratory and in situ experiments to model rock mass behavior, accompanied by numerical analyses which simulate the physical experiments and whose results are directly compared with the experimental data. The laboratory experiments described and simulated in this report (Perry et al., 1995) are intended to provide highly controlled initial and boundary conditions which should be relatively easy to model; these efforts will give an indication of the expected difficulties in modeling in situ processes, and the types of in situ data or experiments which may provide the most effective validation of the code. This validation effort is intended to develop an understanding of the regimes and conditions to which the various rock-mass models are applicable. As an understanding develops of how these models can represent experimental data, so will the confidence in using these models. Over time, this ongoing effort will provide the required validation of the rock-mass models used for design and performance assessment as planned for site characterization and will be required to satisfy federal regulations.

Data from laboratory intact rock tests and rock-mass field tests are required to validate any rock mass models used for the YMP. Major problems associated with using data from rock-mass field tests are that the data are relatively sparse or limited, boundary conditions are hard to

replicate, joint geometries are difficult to model, and material properties are not known precisely. These problems make the use of field test data difficult albeit necessary for model validation efforts. To address these problems, a series of lab-scale experiments of increasing complexity is underway. These experiments examine the behavior of well-defined jointed rock structures or models of jointed structures under uniaxial loading. The laboratory environment allows control over the boundary conditions, material properties, and quality and quantity of the data obtained. Such experiments are ideal for model validation purposes and provide a foundation on which to base future validation efforts using field rock-mass data.

The objective of the work documented in this report is to perform code validation calculations of layered polycarbonate (Lexan) plate experiments performed for Sandia National Laboratories (SNL) at the Idaho National Engineering Laboratory (Perry et al., 1995). In addition, the results of a similar series of experiments for which granite is the test medium will be predicted by the same rock mass codes. The experiments will be modeled using three rock-mass computer models: the discrete element code UDEC, Version 1.82 (Itasca, 1992); and the finite element codes JAC2D Version 5.10 (Biffle and Blanford, 1994) and JAS3D Version 1.1[1]. The codes UDEC and JAC2D are in the Software Configuration Management System and their use is controlled by SNL-YMP Quality Assurance Implementation Procedure 19-1 (Software QA).

[1] The 3-D compliant joint model JAS3D has not yet been submitted to the SNL-YMP Software Configuration Management System. The initial code validation and benchmark calculations are near completion as of the writing of this report, and thus JAS3D should be submitted under Software QA controls in 1996. The version 1.1 listed here is a number used by the code authors and should not be used for QA purposes. The user documentation of this code, which is currently in preparation, is a SAND report by Blanford, M.L., JAS3D, A Multi-Strategy Iterative Code for Solid Mechanics Analysis.

2.0 Description of the Layered Rock Experiments

The Idaho National Engineering Laboratory (INEL) has performed experiments to model rock-mass behavior using layered plates of two different simulated rock materials, a polycarbonate (Lexan) and granite. The methodology and results of the experiments performed on Lexan plates are reported in Perry, et al. (1995); the methodology of the tests with granite plates is nearly identical, but the results have not yet been reported. Results from the Lexan tests will be directly compared to the calculations described later. Both experiments involve applying a vertical loading to a stack of plates with a hole drilled in the middle to induce stress-related slippage. The experimental data is obtained using the technique of phase shifting moiré interferometry employing lasers. Figure 1 (from Perry et al., 1995) shows the Lexan plates load test setup, and Figure 2 (also from Perry et al., 1995) shows the interferometer schematic. The dimensions of the test specimens differ slightly; there were 24 Lexan plates, each with the reported dimensions of 12"×2"×0.25" (304.8×50.8×6.35 mm), with a 1.5"- (38.1 mm-) diameter hole drilled in the middle, whereas for the granite tests there were 16 plates, each 10"×2"×0.375" (254×50.8×9.53 mm), with the same size of hole.

The following material properties are required for the characterization of the test media:

ν = Poisson's ratio;
E = Young's modulus, or modulus of elasticity (in GPa);
G = Shear modulus (in GPa);
K = Bulk modulus (in GPa);
μ = Friction coefficient;
ρ = material density (in kg/m^3);
V_p = compressional wave velocity (in m/s); and,
V_S = shear wave velocity (in m/s); where

$$\nu = \frac{(V_p^2 / V_s^2) - 2}{2[(V_p^2 / V_s^2) - 1]};$$

$$G = \rho V_s^2; \qquad \text{also } G = \frac{E}{2(1+\nu)};$$

$$E = 2(1+\nu)\rho V_s^2; \text{ and}$$

$$K = \frac{E}{3(1-2\nu)}.$$

The values of ρ, V_p, V_S, and μ were measured for the Lexan and granite specimens (except for μ, which had not yet been measured for the granite specimens as this report was being written). These values are listed in Table 1. The values listed for Lexan are taken from Perry et al. (1995), except the value for K, which is calculated from the measured data. The value for the density of

the granite used in the experiments was measured at SNL[2]; the compression and shear wave velocities for the granite specimens were measured at INEL[3]. The three geomechanical codes each require some subset of the values as input parameters: UDEC requires ρ, G, K, and μ; and JAC2D and JAS3D require ρ, ν, E, and μ.

Table 1: Measured Lexan and Granite Properties

	Compression Wave Vel., m/s	Shear Wave Vel., m/s	Rock Density, kg/m³	Poisson's Ratio	Young's Modulus (E, GPa)	Shear Modulus (G, GPa)	Bulk Modulus (K, GPa)	Friction Coeff.
Lexan (Perry, et al.)	2200	920	1200	0.39	2.84	1.02	4.3	0.47
Granite (see footnotes 1 and 2)	6200	3630	2960	0.239	96.7	39.0	61.8	(No value for granite yet available)

For the Lexan experiments described in Perry et al. (1995), the displacements from the experimental data were "nulled," meaning they are absolute measurements representing the deformation accumulated during the application of the load. The displacement data were differenced above and below the joints to produce the relative slip between each pair of plates. A constant value was then added to each set (i.e., for each contact surface) of relative slip data, so that the slip at the hole or vertical centerline would be zero. Thus, plots of relative slip, with zero slip arbitrarily assigned to the edge of the hole, were obtained from the Lexan loading tests and published in Perry et al. (1995). Plots of experimentally determined slippage at loads of 0.14, 0.43, and 0.56 MPa are given in Figures 3 through 5, respectively[4]. At 0.14 MPa, the slip between the plates appears to be uniformly distributed around the hole. However, at 0.43 MPa, the slip along the first and second interface from the top of the measured section has increased dramatically. Finally, at 0.56 MPa, the second interface from the top has become the primary location for slip, while the top interface indicates no slip directly above the hole, and a reduced value of slip far from the hole.

The preliminary results of the Lexan experiments confirmed the feasibility of using phase shifting moiré interferometry for quantifying slip during laboratory experiments with layered rock models. Results for the Lexan show a clear evolution of slip as a function of load. The trends apparent in these experiments were reproducible between experiments. As a second phase in the development of laboratory data to be used for rock mass model validation, similar experiments have been performed on granite plates. Granite was chosen because it was easily available, easily machineable, and chemically similar to the tuff which is the primary rock type at Yucca Mountain. The analysis of the experimental data and reporting of the results are in progress as of the

[2] Specifically, the mass and volume of a sample of the granite used in the INEL lab tests were measured at SNL. The granite sample was found to have a mass of 33.69 g, and a volume of $11.4 \pm .2$ cm³. The resulting density was 2.96 ± 0.05 g/cm³.

[3] These values were documented in a memo from Karen Wendt to Hugh Bruck (both of INEL) dated June 29, 1995. A copy of this memo is included in the records files for work agreements WA-0165 and WA-0190 in the SNL YMP Local Records Center.

[4] Note that the hole cuts into the fourth plate above the horizontal centerline. The reported hole diameter of 1.5" is correct, but the plates were about 0.01" thinner than reported. It is this reason which explains why the third interface above the horizontal centerline is not tangent to the hole, as the reported dimensions would indicate. This information was reported in a personal communication (via e-mail) from Brent Buescher, INEL to Steven R. Sobolik, SNL, dated September 20, 1995.

completion of this report, so no experimental results of slip are available. However, most of the material properties of the granite are known (see Table 1). At the time rock-mass model calculations were performed, the maximum load tested by INEL was approximately 13 kN (3000 pounds), which for the size of plates tested translates to about 1 MPa. The granite is a much stiffer material than the Lexan, so naturally less contact displacement was expected; indeed, qualitative observations of the raw data from initial loading tests confirmed this assumption.

The uniaxial loading tests performed by INEL were designed to produce experimental data quantifying the behavior of a jointed rock mass under loaded conditions. The frictional slip of intact rocks along joints such as fractures is a characteristic of rock mass behavior which is important to the characterization of an underground facility such as the ESF at Yucca Mountain. Because of the simple geometries and controlled boundary conditions of the laboratory experiment, sensitivities of the codes to items such as material and joint properties, gridding schemes, and incremental accumulation of the static load may be easily tested. The laboratory experiments simulated by the calculations described here do not measure such values as principal stresses, rock mass strength, and thermal effects on these properties. However, increasingly complex laboratory experiments have been planned to predict frictional slip for similar sets of plates undergoing biaxial loading, followed by the prediction of the frictional slip of a "blocky" model consisting of evenly-spaced, orthogonal, discontinuous fractures. These experiments would be conducted using the same granite material used previously, as well as plates made from welded tuff obtained from the Yucca Mountain area.

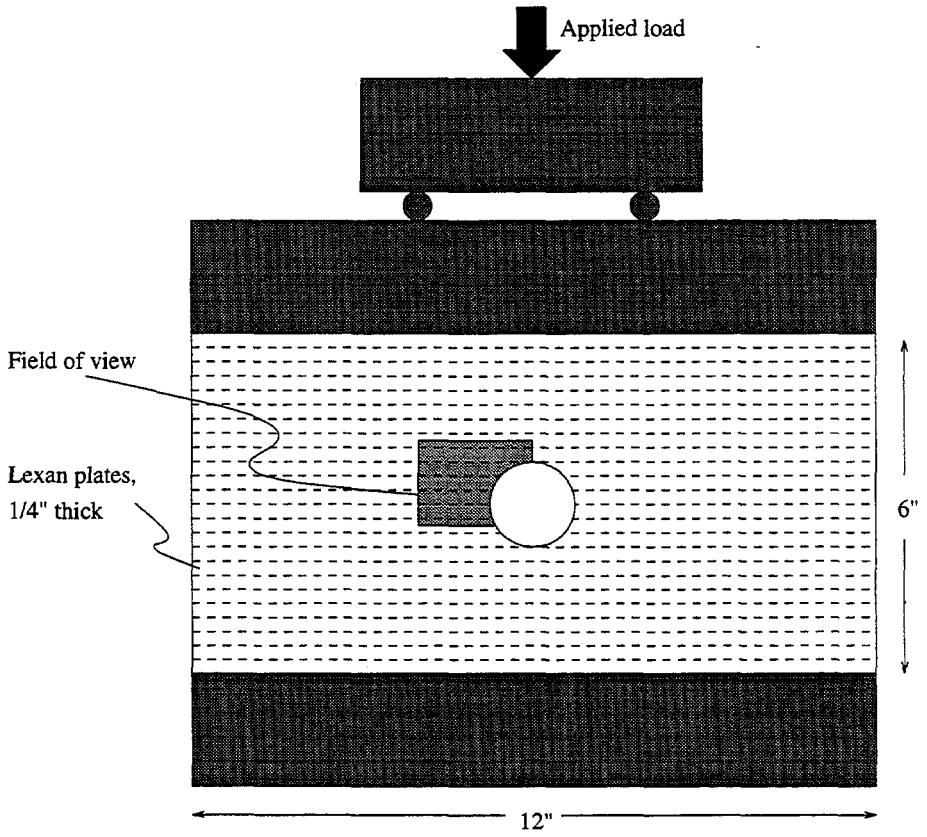

Figure 1: Schematic of load frame.

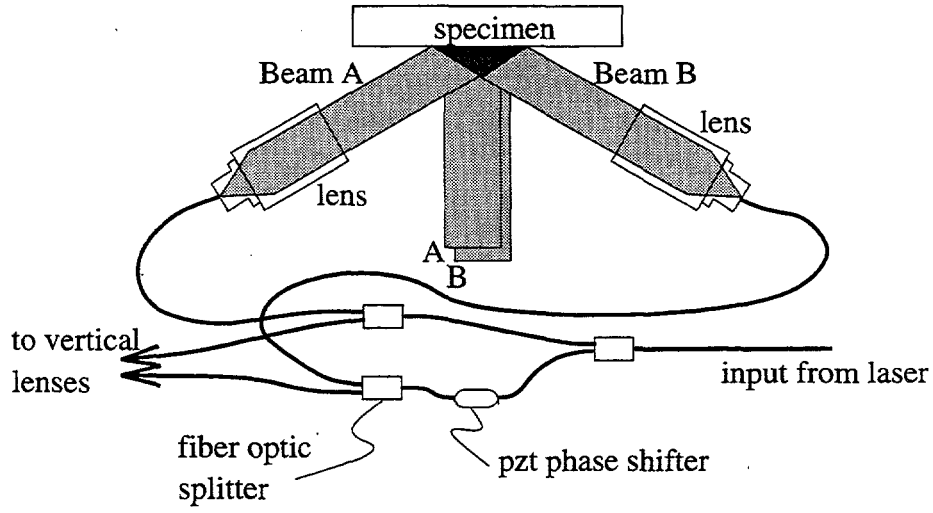

Figure 2: Schematic of four beam moiré interferometer.

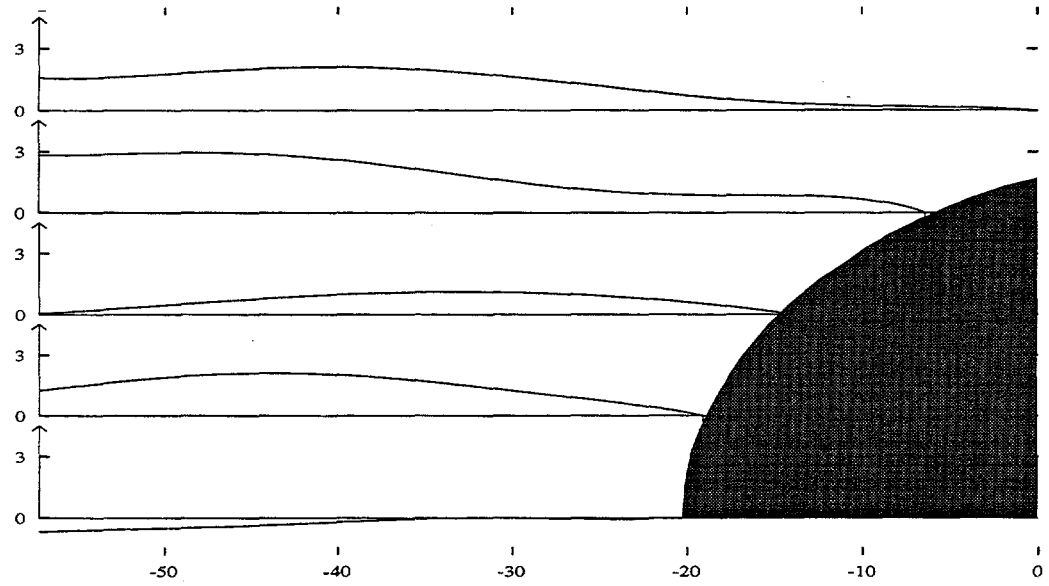

Figure 3: Slip along interfaces at $\sigma_0 = 0.14\,\mathrm{MPa}$. The position scale is in millimeters, and the slip is in microns.

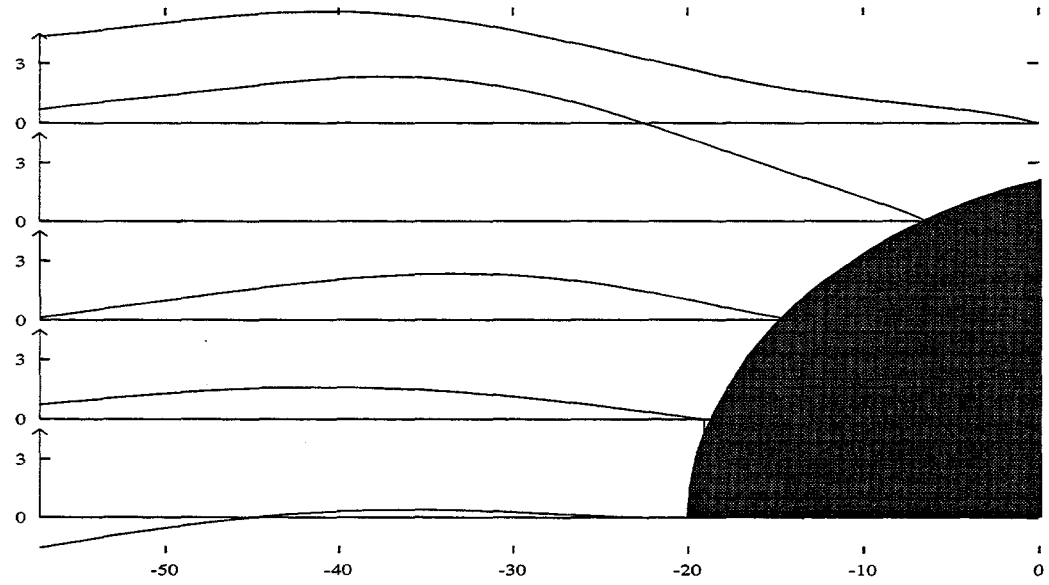

Figure 4: Slip along interfaces at $\sigma_0 = 0.43\,\mathrm{MPa}$. The position scale is in millimeters, and the slip is in microns.

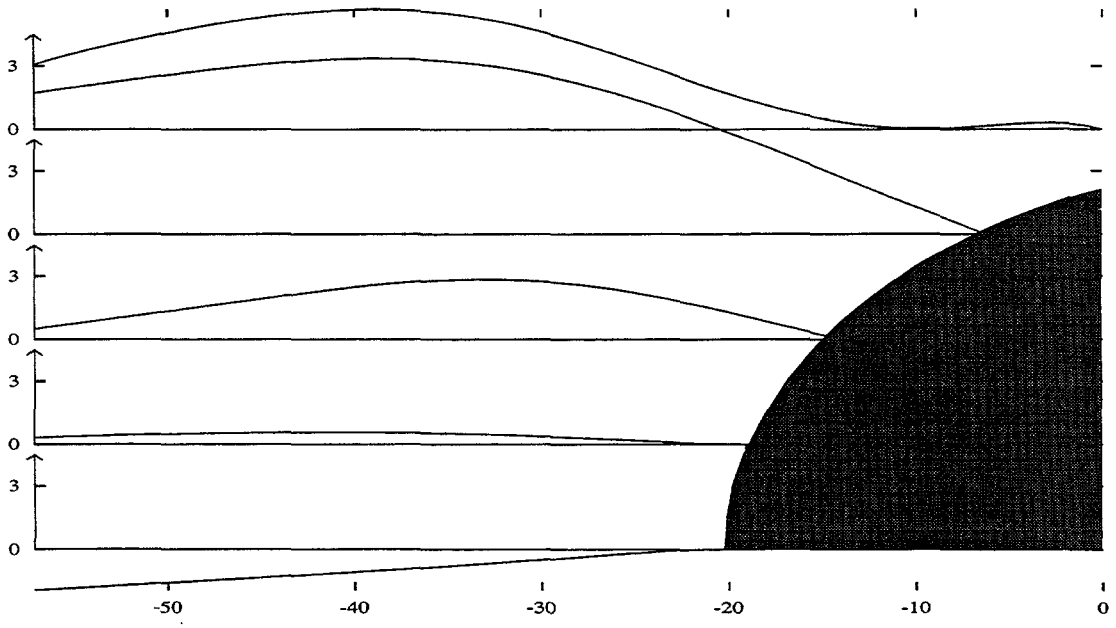

Figure 5: Slip along interfaces at $\sigma_0 = 0.56\,\mathrm{MPa}$. The position scale is in millimeters, and the slip is in microns.

3.0 Calculations Using UDEC

Calculations of uniaxial loading of layered Lexan and granite plates have been performed with the discrete element code UDEC (Itasca, 1992). These initial calculations are intended to determine if the results reported by UDEC may be realistically compared to experimental data obtained under heavily controlled conditions, such as the INEL lab tests, and if the computed values reasonably predict the experimental results.

The Universal Distinct Element Code, also known as UDEC (Itasca, 1992), is a two-dimensional numerical program based upon the distinct element method for noncontinuum modeling. UDEC simulates the response of discontinuous media (such as a jointed rock mass) subjected to either static or dynamic loading. The discontinuous medium is represented as an assemblage of discrete blocks. The discontinuities are treated as boundary conditions between blocks; large displacements along discontinuities between blocks are allowed. Deformable blocks are subdivided into a mesh of finite difference elements and each element responds according to the prescribed stress-strain law (constitutive model). The block constitutive model applied to the plate materials for these calculations was the classic elastic, isotropic model (which is the default model in UDEC). The relative motion of the discontinuities is also governed by linear or non-linear force-displacement relations for movement in both the normal and shear directions. The default joint constitutive model, a joint area contact elastic/plastic model with Coulomb slip failure, was employed for these calculations. UDEC is based on a Lagrangian calculation scheme which is well suited to model large movements and deformations of a blocky system.

3.1 Lexan Modeling with UDEC

The mesh used for the Lexan calculations is shown in Figure 6. Each of the 24 plates was subdivided into finite difference zones, and the plates from which the hole was drilled were given a higher concentration of elements. All of the plates were allowed to slip along the contact surfaces between plates. The boundary conditions imposed on the problem included the downward load across the top of the stack of plates (ranging from 0.15-0.55 MPa), a zero velocity (and therefore, zero displacement) boundary for the bottom surface, and free surfaces at the sides. The material properties used for Lexan are those described in Table 1. In addition, the joint constitutive model employed for these calculations required the input of joint stiffness properties. The joint normal stiffness and joint shear stiffness were both set to 10 GPa/m; a discussion of the choice of parameters for these values is reserved for later in this chapter.

Most of the results from these calculations will be expressed as displacements or slips occurring at the sliding interfaces (i.e., joints) between plates. Figure 7 uses the UDEC Lexan model to describe the location of the horizontal centerline and the first four interfaces above the centerline. The prescribed diameter of the hole (1.5 inches) and thickness of the plates (0.25 inches) place the third interface above the horizontal centerline tangent to the top of the hole. As stated in Chapter 2 (see Figures 3-5), the actual thickness of the plates displayed in the plots of experimental data was somewhat smaller than 0.25 inches, which is why the third interface above the horizontal centerline from the actual experiment is not tangent to the hole. Any interface above or below the centerline in the UDEC calculations would be expected to have less slip than those interfaces

intersecting the hole. For this reason, the displacement and slip at the second interface in the UDEC calculations may be the best choice to compare to those at the third interface in the experimental results.

Figures 8 through 12 are contour plots displaying the predicted horizontal displacements of the Lexan plates under loads of 0.15, 0.30, 0.45, 0.50, and 0.55 MPa, respectively. These displacements are absolute to the original frame of reference, and represent both the slippage between plates and elastic deformation of the Lexan. Note that Figures 8, 9, and 10, which display displacement for 0.15, 0.30, and 0.45 MPa respectively, are nearly identical other than the magnitude; i.e., the displacements shown for 0.30 MPa are approximately twice those shown for 0.15 MPa, and those for 0.45 MPa are three times the magnitude of those for 0.15 MPa. The UDEC program uses the displacements of pairs of points on opposite sides of plate contact surfaces to calculate the relative slip between the plates at each location. These slip values are plotted for the 0.15 MPa loading case in Figure 13. A positive slip in Figure 13 indicates the bottom plate at a contact location is slipping further to the left than the top (or, the top plate is slipping further to the right than the bottom plate). The results of the calculations indicate that the portions of Lexan plates near the hole are deforming towards the hole, while the outlying portions of the plates are slipping away from the hole.

Plots of experimentally determined slippage at loads of 0.14 MPa, 0.43 MPa, and 0.56 MPa are given in Figures 3, 4, and 5. These plots of relative slip may be compared to the UDEC calculations for 0.15 MPa, 0.45 MPa, and 0.55 MPa presented in Figures 14, 15, and 16. A comparison of the third interface in Figure 3 and the second interface of Figure 14 shows fair agreement in terms of general trends and magnitude of the observed slip. The interface above the hole in Figure 14 shows negative slip for a distance, which is unlike the measured slip. There is a more noticeable difference in the magnitudes of slip displayed in Figures 4 and 15. The third interface of Figure 4 shows a slip of 6 microns, whereas the second interface in Figure 15 predicts a slip of about 10 microns. A similar difference can be seen between Figures 5 and 16. The other interfaces in these figures are slightly different both in magnitudes and trends. UDEC has the capability of plotting x-y and principal stress fields that correlate to the slip patterns shown here, so relationships between slip distances and stress may be estimated. Some plots of y-direction stress corresponding to the slips shown in Figures 14 through 16 will be discussed later in this chapter.

3.2 Granite Modeling with UDEC

Similar calculations were performed to simulate the granite experiments. The grid used for the granite calculations is shown in Figure 17. Note that the second interface above the centerline is tangent to the top of the hole, not the third as in the case of the Lexan simulations. The material properties used for granite were those listed in Table 1; due to a lack of better information, the values for friction coefficient and joint properties used for the Lexan plates were also used for the granite plates. The granite is a much stiffer material than the Lexan, so naturally less contact displacement is expected. Simulations were run for loads of 0.5 and 1 MPa. Two horizontal displacement plots are displayed in Figures 18 and 19 for loads of 0.5 and 1 MPa, respectively. The magnitude of maximum displacement for a load of 0.5 MPa are about one-third less for the

granite than for the Lexan (see Figures 11 and 18). Figures 20 and 21 show the slip predicted by the calculations after the slip values were zeroed at the hole. Again, the trends are similar to those for Lexan, but the slip magnitude is less by approximately one third for the closest corresponding load. Of course, some uncertainty exists in these calculations because of the lack of a measured friction coefficient for the granite. Additionally, the selection of joint stiffness properties may be important in determining the predicted slip; this possibility is discussed in the next section.

3.3 Results and Discussion

The discrete element code UDEC has been used to predict frictional slip measured in uniaxial loading of Lexan and granite plates with parallel interfaces. The predictions of slip for the Lexan experiments have been compared to experimental results and found to have inconsistent agreement with the magnitude and direction of the slip. The prediction of slip for the granite experiments indicates a stiffer system, as would be expected. The validity of the prediction of slip (and, subsequently, the prediction of the related principal stress field) by UDEC is highly dependent on three factors: the choice of material and joint properties, the ability to determine when a "steady-state" solution is reached, and the physical reality of the steady-state solution based on the predicted overlap of discrete blocks.

The results of these UDEC calculations are dependent on the assumptions regarding the choice of both material and joint properties. Because the dynamic measurements of compression and shear wave velocities were obtained in a laboratory environment with unfractured samples, the use of these values to determine bulk modulus and Poisson's ratio should produce representative intact rock values. The granite calculations should be re-done with a measured friction coefficient from the samples used in the load tests.

The choice of joint stiffness properties used for these calculations is more uncertain than the collection of the material properties. The joint normal stiffness is derived by dividing the half-closure stress by the maximum joint closure value. The half-closure stress is the compressive stress that it takes to close the joint to half the maximum joint closure value. The maximum joint closure is usually assumed to be the average joint normal opening when the joint is in an unstressed condition. The elastic shear stiffness is the slope of the curve (actually a straight line) of shear stress versus joint deformation, analogous to the elastic modulus being the slope of the line for stress vs. strain. The change from elastic to inelastic slope is governed by the Mohr-Coulomb failure criterion (which depends on the normal stress, coefficient of friction, and cohesion). These types of data can be obtained from laboratory experiments. There are no readily available data concerning joint stiffness properties of Lexan. Table 2-6 in the Site Characterization Plan Conceptual Design Report (SNL, 1987) lists a lower-bound value of 100 GPa/m for joint shear stiffness for all tuff units at Yucca Mountain, to which granite is a chemically-similar material. Several calculations by SNL personnel for informal investigations of tunnel, drift, grout, and fill design concerns used values for both normal and shear stiffness ranging from 1 to 1000 GPa/m. The median value seemed to be about 10 GPa/m, and this value was chosen for both joint normal and shear stiffness for the Lexan and granite calculations presented in Figures 8 through 21. Joint shear stiffness values are included for tuffs at various

Rock Mass Quality Category numbers in the Reference Information Base (RIB) (DOE/YMP, 1989). Values for the half-closure stress and the maximum joint closure value may be taken from the RIB for determining joint normal stiffness properties to be used with a continuum joint model. Clearly, site data for determining joint normal and joint shear stiffness are either available or can be obtained. In addition, the documentation for the UDEC code (Itasca, 1992) suggests a way to estimate the joint normal stiffness, k_n, and the joint shear stiffness, k_s, based on bulk and shear moduli:

$$k_n = k_s = 10 \bullet \max\left[\frac{(K + \frac{4}{3}G)}{\Delta z_{\min}}\right]$$

where $\Delta z_{\min}$ is the smallest width of an adjoining zone (finite difference element) in the normal direction. The max[ ] notation indicates that the maximum value over all zones adjacent to the joint is to be used. For the Lexan and granite calculations, a good value for $\Delta z_{\min}$ was 0.01 m. As a result, according to the above equation recommended values for joint stiffness were 5660 GPa/m for Lexan and 100,000 GPa/m for granite.

Calculations for the Lexan experiments using joint stiffness values ranging from 2 to 5660 GPa/m at 0.45 MPa loading indicated significant dependence of the predicted slip on these variables. The calculations at k_n=k_s=2 GPa/m suffered numerical problems and could not converge to a solution. The horizontal displacement predicted using k_n=k_s=5 GPa/m is shown in Figure 22. Note that the displacement in the plates above and below the hole are approximately the same for both stiffnesses (compare to Figure 10), but that there is significantly more displacement in the plates on either side of the hole for the lower stiffness. Similar horizontal displacement plots for joint stiffnesses of 100 GPa/m and 5660 GPa/m are shown in Figures 23 and 24. As the joint stiffness increases, the response is increasingly more similar to a solid block rather than individual plates. The corresponding slip profiles for these calculations are presented in Figures 25 through 27. Note that the magnitude of slip predicted over this range of stiffness values is approximately two orders. Especially interesting is that the magnitude of slippage exhibited by the Lexan experiments is bounded by the results predicted by joint stiffnesses of 10 and 100 GPa/m, indicating a considerable amount of sensitivity to these variables. Figures 28 and 29 show the slip and horizontal displacement of the granite plates with 0.5 MPa load at the UDEC-recommended stiffness of 10^5 GPa/m. In comparison to Figures 20 and 18, respectively, at a stiffness of 10 GPa/m, Figures 28 and 29 indicate a much stiffer system with the primary displacement being the deformation equivalent to a solid block of granite. Obviously, more information is needed to determine the true physical and numerical dependencies of frictional slip on the joint stiffness.

One of the concerns with using UDEC to predict the resultant stress and displacement fields due to a static loading condition is the difficulty in determining when a "steady-state" condition is attained. UDEC performs static loading problems by creating a dynamic pulse with a very small timestep. A steady-state solution is achieved when the static load modeled by the dynamic pulse has completed propagated through the modeled system and the maximum unbalanced force calculated for all the finite difference cells is approximately zero. The term "steady-state" refers

to the fact that a static process is being modeled by calculating with a time-dependent (i.e., dynamic) equation, with the notion that a static condition is achieved when all changes to the system have approached zero. The code user must be able to determine how many computational cycles are required for the dynamic pulse to propagate completely through the system. If "steady-state" is not reached at the end of the prescribed number of cycles, problems such as the uniaxial loading experiments modeled here (which should have an essentially symmetric solution across the horizontal axis of symmetry) will exhibit a physically-unrealistic asymmetry. Note the displacements displayed in Figures 8 through 12, 18, 19, 22, 23, 24, and 29; all of these are nearly, but not quite, symmetrical, indicating that steady-state had not yet been reached. The same behavior can be seen in the corresponding y-direction (in the direction of the load) stress fields; Figures 30 through 32 present the vertical stress fields corresponding to the displacements in Lexan predicted by Figures 8, 12, and 23 respectively. The reason for asymmetric displacement across the horizontal centerline was because UDEC did not perform enough computational cycles; the trick is knowing when the results have reached steady-state (over and above just having a solution that "looks" correct). The number of computational cycles is set in the UDEC input file, along with an overlap tolerance. The overlap tolerance is the maximum allowable overlap distance in space of two contiguous discrete blocks, which may numerically cross over one into the other. At each cycle (timestep), a maximum unbalanced force is calculated; theoretically, this number should approach zero at the end of the calculation. The problem lies in the fact that as the number of cycles is increased, thereby allowing more time for the dynamic pulse to extend through the system, the amount of overlap between blocks increases. This overlap, which is a numerical artifact, may increase to levels which may bring into question the physical reality of the solution. This is the type of code difficulty which seems to require a great deal of familiarity with the code to address appropriately; it would seem that the code user, as well as the code itself, should go through a validation process.

The run time for UDEC on these problems was in the range of 20-30 minutes on Sparc 10 workstation, depending on the applied load and the amount of deformation.

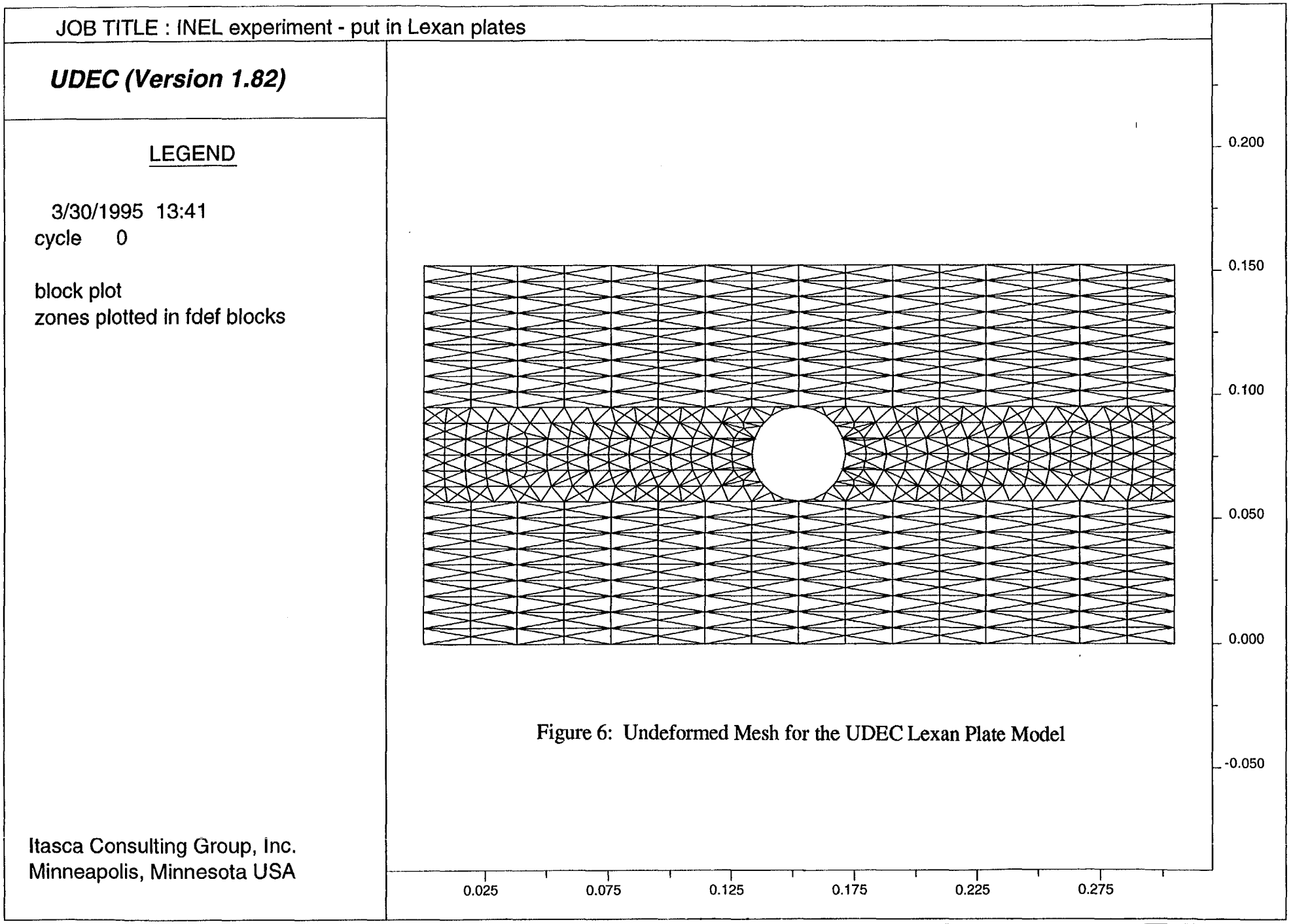

Figure 6: Undeformed Mesh for the UDEC Lexan Plate Model

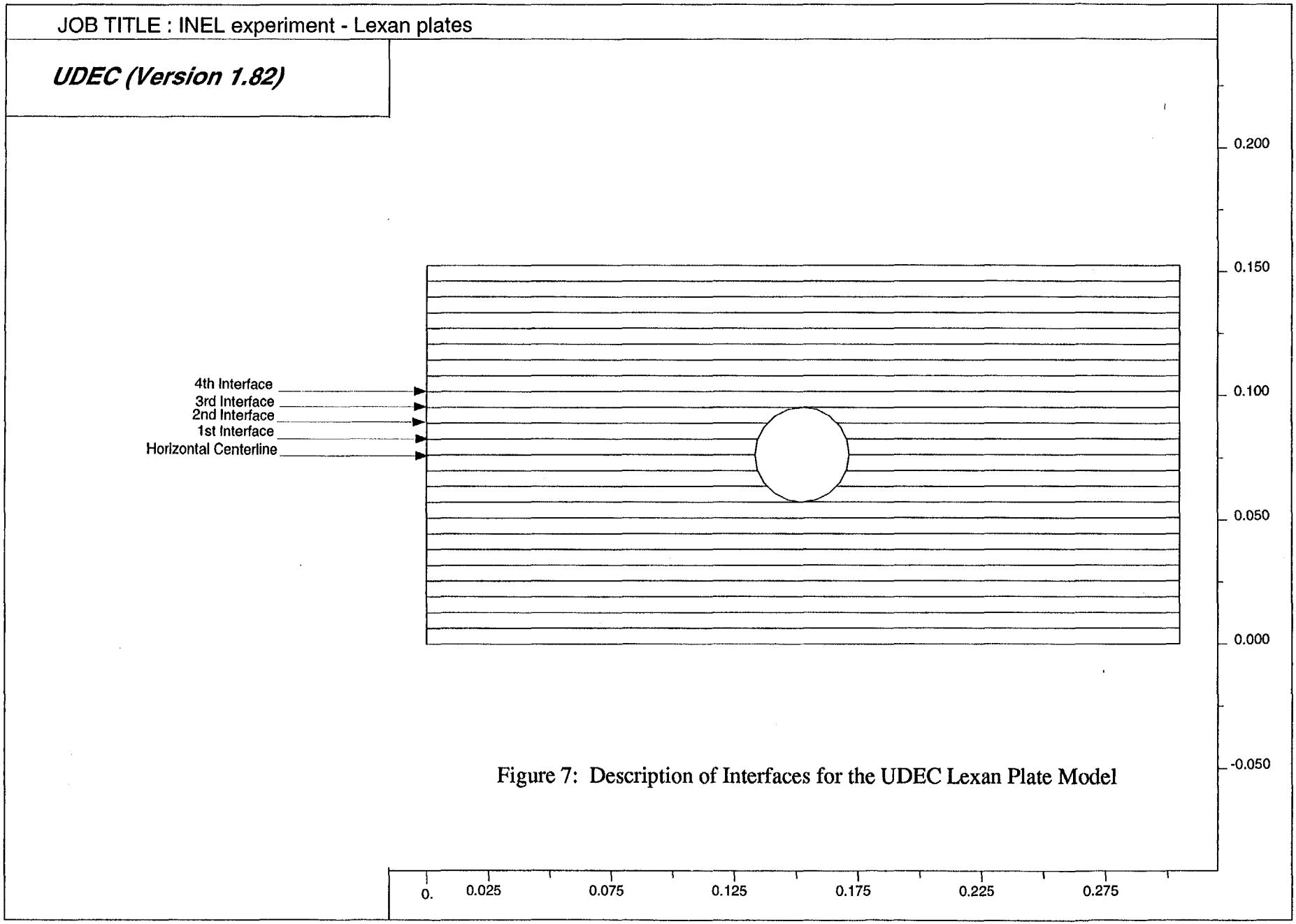

Figure 7: Description of Interfaces for the UDEC Lexan Plate Model

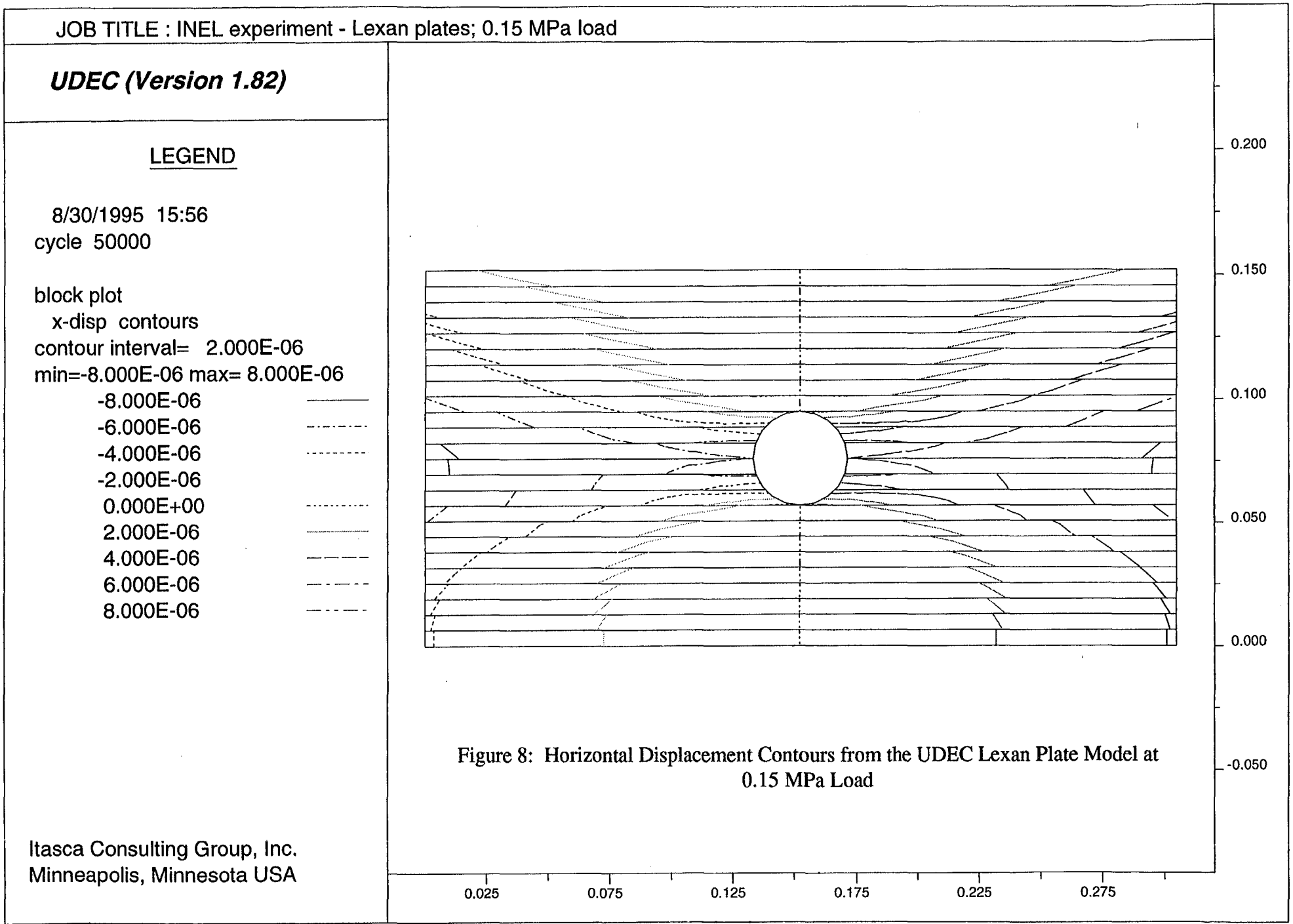

Figure 8: Horizontal Displacement Contours from the UDEC Lexan Plate Model at 0.15 MPa Load

JOB TITLE : INEL experiment - Lexan plates; 0.30 MPa load

UDEC (Version 1.82)

LEGEND

8/31/1995 10:26
cycle 35000

block plot
x-disp contours
contour interval= 2.000E-06
number of contours/color= 2
min=-1.400E-05 max= 1.400E-05
-1.400E-05 -1.200E-05
-1.000E-05 -8.000E-06
-6.000E-06 -4.000E-06
-2.000E-06 0.000E+00
2.000E-06 4.000E-06
6.000E-06 8.000E-06
1.000E-05 1.200E-05
1.400E-05

Itasca Consulting Group, Inc.
Minneapolis, Minnesota USA

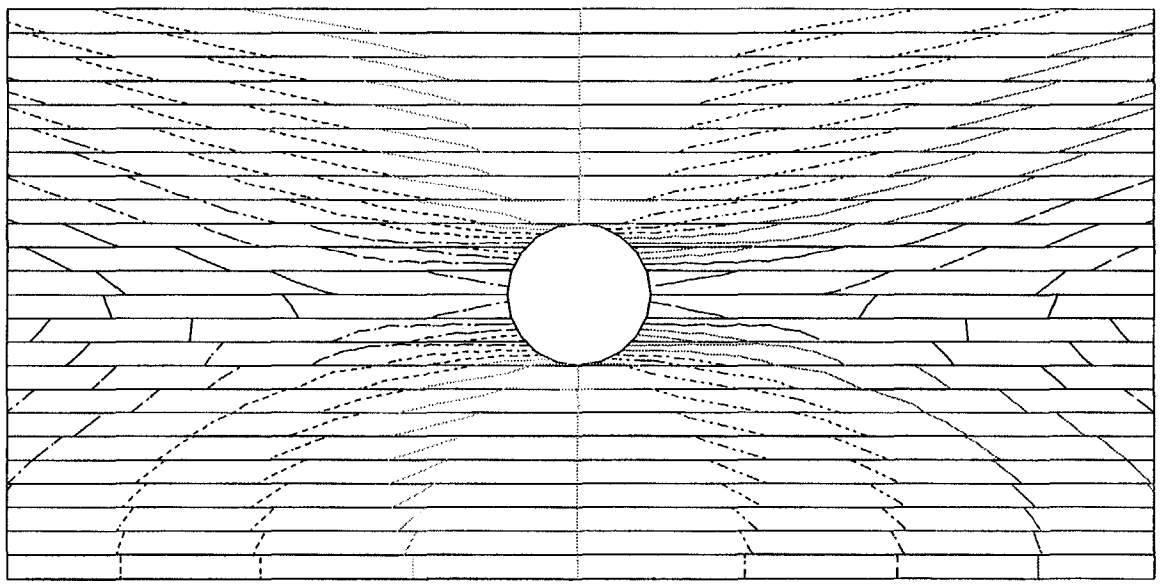

Figure 9: Horizontal Displacement Contours from the UDEC Lexan Plate Model at 0.30 MPa Load

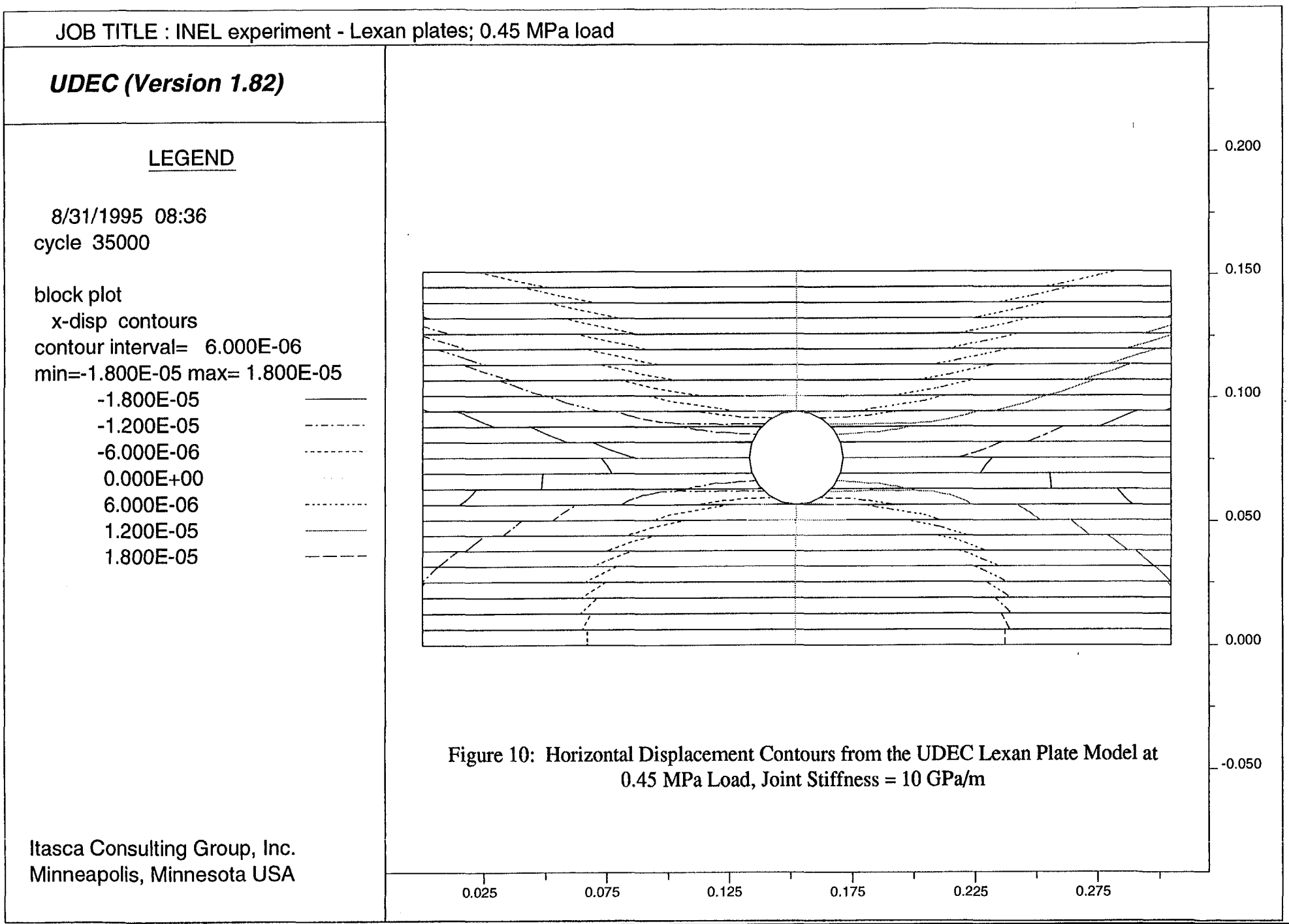

Figure 10: Horizontal Displacement Contours from the UDEC Lexan Plate Model at 0.45 MPa Load, Joint Stiffness = 10 GPa/m

JOB TITLE : INEL experiment - Lexan plates; 0.50 MPa load

UDEC (Version 1.82)

LEGEND

8/31/1995 11:06
cycle 35000

block plot
x-disp contours
contour interval= 3.000E-06
number of contours/color= 2
min=-2.400E-05 max= 2.400E-05
-2.400E-05 -2.100E-05
-1.800E-05 -1.500E-05
-1.200E-05 -9.000E-06
-6.000E-06 -3.000E-06
0.000E+00 3.000E-06
6.000E-06 9.000E-06
1.200E-05 1.500E-05
1.800E-05 2.100E-05
2.400E-05

Itasca Consulting Group, Inc.
Minneapolis, Minnesota USA

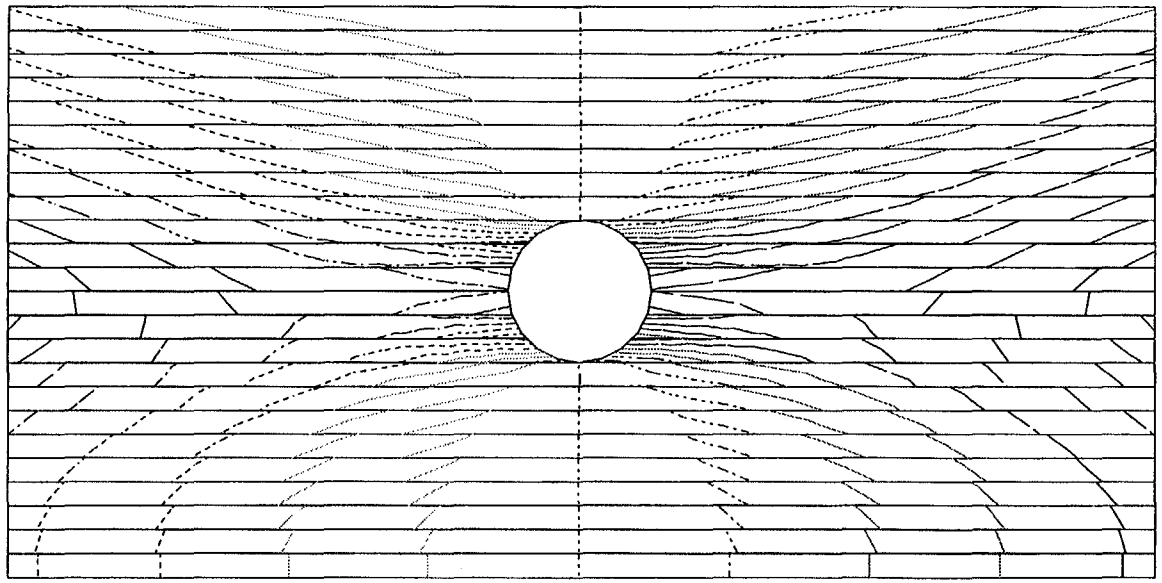

Figure 11: Horizontal Displacement Contours from the UDEC Lexan Plate Model at 0.50 MPa Load

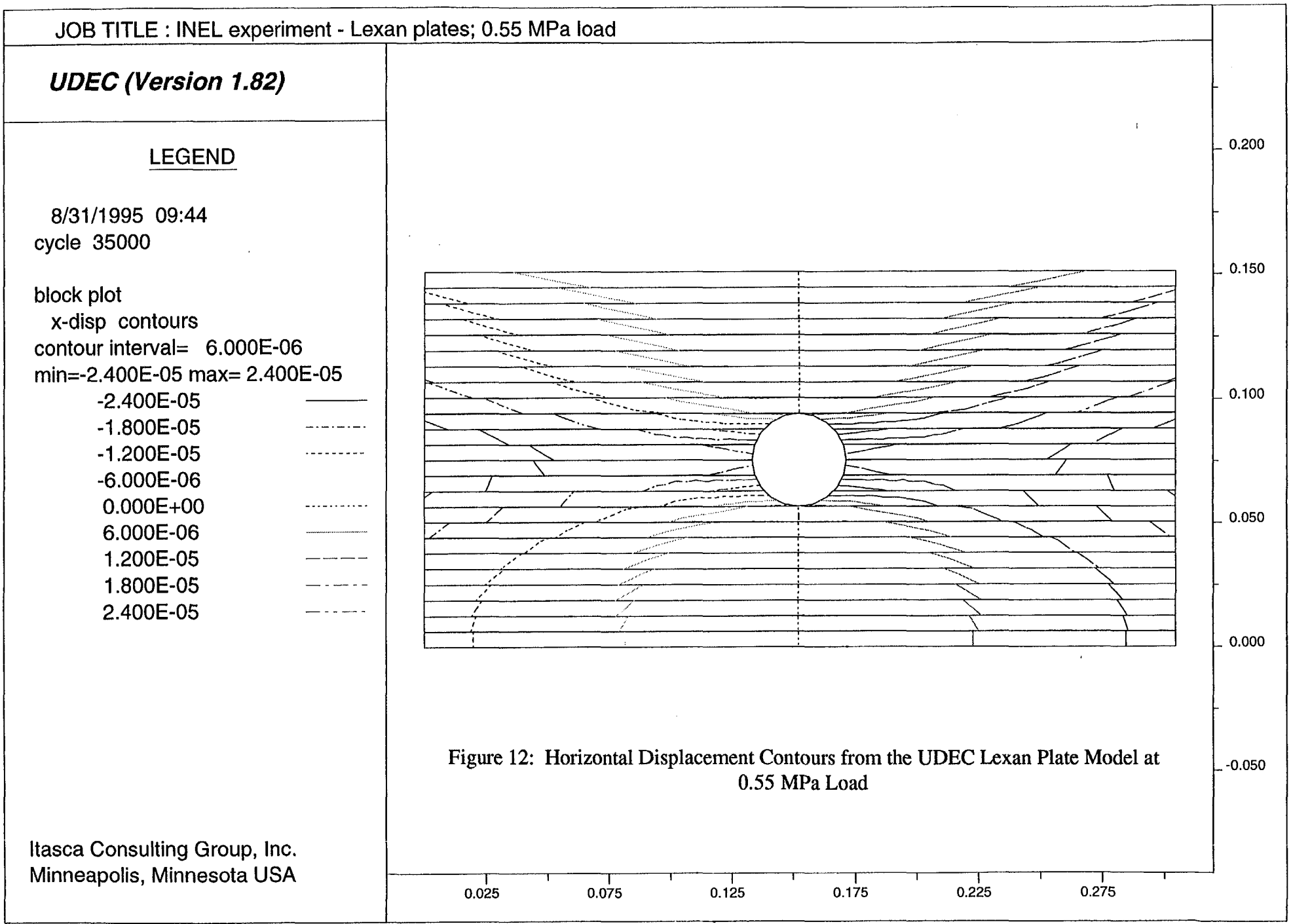

Figure 12: Horizontal Displacement Contours from the UDEC Lexan Plate Model at 0.55 MPa Load

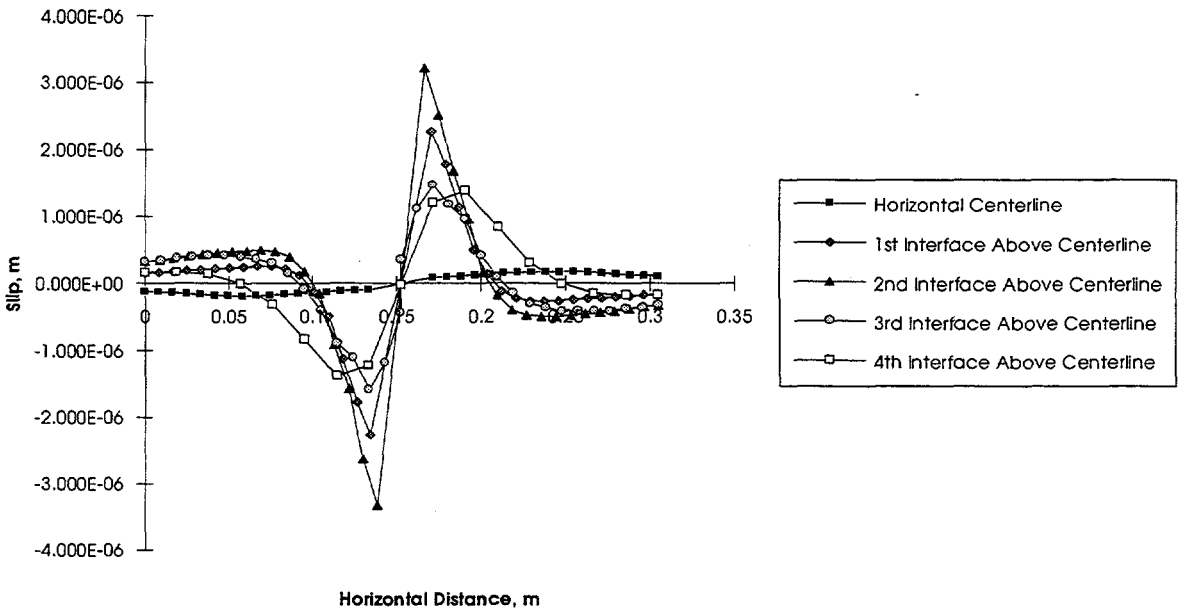

Figure 13: Slip vs. Distance, Lexan Plates, Load=0.15 MPa
(Numbers Directly from UDEC run)

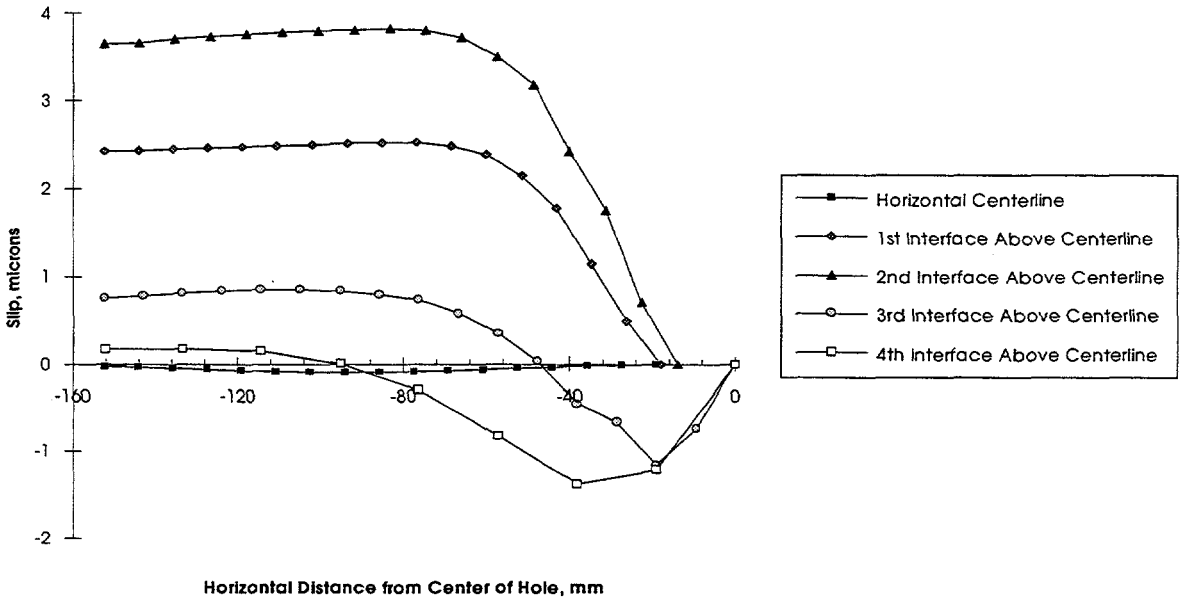

Figure 14: Slip vs. Distance, Lexan Plates, Load=0.15 MPa
(Point at Hole or Vertical Center Used as Zero Reference)

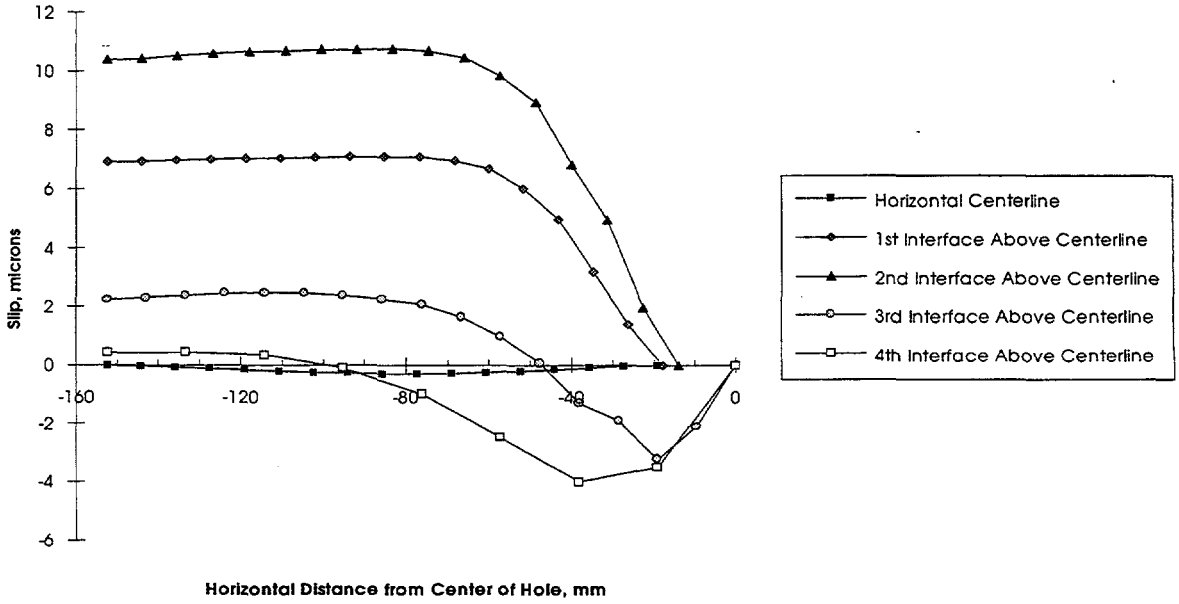

Figure 15: Slip vs. Distance, Lexan Plates, Load=0.45 MPa, Joint Stiffness=10 GPa/m

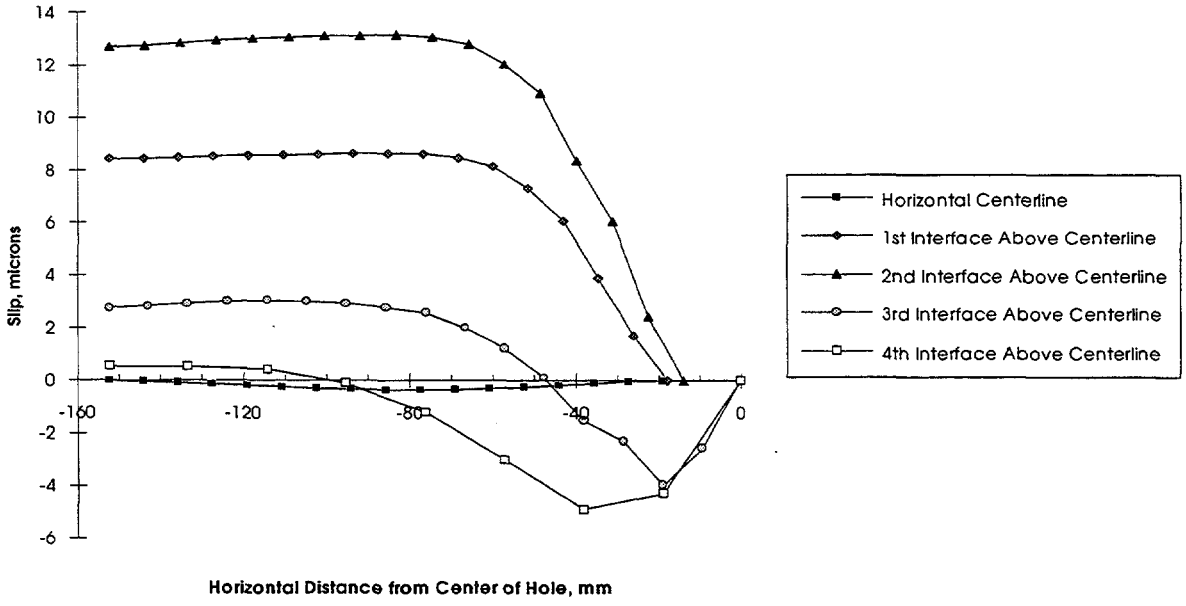

Figure 16: Slip vs. Distance, Lexan Plates, Load=0.55 MPa

JOB TITLE : INEL experiment - Granite plates; 1.0 MPa load (Frict. coef. = 0.47)

UDEC (Version 1.82)

LEGEND

7/18/1995 11:06
cycle 0

block plot
zones plotted in fdef blocks

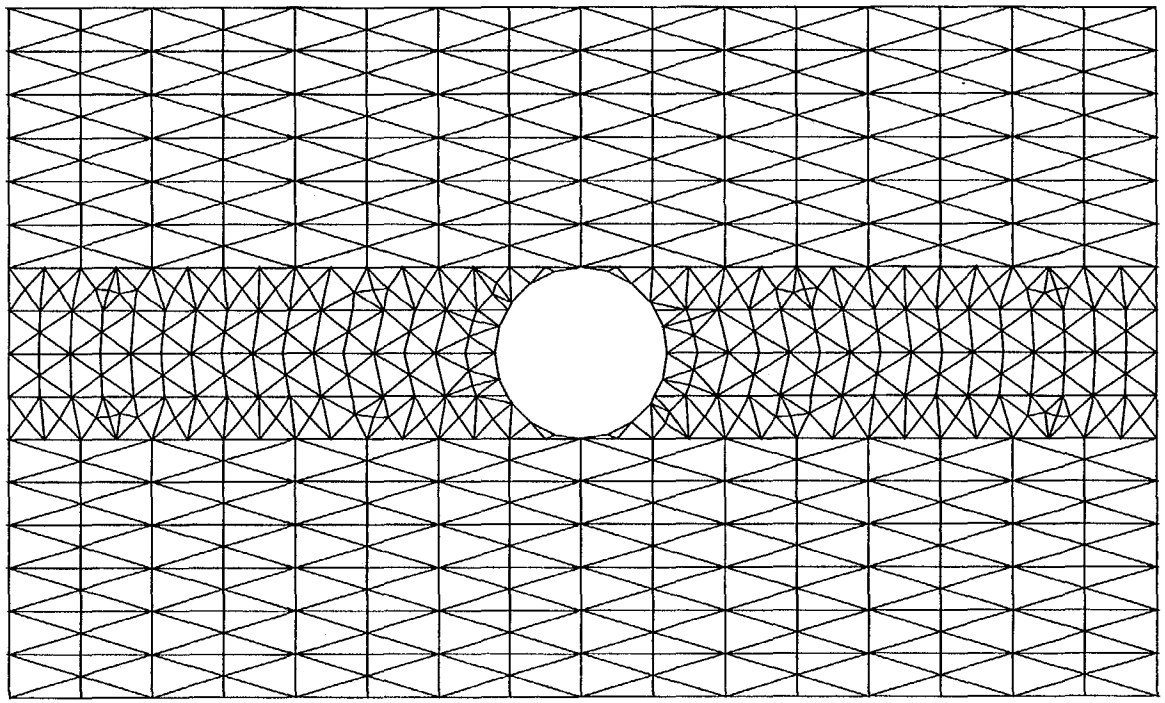

Figure 17: Undeformed Mesh for the UDEC Granite Plate Model

Itasca Consulting Group, Inc.
Minneapolis, Minnesota USA

JOB TITLE : INEL experiment - Granite plates; 0.5 MPa load (Frict. coef. = 0.47)

UDEC (Version 1.82)

LEGEND

8/31/1995 11:48
cycle 35000

block plot
x-disp contours
contour interval= 2.000E-06
min=-6.000E-06 max= 6.000E-06

-6.000E-06	
-4.000E-06	
-2.000E-06	
0.000E+00	
2.000E-06	
4.000E-06	
6.000E-06	

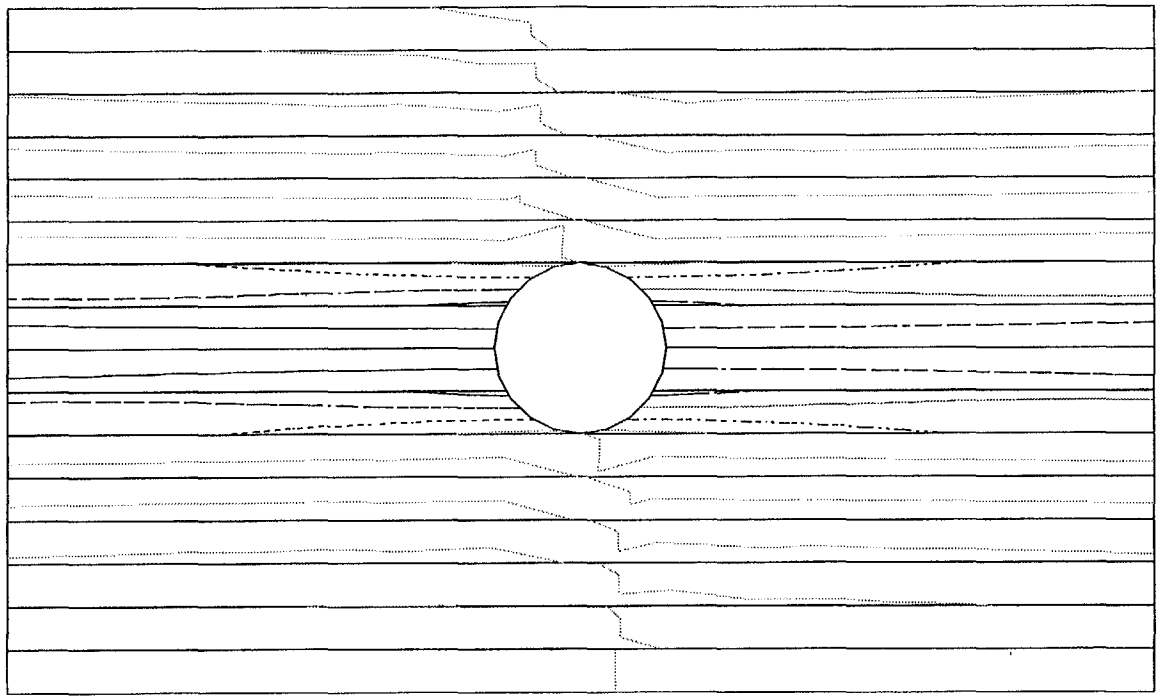

Figure 18: Horizontal Displacement Contours from the UDEC Granite Plate Model at 0.5 MPa Load

Itasca Consulting Group, Inc.
Minneapolis, Minnesota USA

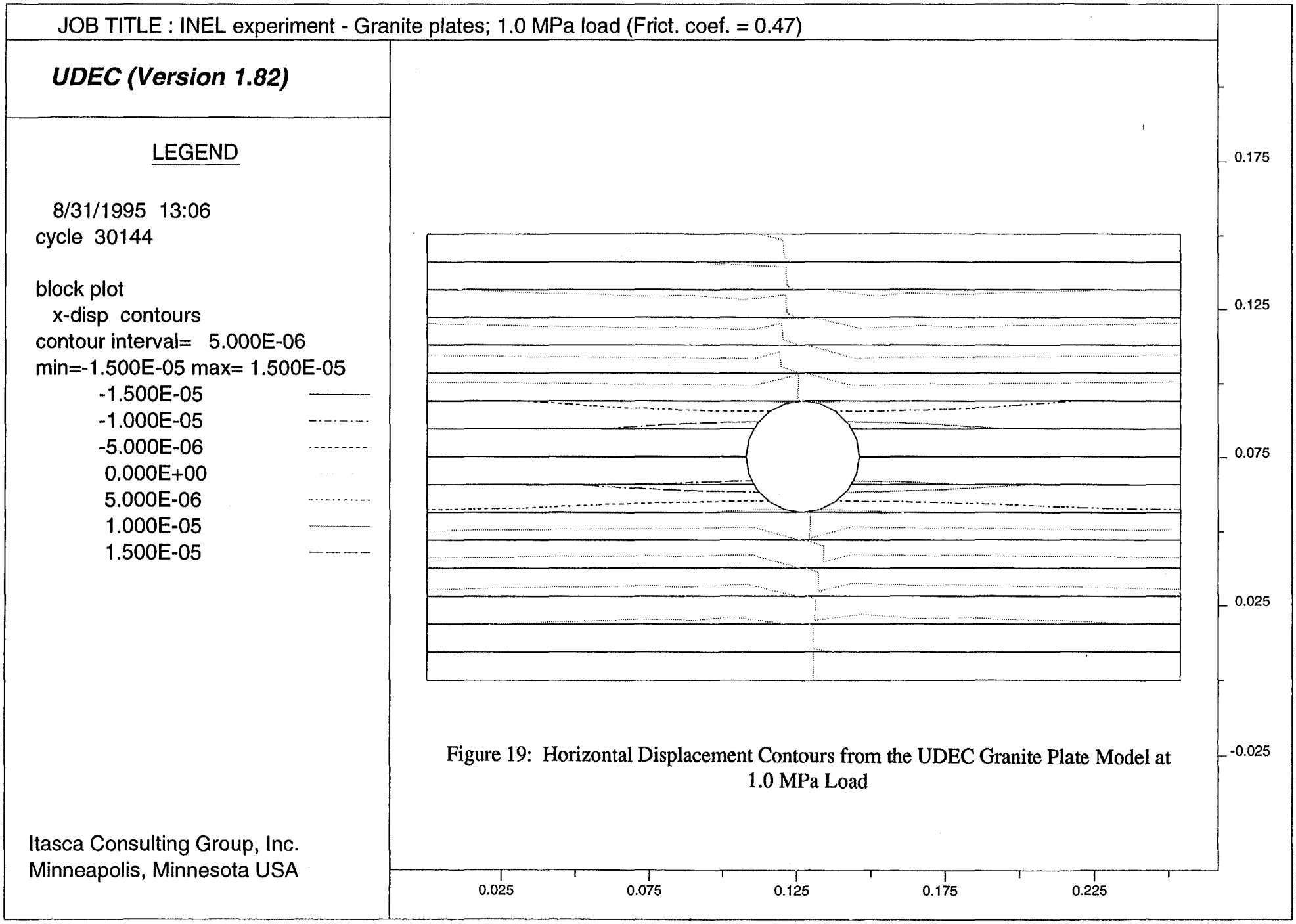

Figure 19: Horizontal Displacement Contours from the UDEC Granite Plate Model at 1.0 MPa Load

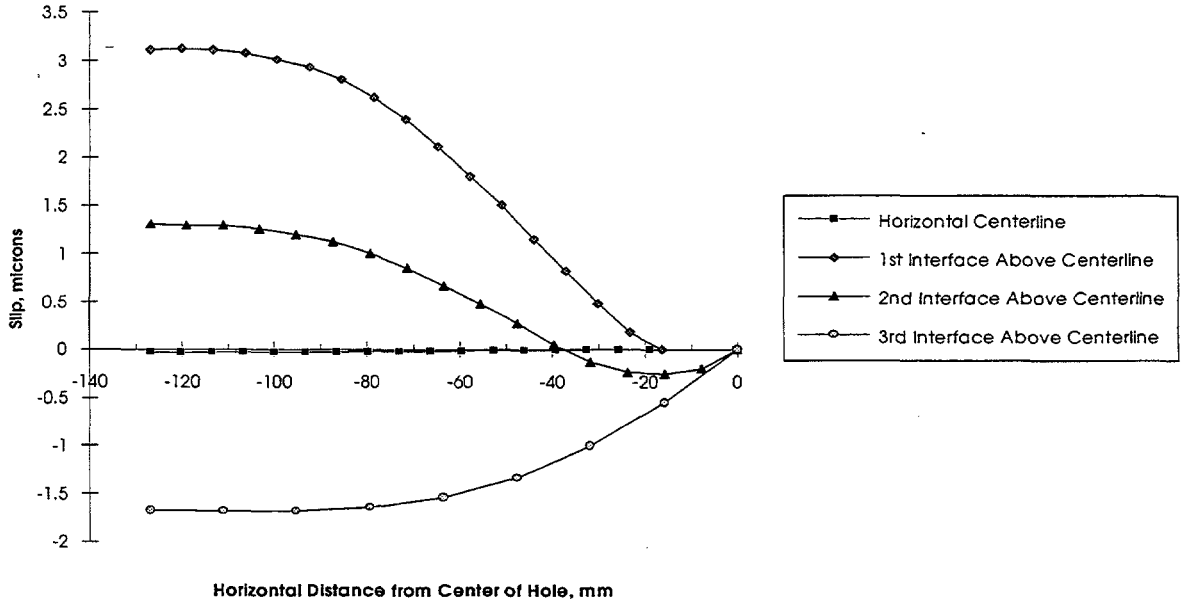

Figure 20: Slip vs. Distance, Granite Plates, Load=0.5 MPa
(Point at Hole or Vertical Center Used as Zero Reference)

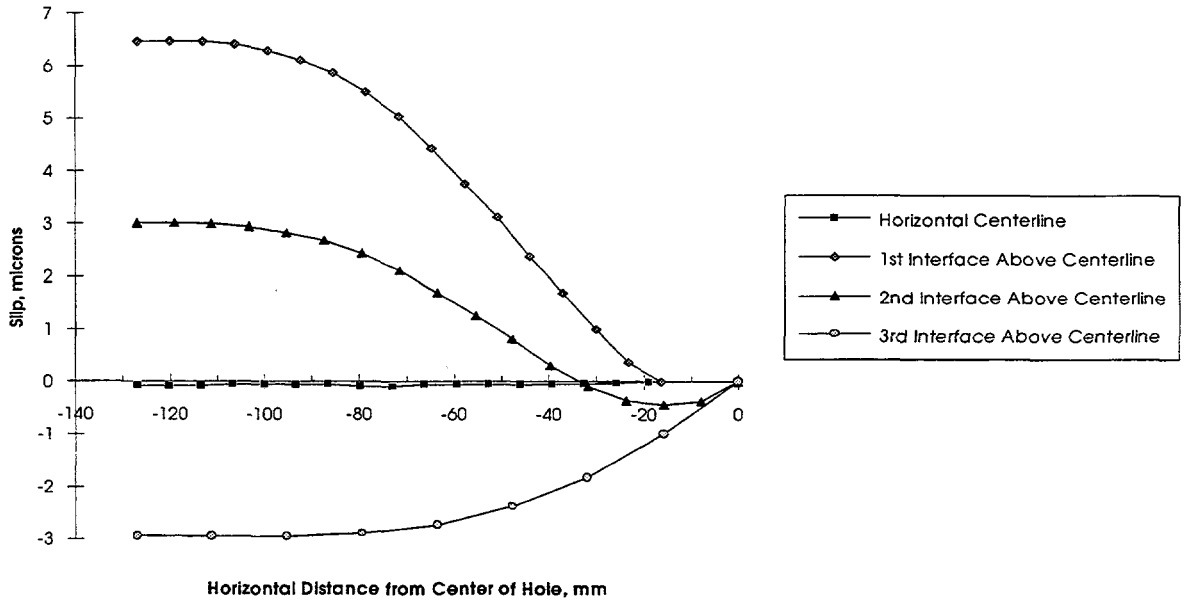

Figure 21: Slip vs. Distance, Granite Plates, Load=1.0 MPa

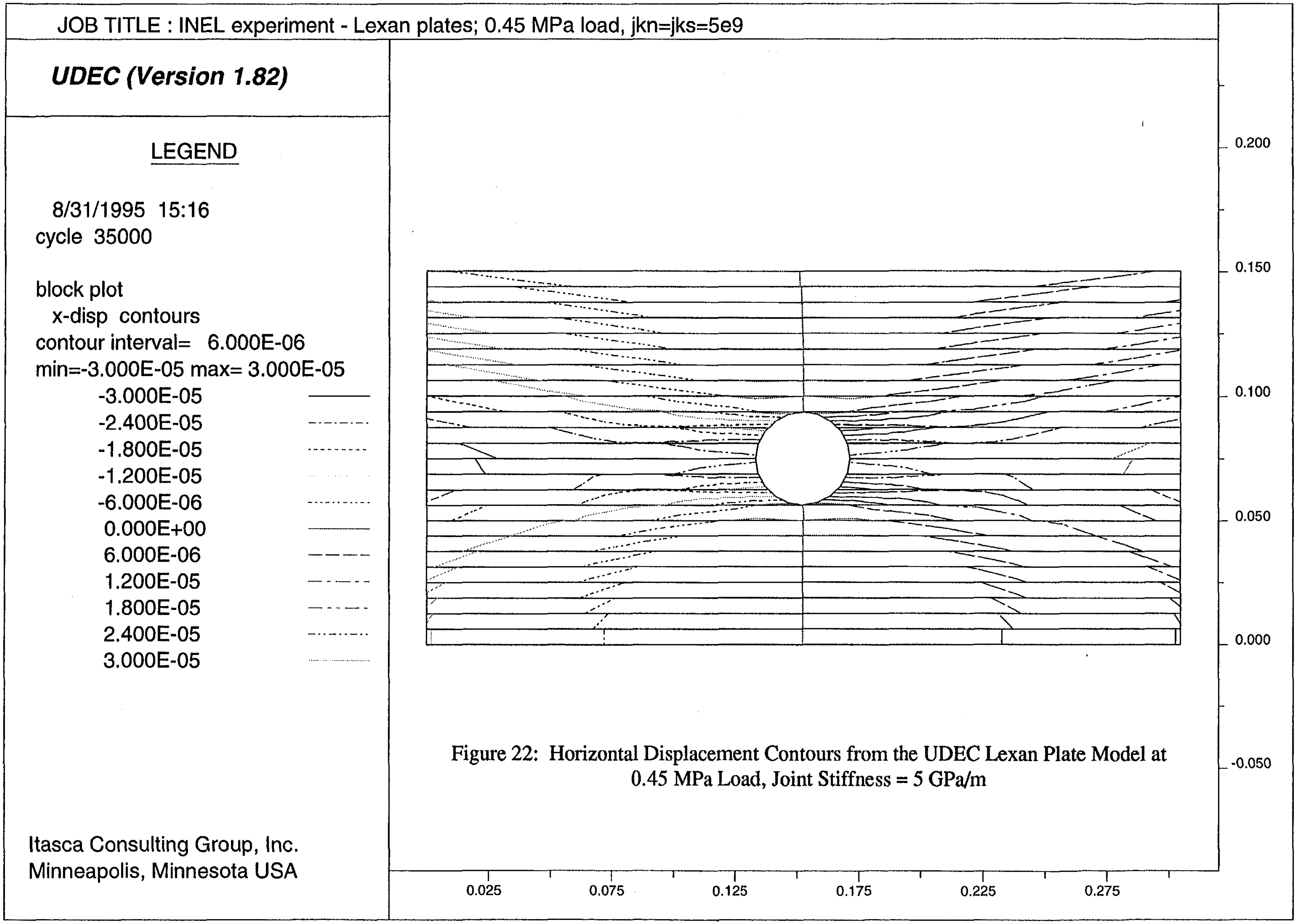

Figure 22: Horizontal Displacement Contours from the UDEC Lexan Plate Model at 0.45 MPa Load, Joint Stiffness = 5 GPa/m

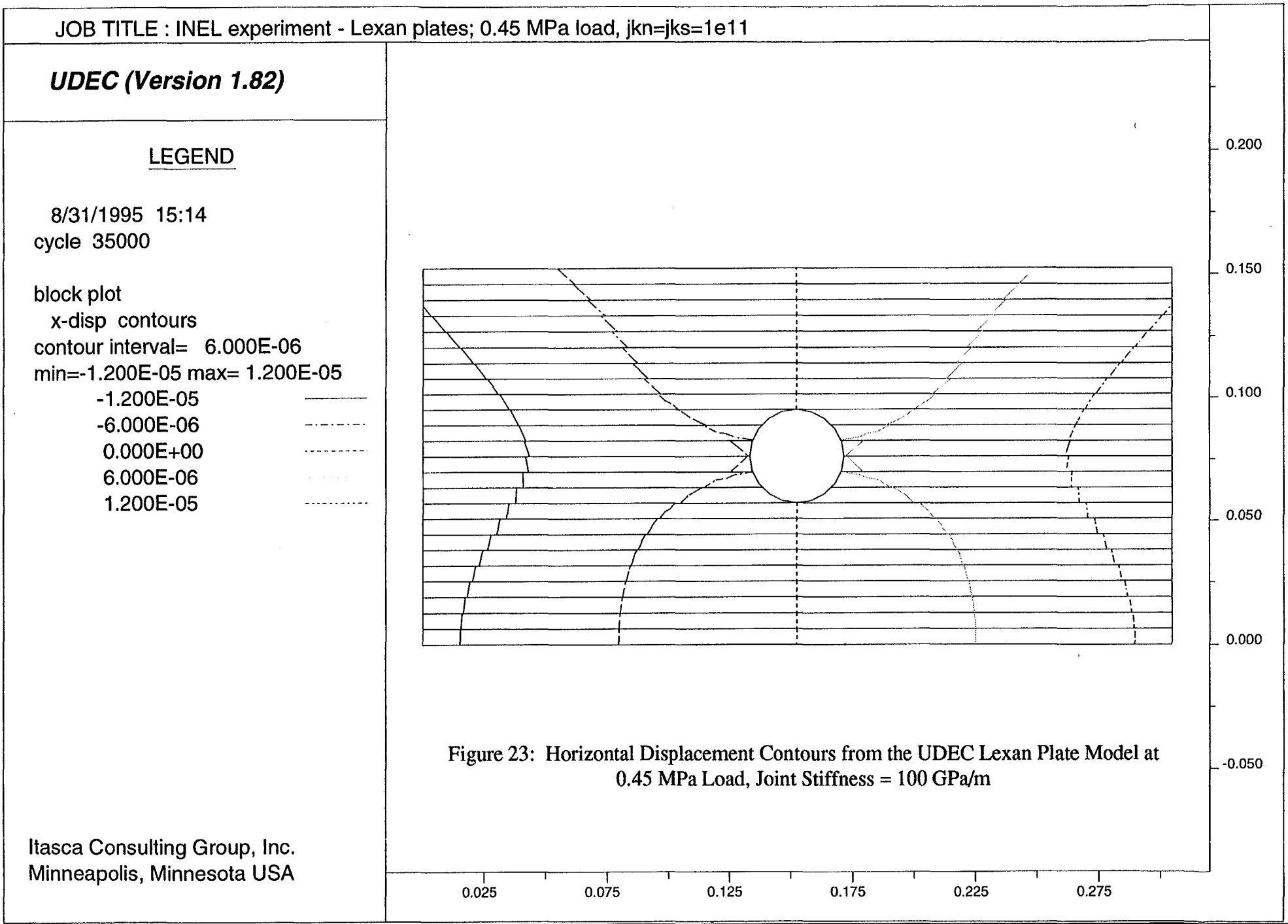

Figure 23: Horizontal Displacement Contours from the UDEC Lexan Plate Model at 0.45 MPa Load, Joint Stiffness = 100 GPa/m

JOB TITLE : INEL experiment - Lexan plates; 0.45 MPa load, jkn=jks=5.66e12

UDEC (Version 1.82)

LEGEND

8/31/1995 14:35
cycle 35000

block plot
x-disp contours
contour interval= 6.000E-06
min=-1.200E-05 max= 1.200E-05
-1.200E-05
-6.000E-06
0.000E+00
6.000E-06
1.200E-05

Itasca Consulting Group, Inc.
Minneapolis, Minnesota USA

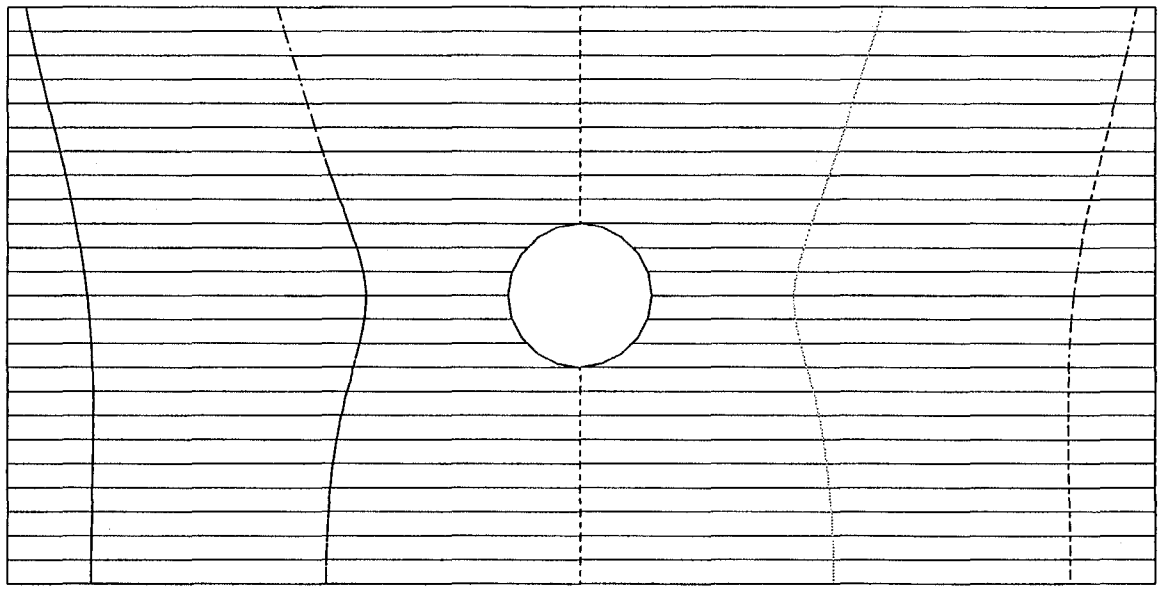

Figure 24: Horizontal Displacement Contours from the UDEC Lexan Plate Model at 0.45 MPa Load, Joint Stiffness = 5660 GPa/m

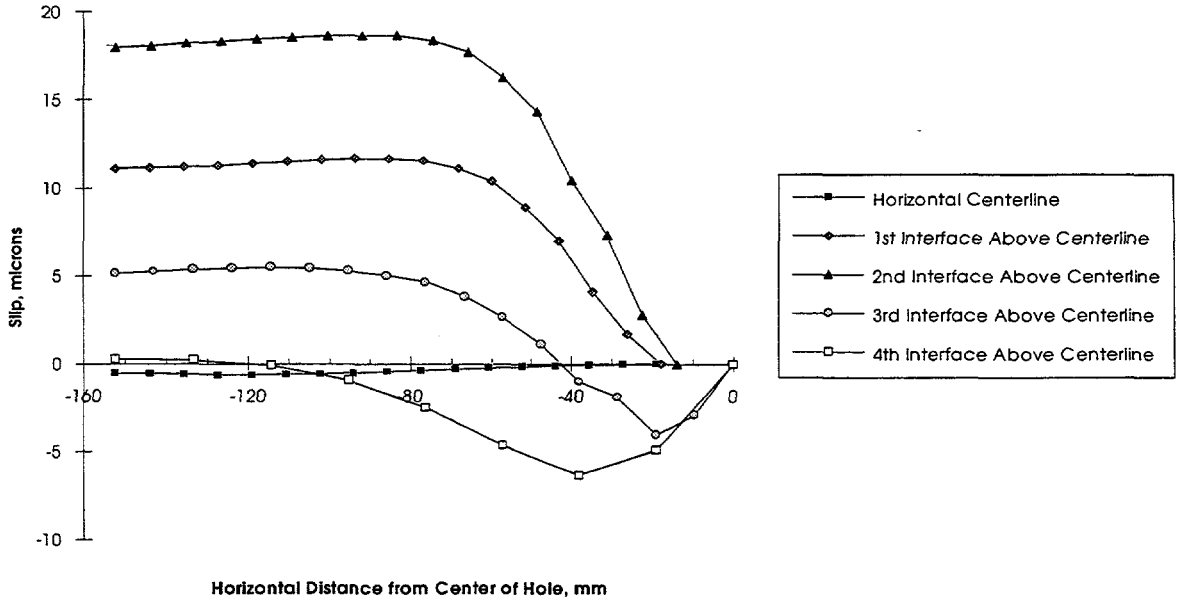

Figure 25: Slip vs. Distance, Lexan Plates, Load=0.45 MPa, Joint Stiffness=5 GPa/m

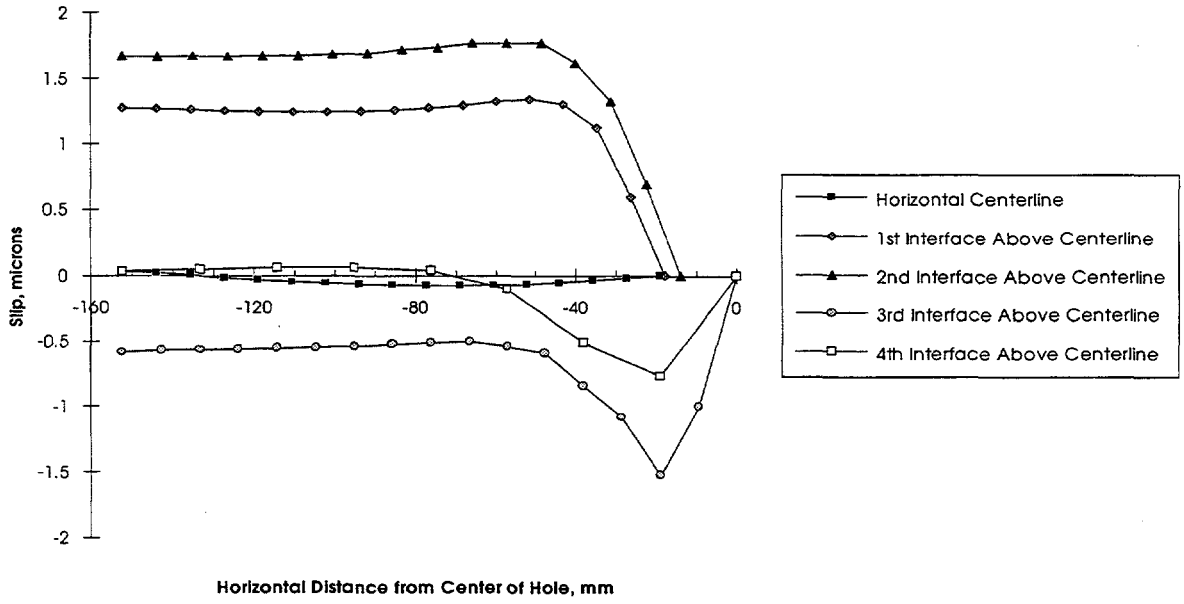

Figure 26: Slip vs. Distance, Lexan Plates, Load=0.45 MPa, Joint Stiffness=100 GPa/m

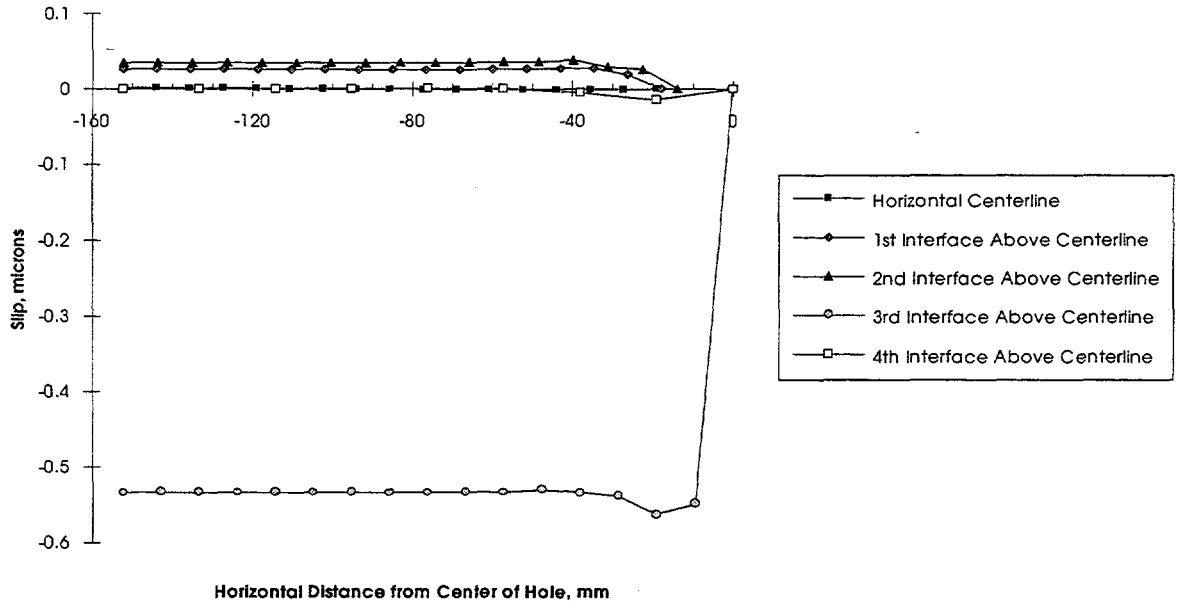

Figure 27: Slip vs. Distance, Lexan Plates, Load=0.45 MPa, Joint Stiffness=5660 GPa/m

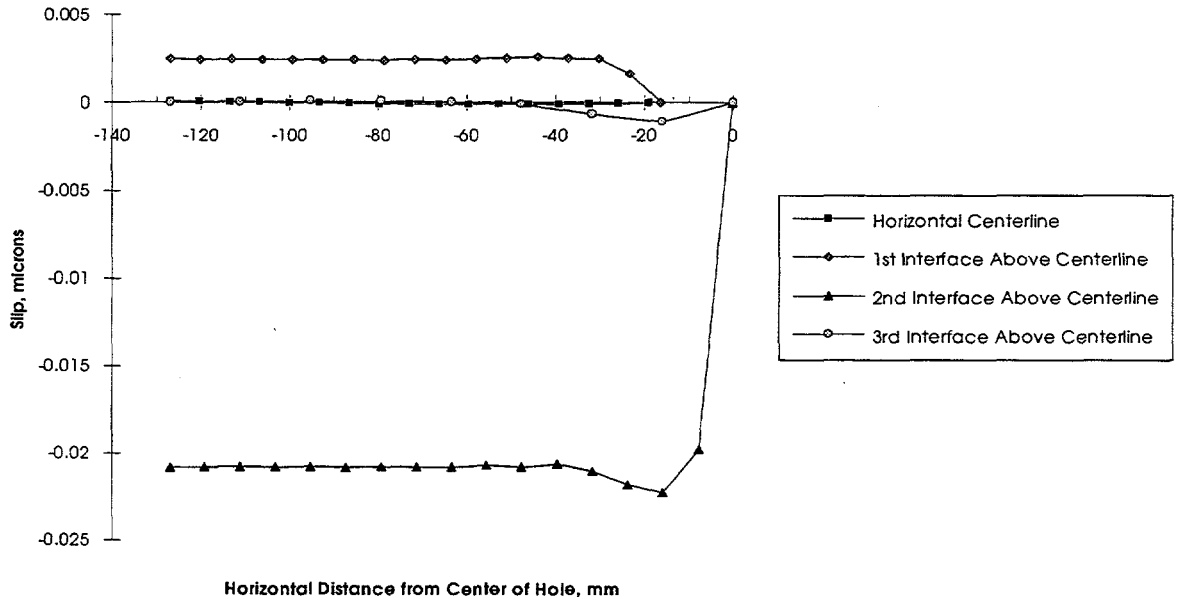

Figure 28: Slip vs. Distance, Granite Plates, Load=0.5 MPa, Joint Stiffness=100,000 GPa/m

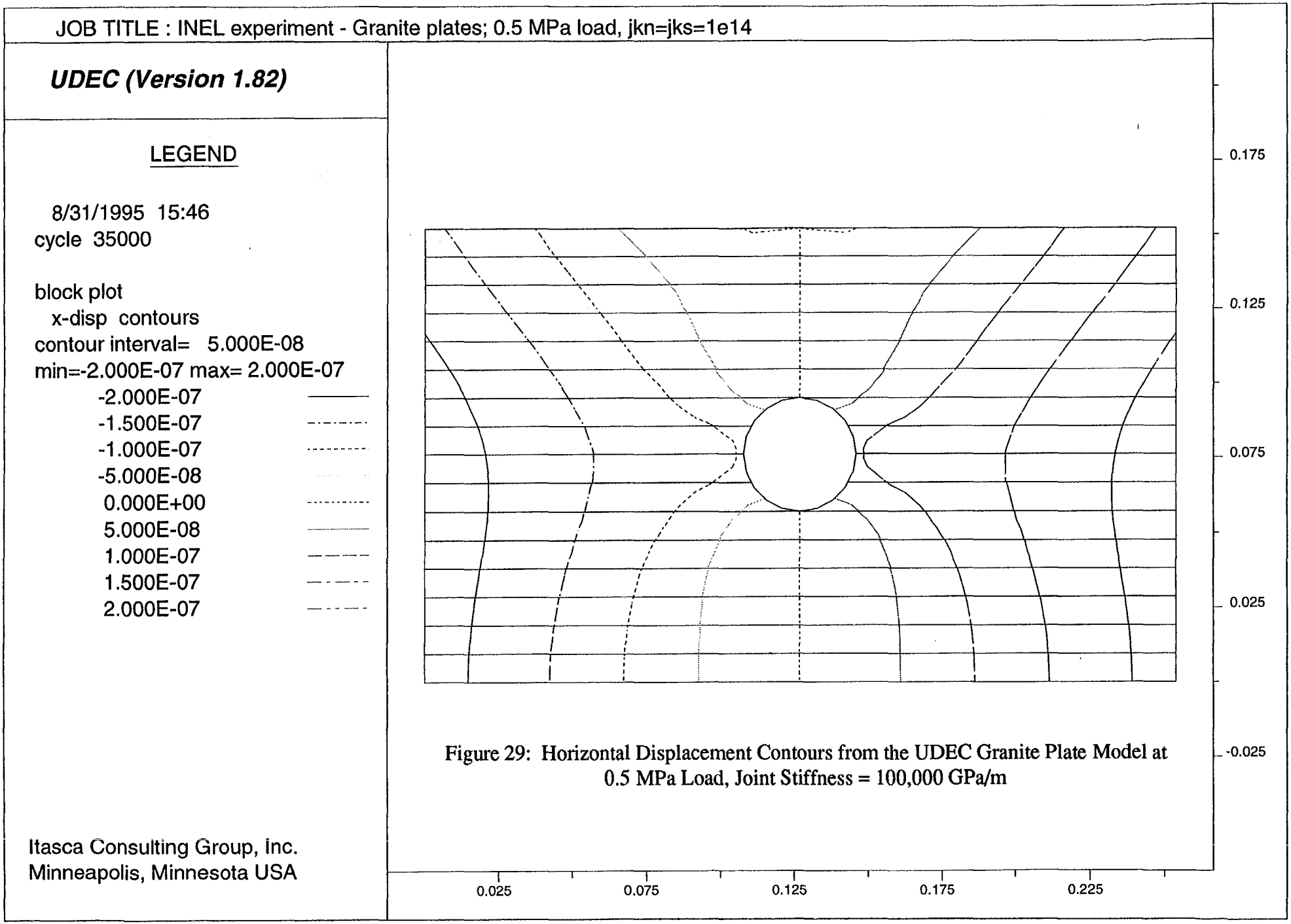

Figure 29: Horizontal Displacement Contours from the UDEC Granite Plate Model at 0.5 MPa Load, Joint Stiffness = 100,000 GPa/m

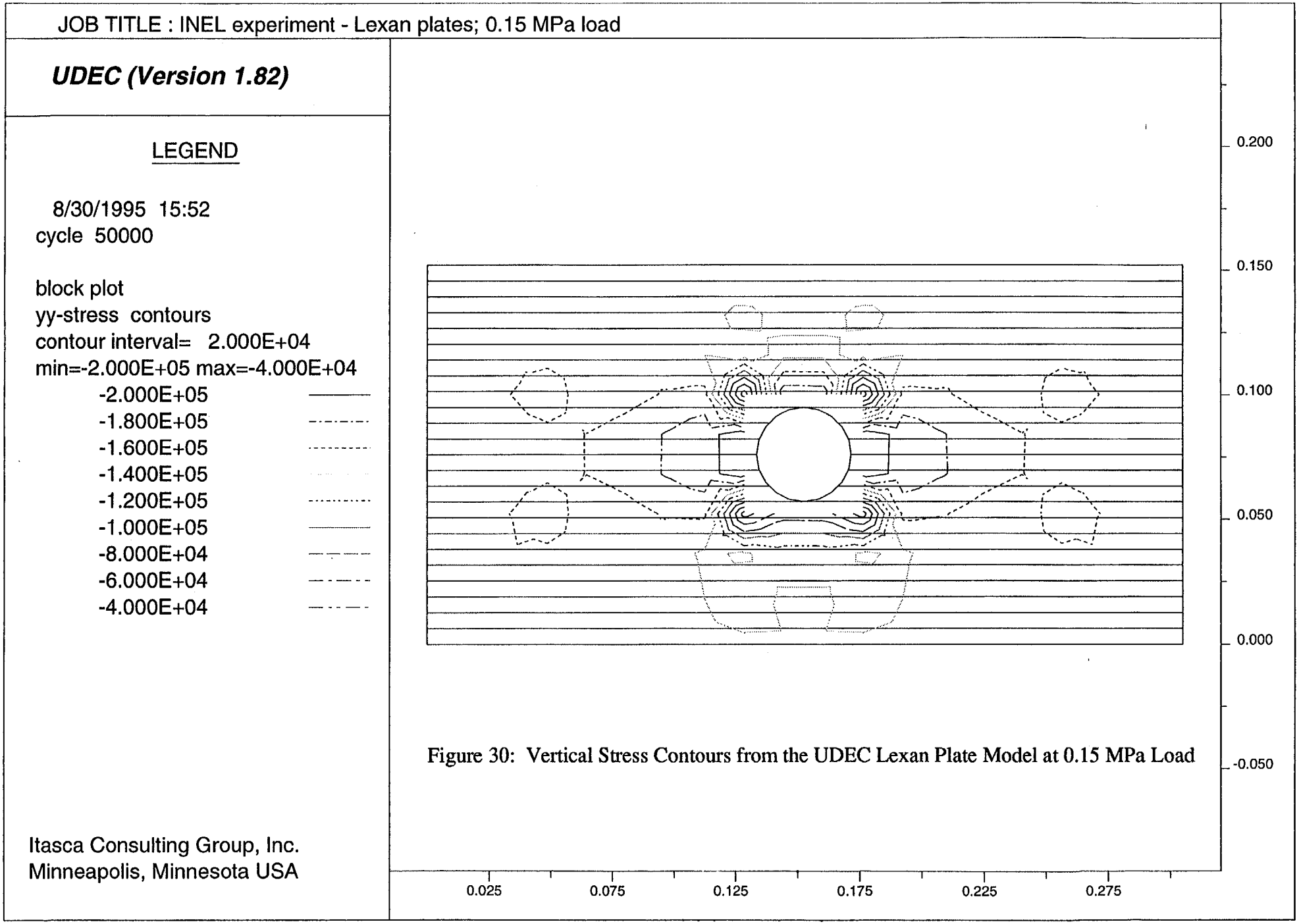

Figure 30: Vertical Stress Contours from the UDEC Lexan Plate Model at 0.15 MPa Load

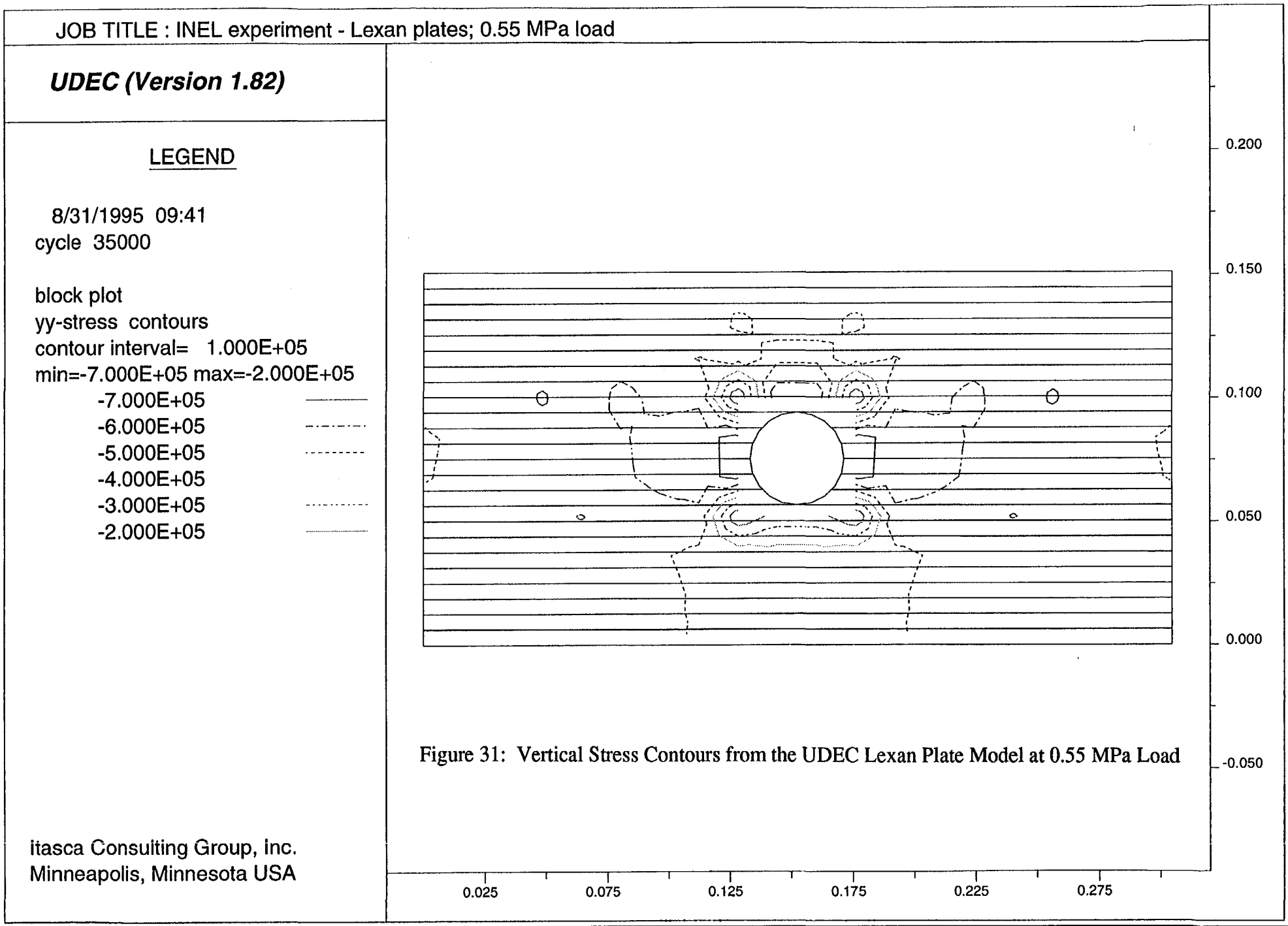

Figure 31: Vertical Stress Contours from the UDEC Lexan Plate Model at 0.55 MPa Load

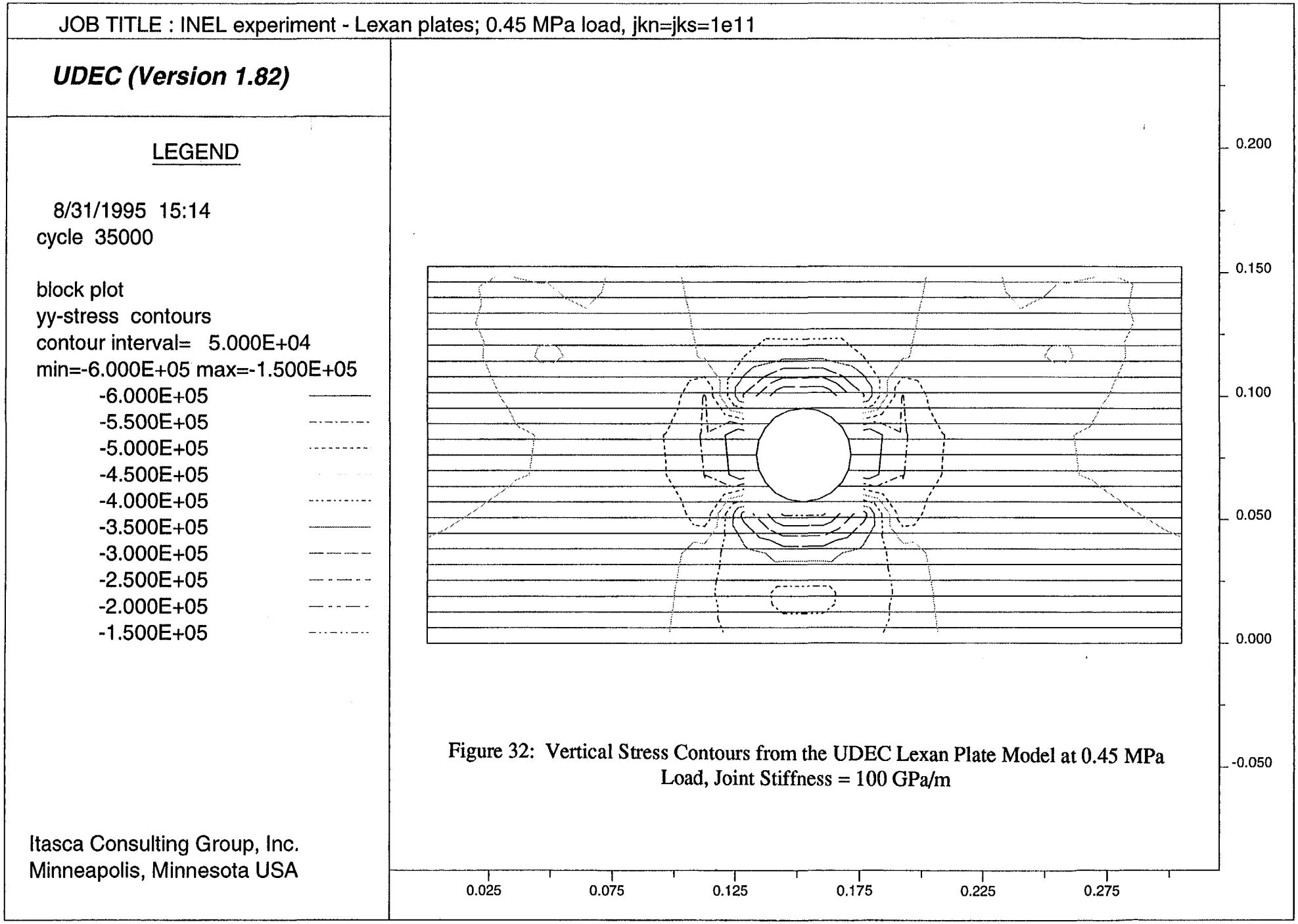

Figure 32: Vertical Stress Contours from the UDEC Lexan Plate Model at 0.45 MPa Load, Joint Stiffness = 100 GPa/m

4.0 Calculations Using JAC2D

Uniaxial loading calculations simulating the INEL plate tests were also performed with the quasi-static finite element code JAC2D (Biffle and Blanford, 1994). JAC2D is a two-dimensional program designed for use on solid mechanics problems using a nonlinear conjugate gradient method to solve a set of continuum equations based on four-node Lagrangian uniform strain elements. Several different material constitutive models are available in JAC2D, including the isothermal (temperature-independent) elastic and elastic-plastic models. The code includes the capability of defining various sliding interfaces in the solution domain, which was used for this application. A compliant joint model (or elastic joint model) is available in JAC2D, but was not appropriate for this work because there was no way to output joint slippage values versus distance results.

The interfaces between the plates, or joints, were defined discretely in JAC2D by a contact surface model using a sliding interface algorithm. The sliding interface algorithm in JAC2D allows general contact between two surfaces of the model. It is a general capability in that it allows the contact to be either fixed, intermittent (i.e., allows gaps to re-open after initial contact), or sliding only (i.e., once in contact the two surfaces are always in contact but may slip in relation to each other) depending on how the model is defined in the input file for the program. The interfaces may include frictional behavior ranging from frictionless to full friction (fixed). The sliding interface definition governs how forces are transmitted across the contacting surfaces. For example, tensile, compressive, and shear forces are all transmitted across a fixed interface, but only compressive (bearing) force may act across a frictionless sliding interface.

4.1 Lexan Modeling with JAC2D

The Lexan plate experiment was modeled as two-dimensional and doubly symmetric about the center hole cut through the plates. The finite element mesh is shown in Figure 33. The mesh included twelve Lexan plates plus an approximation for the steel platen of the testing machine[5]. The assumption of double symmetry translates into a displacement constraint against horizontal displacement along the left edge of the finite element model, which is the vertical centerline through the center of the hole in the actual experiment, and into a constraint against vertical movement of the model along the model's bottom edge--the bottom side of the twelfth plate below the platen. The right edge of the model was not constrained. Twelve sliding interfaces were defined: eleven partial-width ones between the twelve stacked plates and one of full width between the uppermost Lexan plate and the platen. The eleven sliding interfaces between the Lexan plates did not extend across the full width of the (half) plates, but to within one-quarter inch (6.35 mm) of the model's right boundary, where full connectivity between elements of the

[5] The results of the Lexan experiment as reported in Perry, et al. (1995) described the dimensions of the plates in English units (inches), but described the material properties, loads, and displacements in SI units (MPa, microns, etc.). The results of the JAC2D and JAS3D calculations are described in the same manner as the report to provide easier comparison. The calculations performed under JAC2D and JAS3D were performed in English units (thus the mesh dimensions in Figure 32 are in inches, as are the contour plots of displacement) Displacements and slips along plate interfaces were calculated in a manner similar that described earlier and were converted to microns units.

adjacent plates simulated how the stack of plates had been glued together in the actual experiment. Each plate-to-plate interface was assigned a coefficient of friction of 0.47, while the interface between the Lexan plate and the steel platen was modeled as frictionless. The interfaces were not constrained against separation, although each plate was modeled as being initially in contact with adjacent plates. The finite element model consisted of 17,473 elements, 18,989 nodes, and 13 material blocks, since each plate was modeled as a separate material block although all of the Lexan material blocks used the same material property definitions.

Each Lexan plate was modeled as an isothermal elastic material. Only the elastic modulus and Poisson's ratio were necessary to define the material. The elastic modulus value used for Lexan was 2.84 GPa (0.4118×10^6 psi), while 0.39 was the value input for the Poisson's ratio. The steel platen was also modeled as an isothermal elastic material with Young's modulus equal to 206.9 GPa (30×10^6 psi) and Poisson's ratio of 0.30. Because only one element was used to model the platen, it had a relative stiffness compared to the Lexan even greater than the ratios of their moduli suggest.

The downward pressure of the platen on the stack of plates was implemented via pressure loading on the top surface of the one-element platen. The pressure was increased linearly in one hundred increments up to the full value of 1.0 MPa (145 psi). Thus each load step in the calculation represented a 0.01 MPa increase in the pressure load. An EXODUS (Mills-Curran et al., 1988) format plot-file database was written out every fifth load step (at 0.05 MPa increments).

Results of the JAC2D Lexan plate simulation are shown in Figures 34 through 43. Deformed mesh contour plots of the progressive horizontal displacement throughout the Lexan plate model at load increments of 0.15, 0.30, 0.45, 0.50, and 0.55 MPa are shown, respectively in Figures 34 through 38. The displacements shown on the contour plots are always relative to the undeformed state of the mesh, and are shown in the units of inches. In order to discern the relative slippage between plates, the nodal displacements along the sliding interfaces were extracted from the EXODUS database created by JAC2D and plotted separately. The nodal displacements were converted to SI units to facilitate comparison with the reported experimental results and the results reported with the UDEC models. Slippage was calculated by subtracting the horizontal nodal displacement at each node on the lower plate's upper surface from the horizontal displacement value at the node across the sliding interface from it on the upper plate's lower surface. In cases where the two adjoining surfaces did not have matching nodal coordinate values, a spline fit of the horizontal displacement data for each surface was generated so that the ordinates at matching abscissas could be subtracted and the slippage curve plotted. The plate slippage plots, at the load increments corresponding to the five displacement-contour plots, are shown in Figures 39 through 43, respectively, for the five inter-plate sliding interfaces beginning at the horizontal centerline of the hole and progressing upward. Due to the vertical symmetry assumption, there is of course no slip along the bottom plate boundary although there is horizontal displacement, which is shown in Figure 39. Positive slip indicates that the lower surface of the upper plate has displaced to the right, outward from the hole, relative to the upper surface of the plate below it.

The horizontal displacement contour plots indicate that there is some inward displacement

around the hole, but this is relatively minor in extent. Most of the horizontal displacement is outward, away from the hole, growing larger as the plates are squeezed under more pressure. Most of the slippage occurs between the third and fourth plates above the horizontal centerline (in the third sliding interface above the horizontal centerline), which is the sliding interface exactly level with the top of the hole. In this interface, slippage of as much as five microns (at 0.50 MPa pressure load) was recorded over a distance of about ten to twelve centimeters horizontally from the center of the hole. No other interface exhibited any significant slippage.

4.2 Granite Modeling with JAC2D

The granite plate model was similar to the Lexan plate model. The finite element mesh is shown in Figure 44. The basic difference between the two models was the granite plate model's dimensions matched those of the actual experiment: each granite plate was ten inches (254 mm) long by 0.375 inches (9.53 mm) high. Otherwise the meshing scheme (with minor adjustments), boundary conditions, symmetry assumptions, and loading conditions were carried over virtually the same way they were defined for the Lexan plate model. The granite plate model included 17,497 elements, 18,561 nodes, 9 material blocks, and 8 sliding interfaces. Granite was assumed to be an isothermal elastic material with a Young's modulus of 14×10^6 psi (96.7 GPa) and Poisson's ratio equal to 0.239.

Results from the two-dimenstional JAC2D granite plate model are plotted in Figures 45 through 53. Figures 45 through 49 show horizontal displacement contours overlying the deformed mesh at load increments of 0.15, 0.30, 0.45, 0.50, and 0.55 MPa, respectively, while Figures 50 through 53 show the slippage along the four inter-plate contact surfaces passing through and nearest the hole. As in the Lexan model, the bottom of the model is a symmetry plane representing the contact interface between the two middle-most plates. The symmetry assumption precludes relative slippage but allows horizontal displacement, which is shown in Figure 50. Again, slippage was calculated by subtracting the horizontal nodal displacement at each node on the lower plate's upper surface from the horizontal displacement value at the node across the sliding interface from it on the upper plate's lower surface. Positive slip indicates that the lower surface of the upper plate has displaced to the right, outward from the hole, relative to the upper surface of the plate below it.

The granite is a much stiffer material than Lexan, which is evident in the much smaller values recorded in the contour plots of horizontal displacement. The displacement results for the granite model are two to three orders of magnitude less than the results for the Lexan model. Relatively more of the granite plate deflects inward horizontally, however, as the line separating inward from outward displacement extends more or less directly above the entire hole (however, note that the granite plates are not as wide as the Lexan ones, so the same size hole is relatively larger in the granite model).

Slippage between the plates of the granite model is also proportionately reduced from the Lexan model, although it appears to have been more evenly distributed among the sliding interfaces than in the other two-dimensional model. Slippage magnitudes of from five to ten thousandths of a micron (at pressure loads of 0.30 MPa or greater) over a horizontal distance of 30 millimeters or so from the hole center are seen in the first interface (between the first and second

plates) above the horizontal centerline. The peak value of slippage of about thirty-five thousandths of a micron was recorded in the second interface above the horizontal centerline, which, as was the case in the Lexan model, was located exactly at the top of the hole. Slippage reaching over ten thousandths of a micron was reached in the third interface above the horizontal centerline.

The run time for JAC2D was dependent primarily on the number of contact surfaces modeled for each experiment. For the Lexan problems, JAC2D required approximately 35 CPU-hours (125713 CPU-seconds) on an HP9000/730 computer. On the same computer, the granite simulations required approximately 20 CPU-hours (71,438 CPU-seconds). A two-dimensional model has three degrees of freedom at unconstrained nodes (x-displacement, y-displacement, and rotation about the z-axis), and there are additional equations to solve for any contact conditions at the nodes. The Lexan model had about 19,000 nodes and 12 contact surfaces, and the granite model had about 18,600 nodes and 8 contact surfaces. A comparison of the two problems indicates that the number of contact surfaces was the determining factor in the difference in run times. The 2-D Lexan problem had 1.5 times as many contact surfaces as the 2-D granite problem, and the ratio of CPU-seconds is about 1.76. The predicted magnitudes of deformation may have also contributed to the difference in run times, as increasing gradients in the primary variables tend to add computational complexity to finite element calculations.

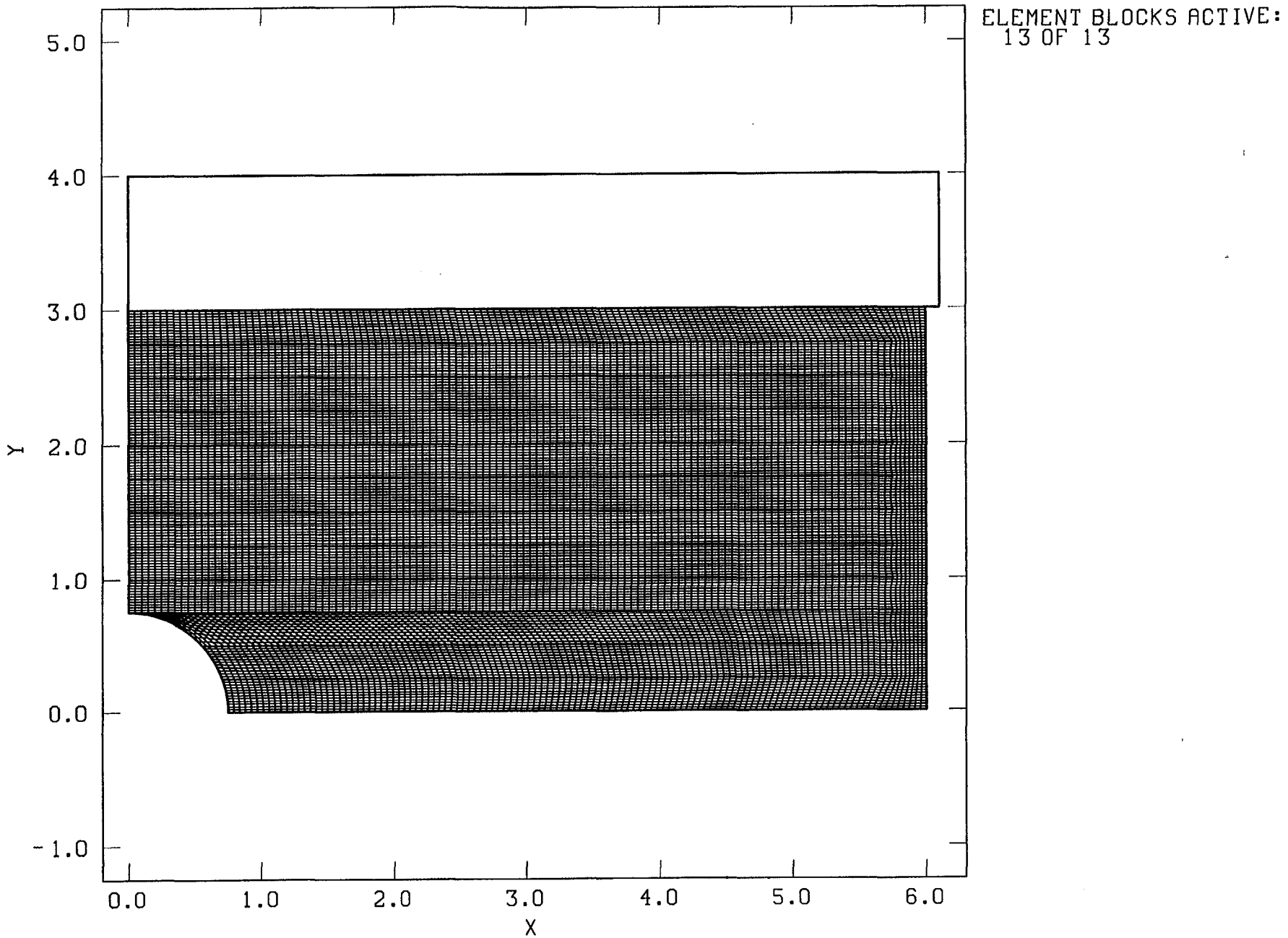

Figure 33: Undeformed Mesh for the JAC2D Lexan Plate Model
(all units in inches)

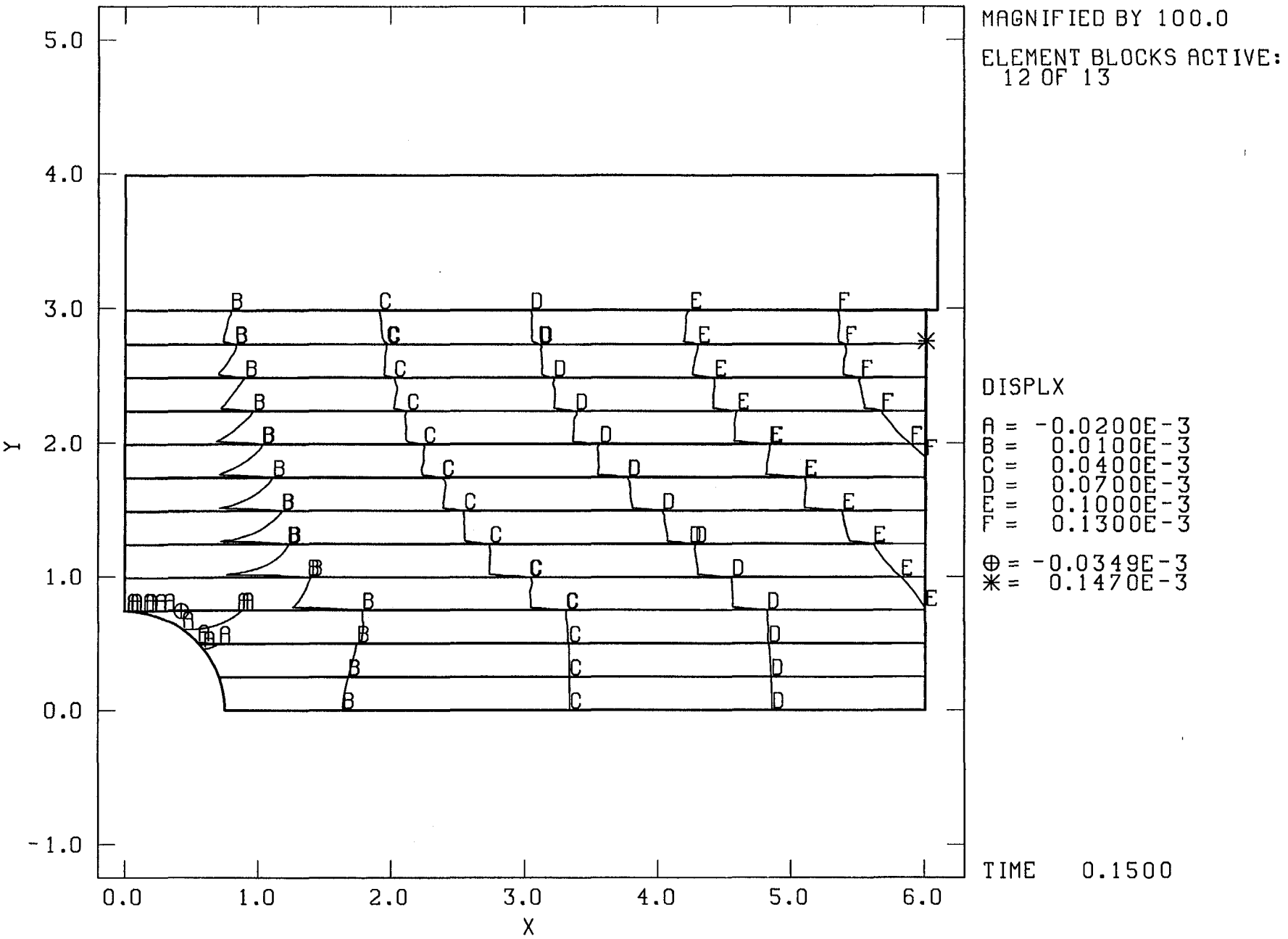

Figure 34: Horizontal Displacement Contours from the JAC2D Lexan Plate Model at 0.15 MPa Load
(all units in inches)

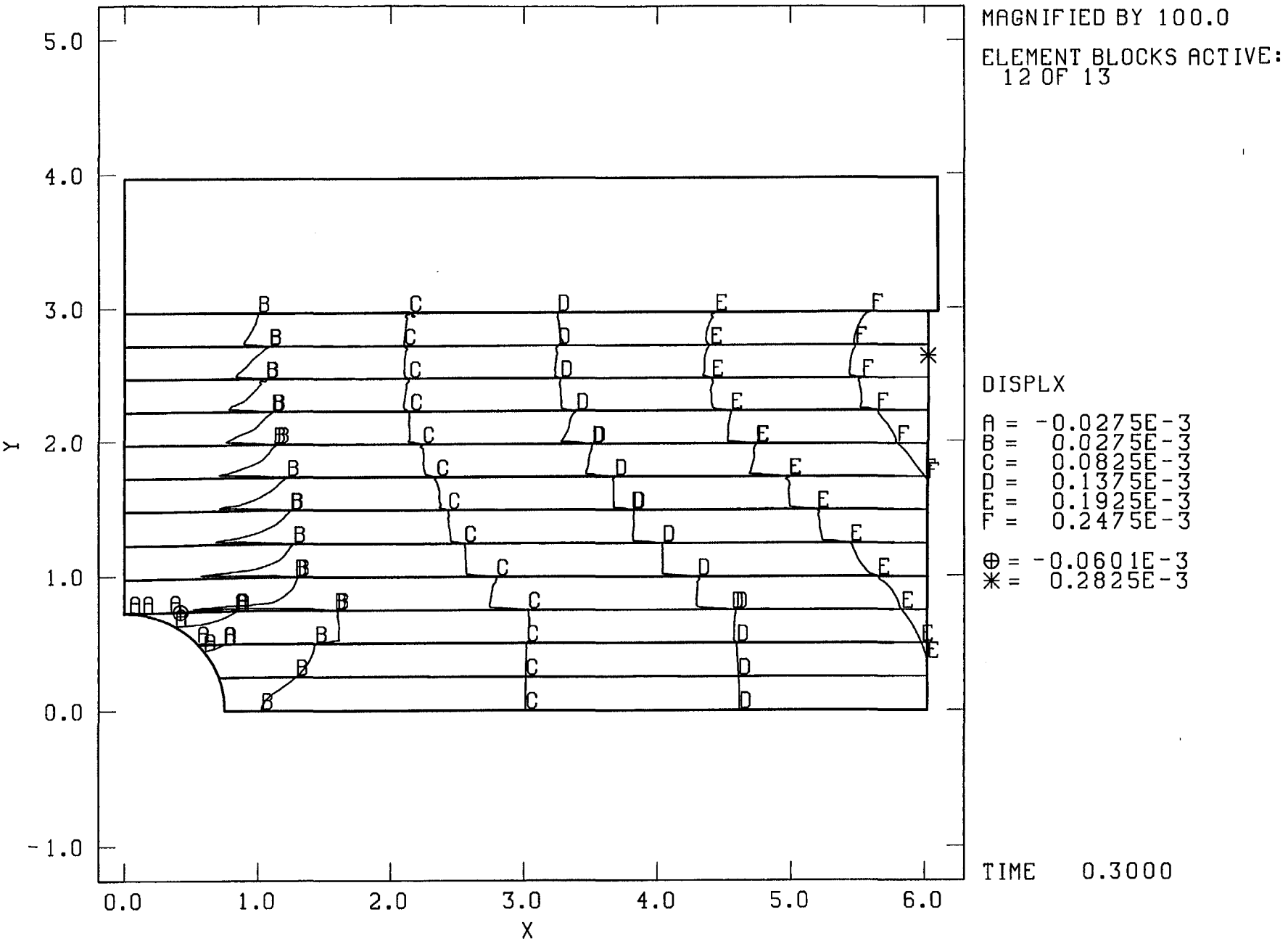

Figure 35: Horizontal Displacement Contours from the JAC2D Lexan Plate Model at 0.30 MPa Load
(all units in inches)

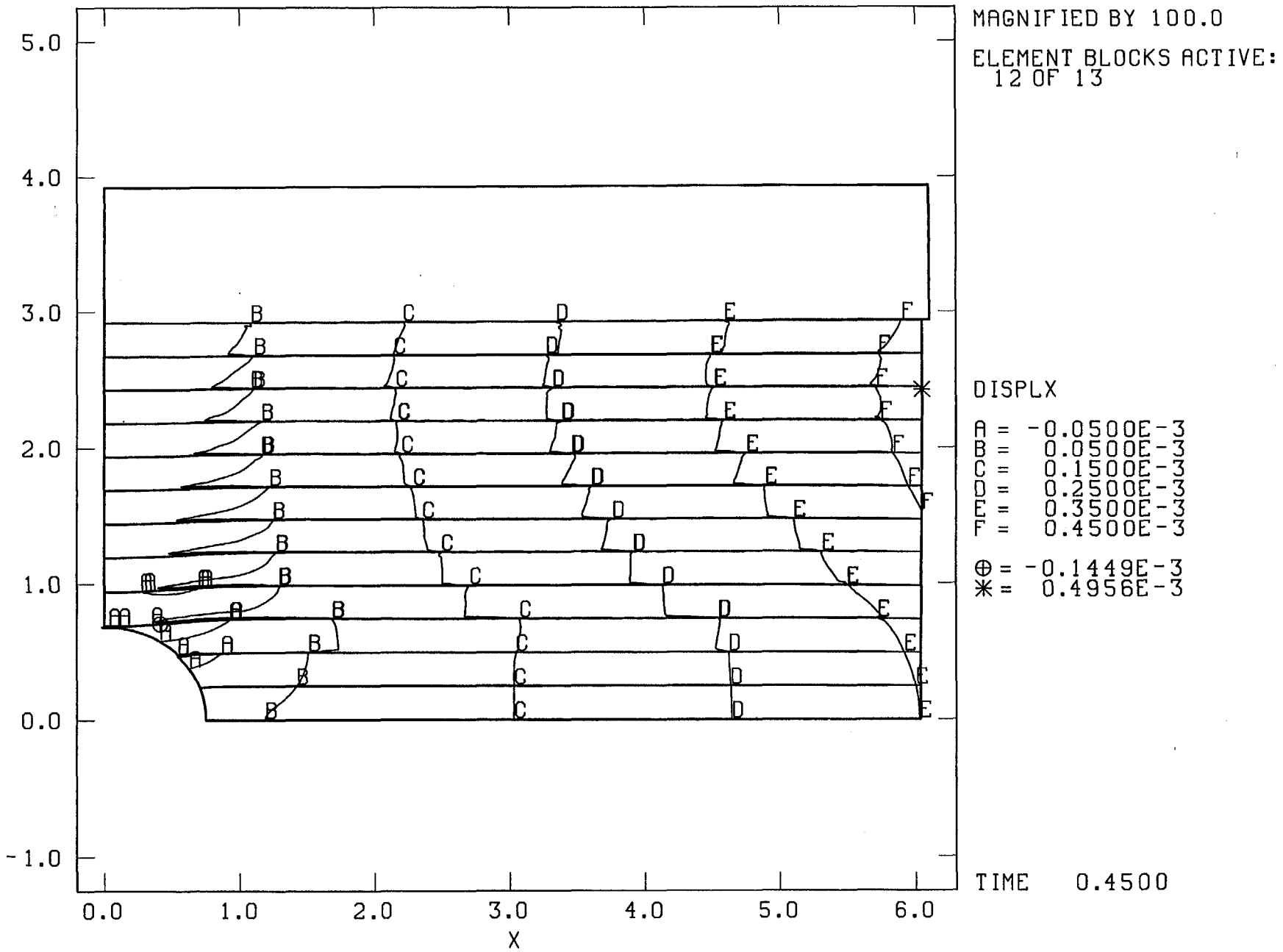

Figure 36: Horizontal Displacement Contours from the JAC2D Lexan Plate Model at 0.45 MPa Load
(all units in inches)

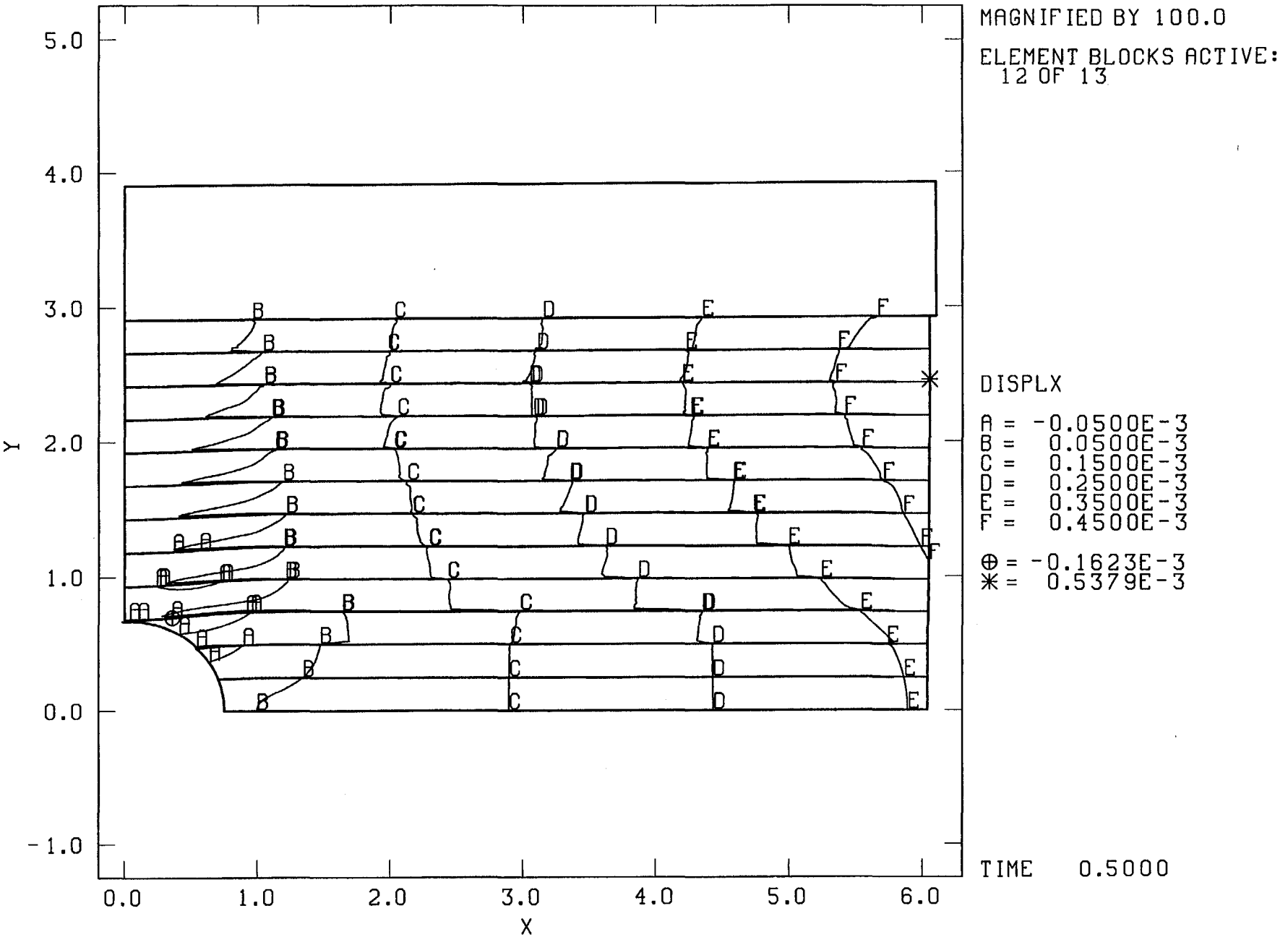

Figure 37: Horizontal Displacement Contours from the JAC2D Lexan Plate Model at 0.50 MPa Load
(all units in inches)

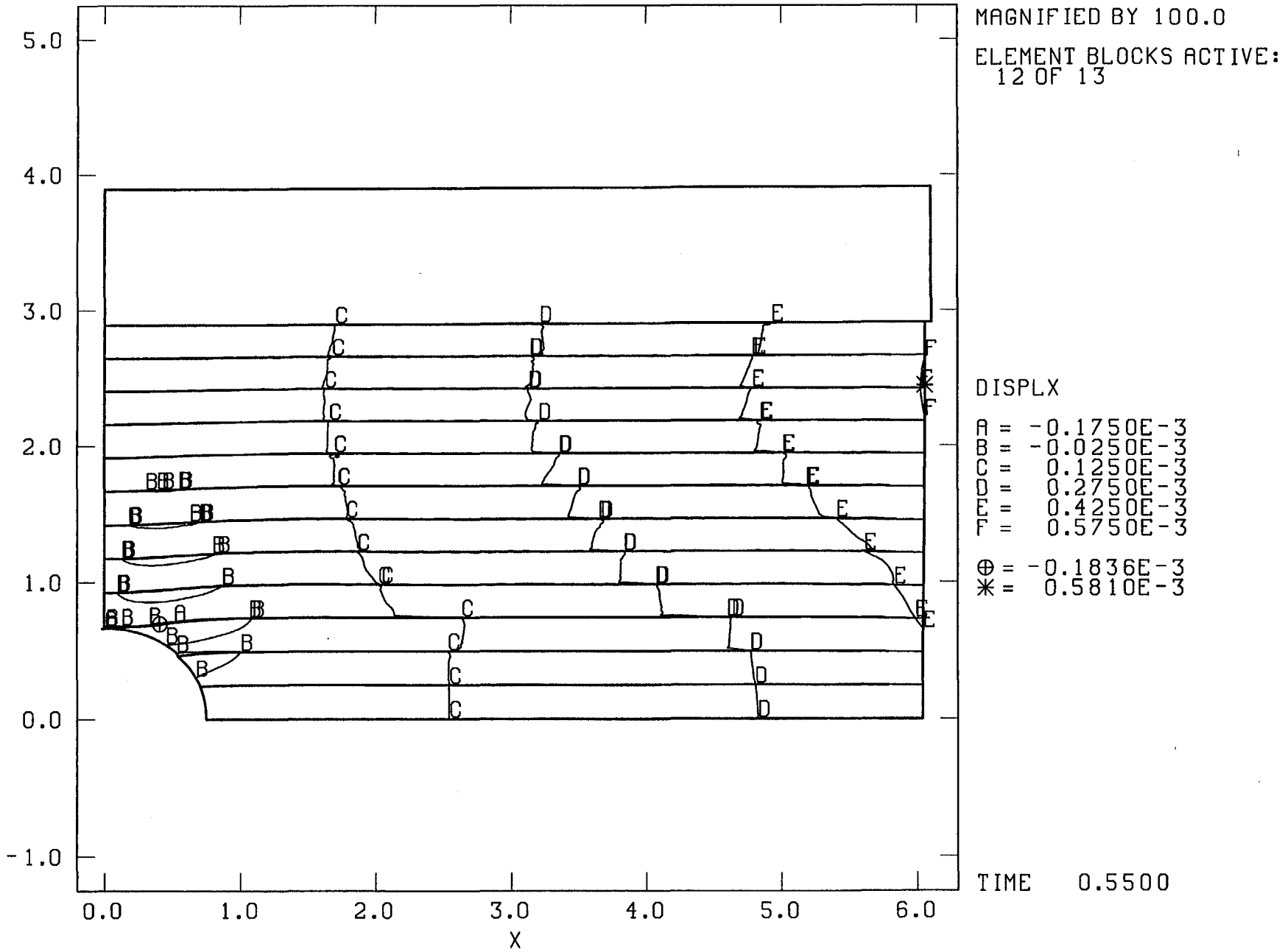

Figure 38: Horizontal Displacement Contours from the JAC2D Lexan Plate Model at 0.55 MPa Load
(all units in inches)

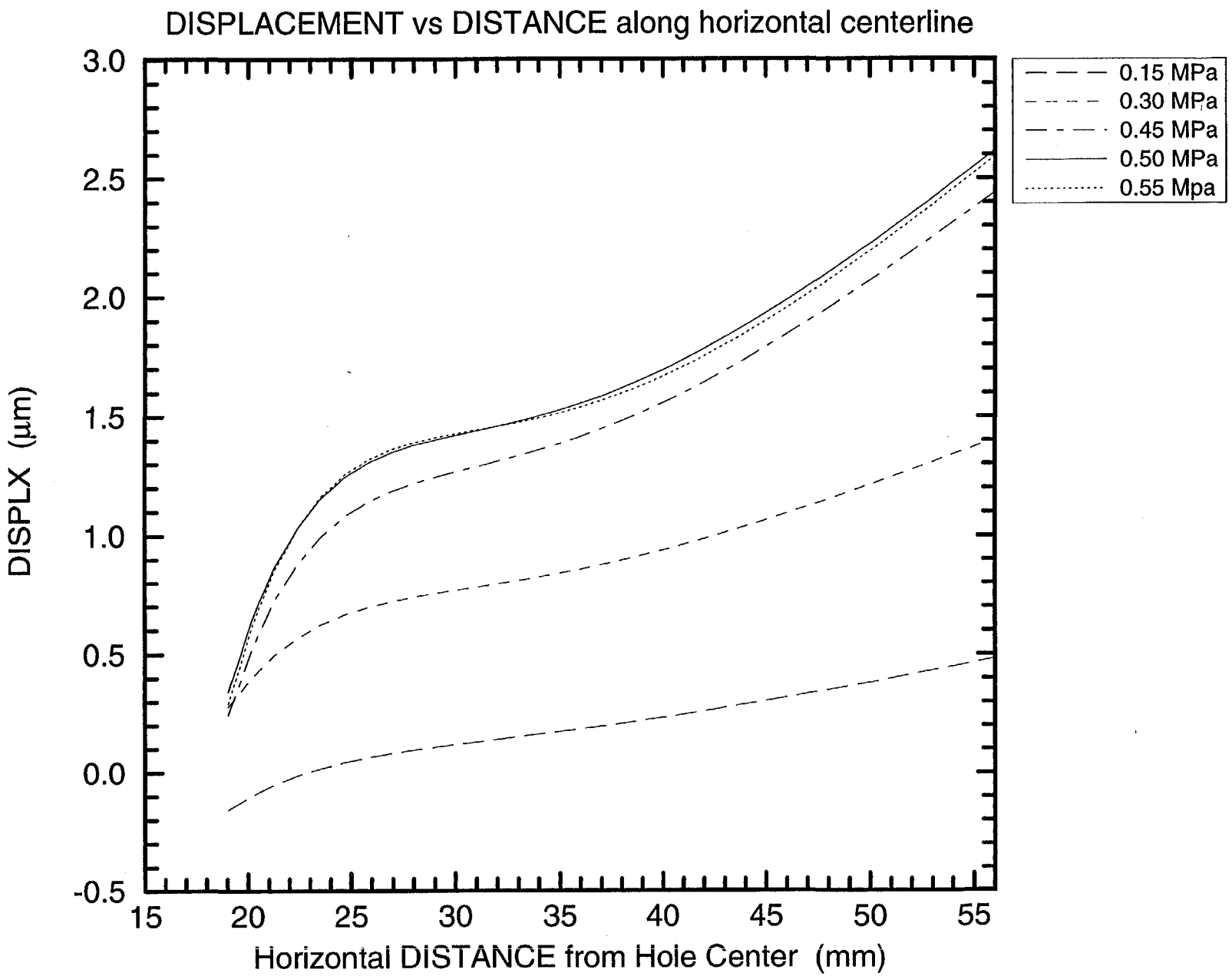

Figure 39: Displacements Along Horizontal Centerline of the JAC2D Lexan Plate Model

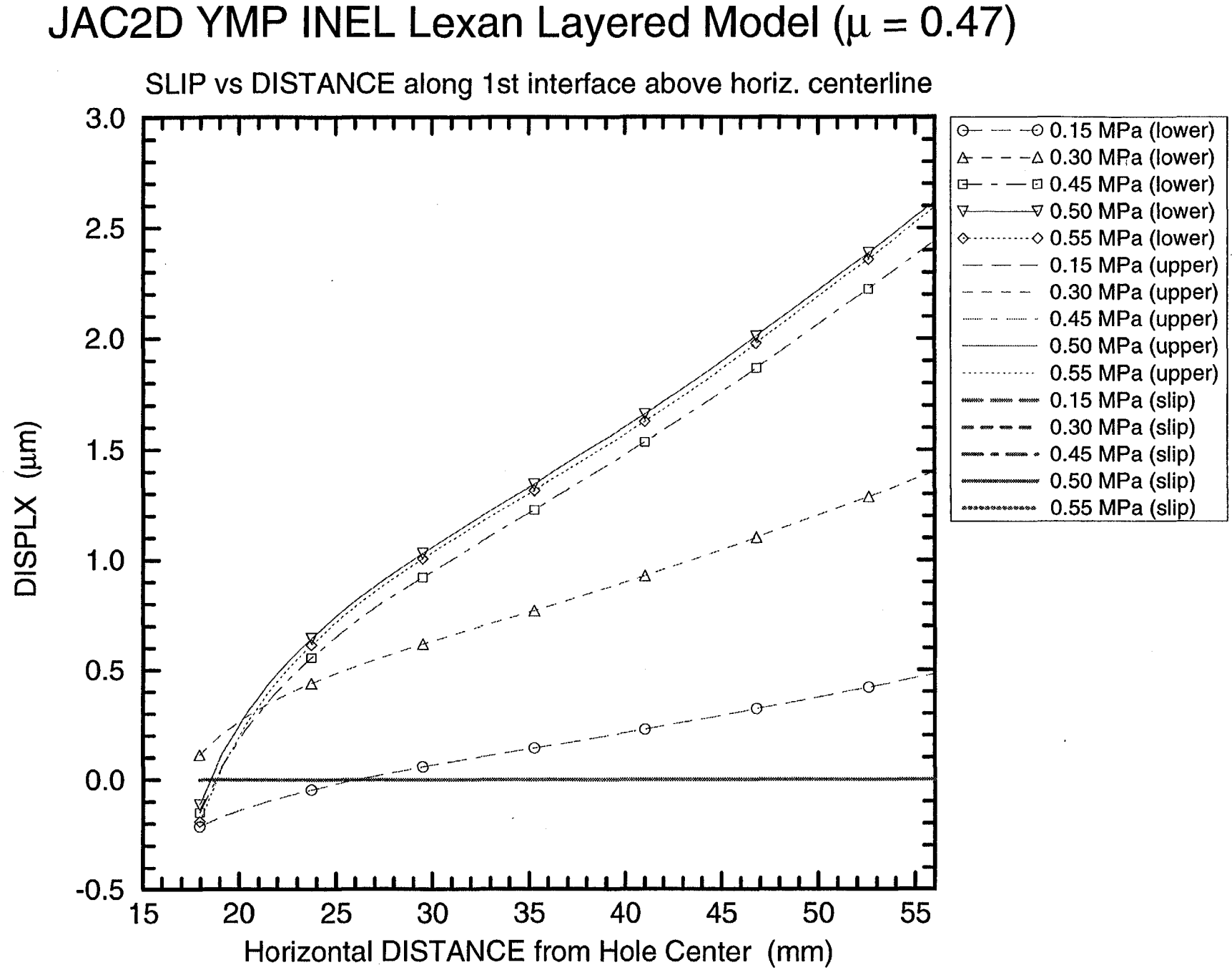

Figure 40: Displacements and Slip Along First Plate Interface above the Horizontal Centerline of the JAC2D Lexan Plate Model

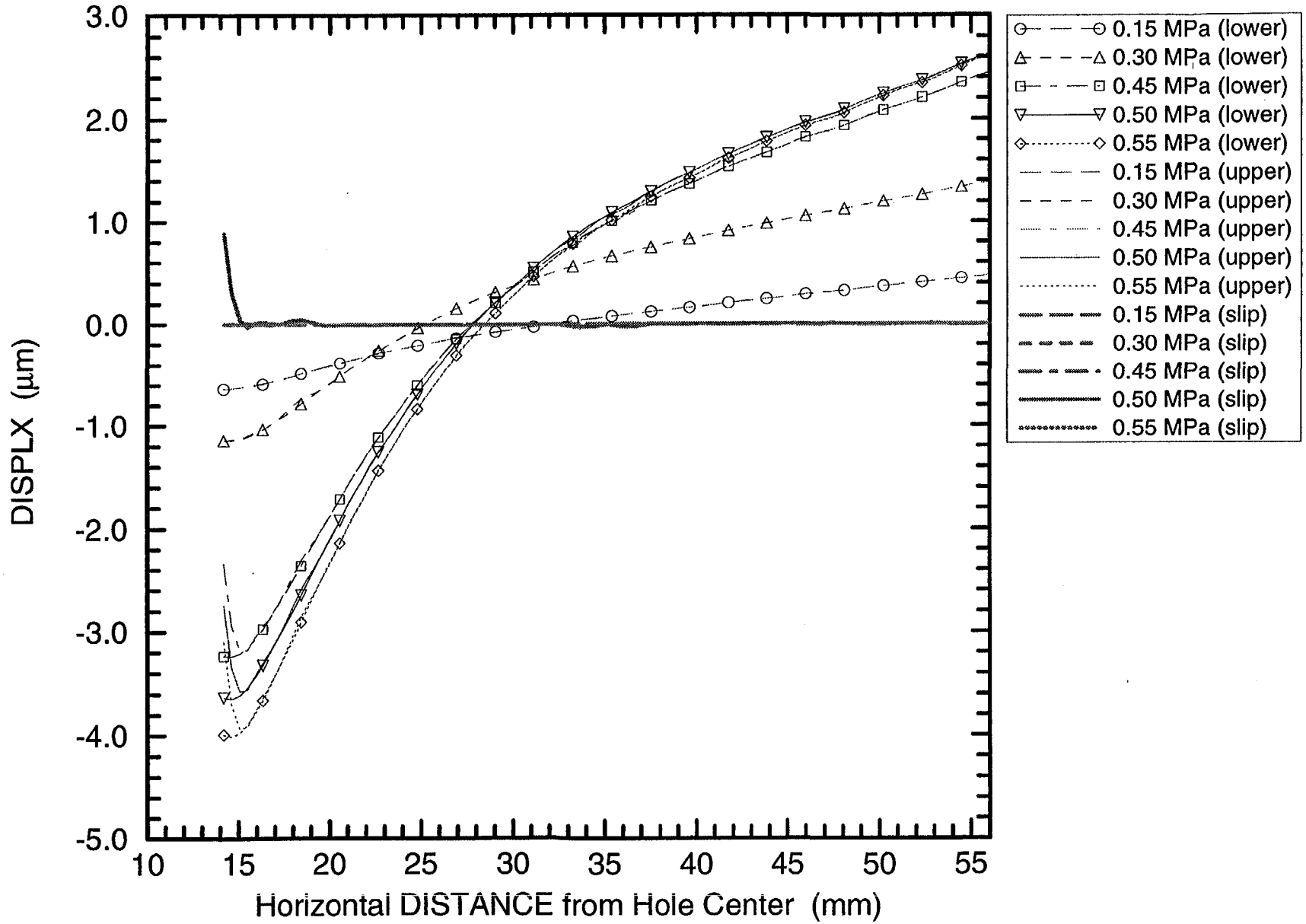

Figure 41: Displacements and Slip Along Second Plate Interface above the Horizontal Centerline of the JAC2D Lexan Plate Model

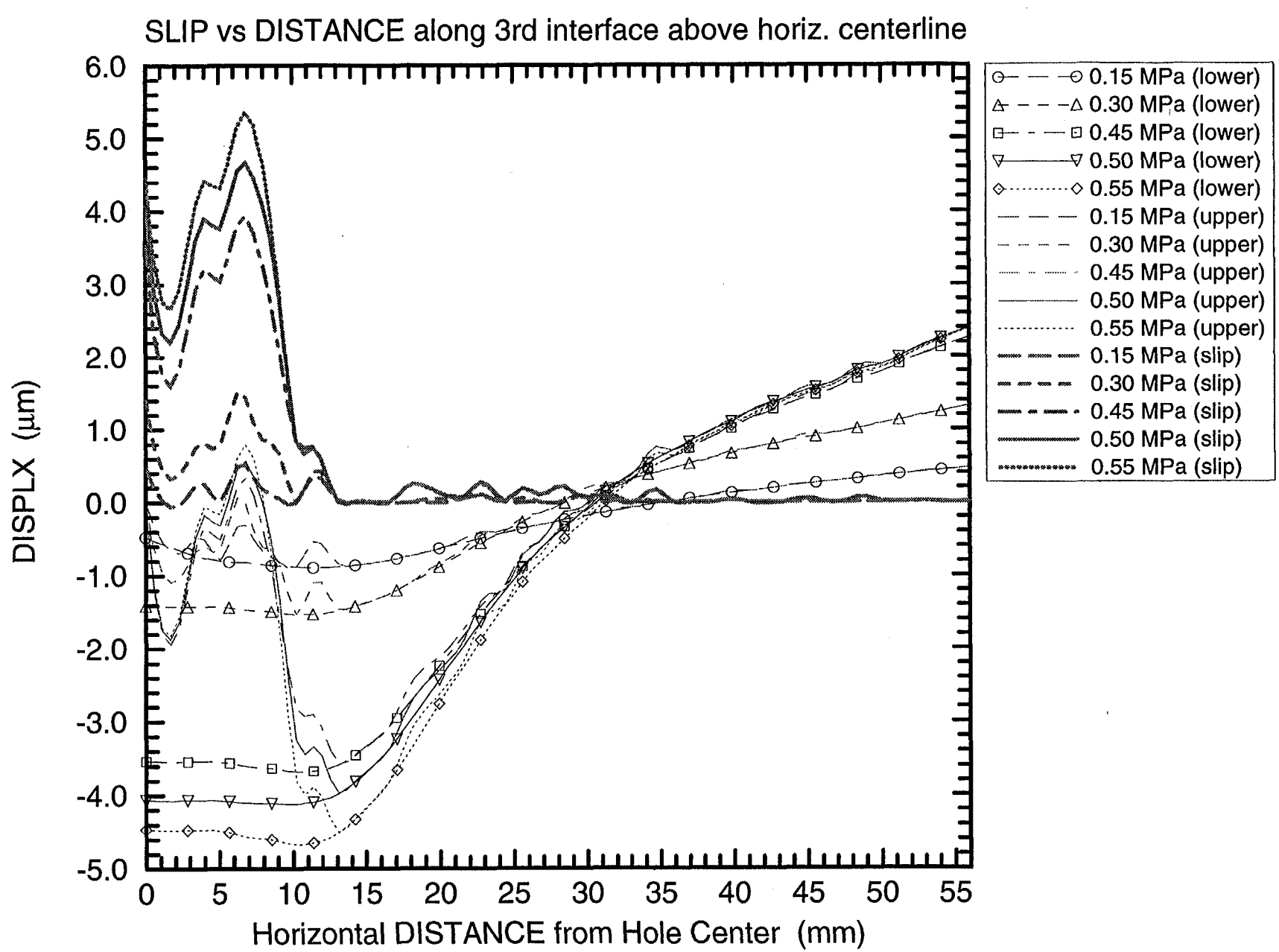

Figure 42: Displacements and Slip Along Third Plate Interface above the Horizontal Centerline of the JAC2D Lexan Plate Model

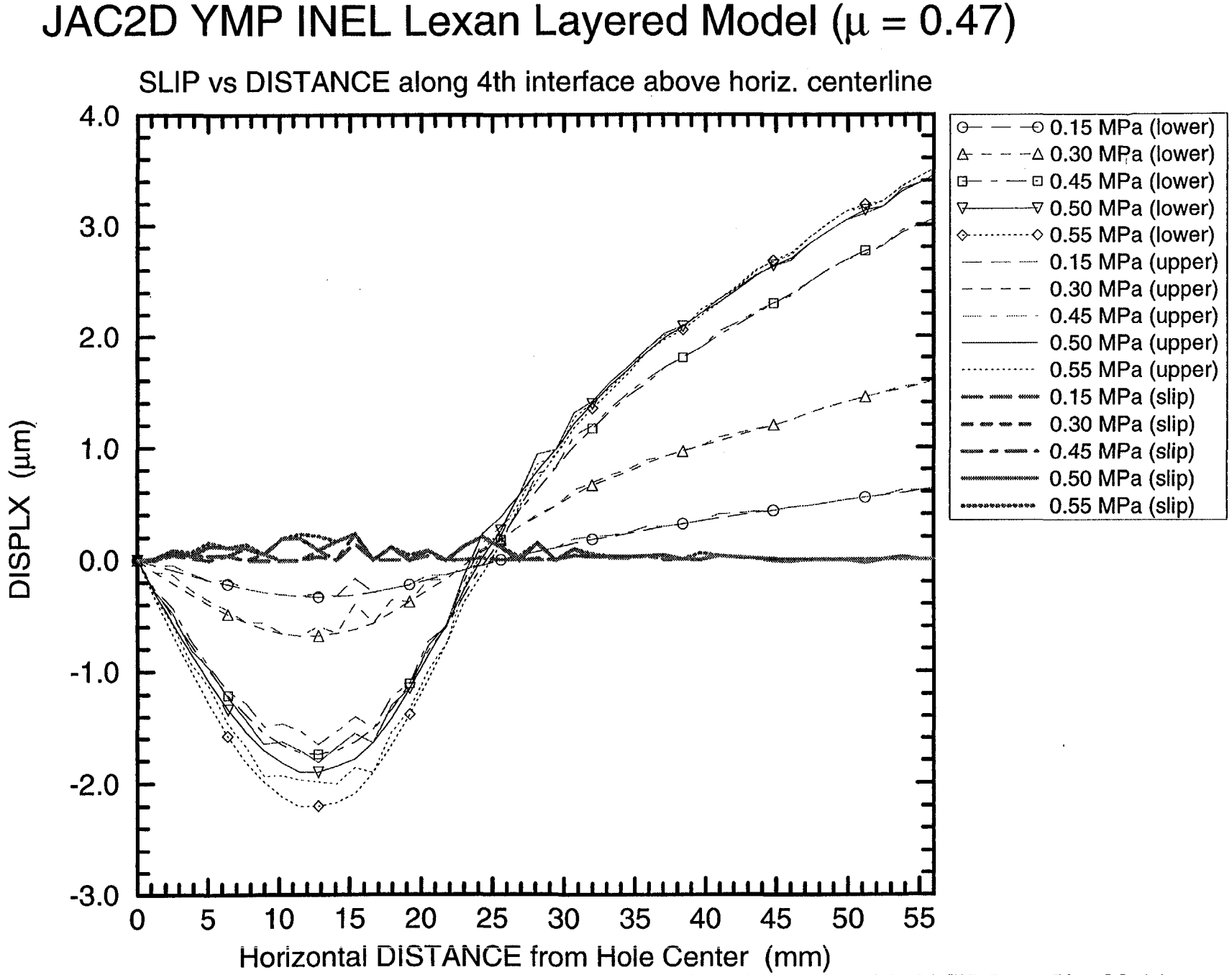

Figure 43: Displacements and Slip Along Fourth Plate Interface above the Horizontal Centerline of the JAC2D Lexan Plate Model

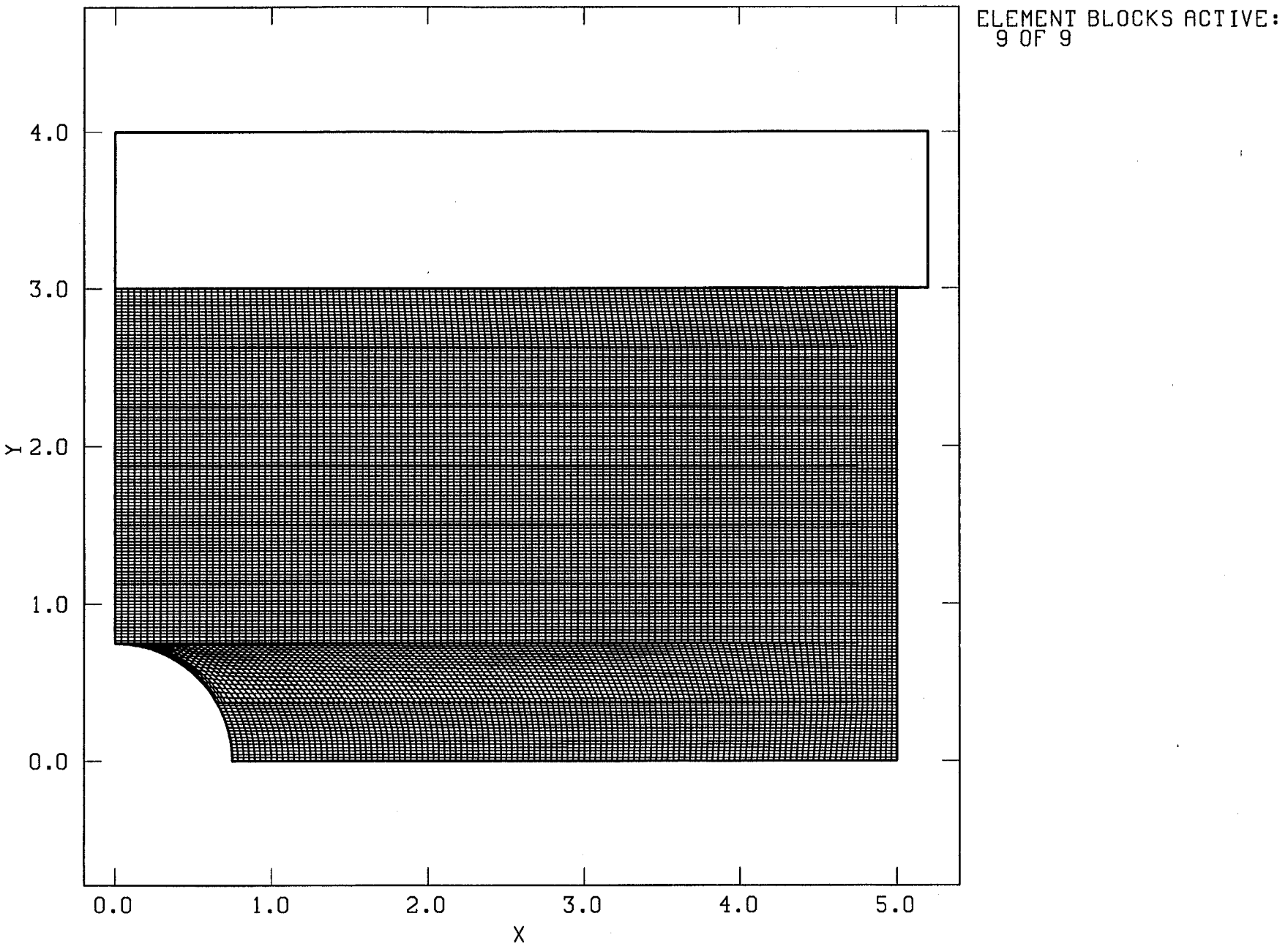

Figure 44: Undeformed Mesh for the JAC2D Granite Plate Model
(all units in inches)

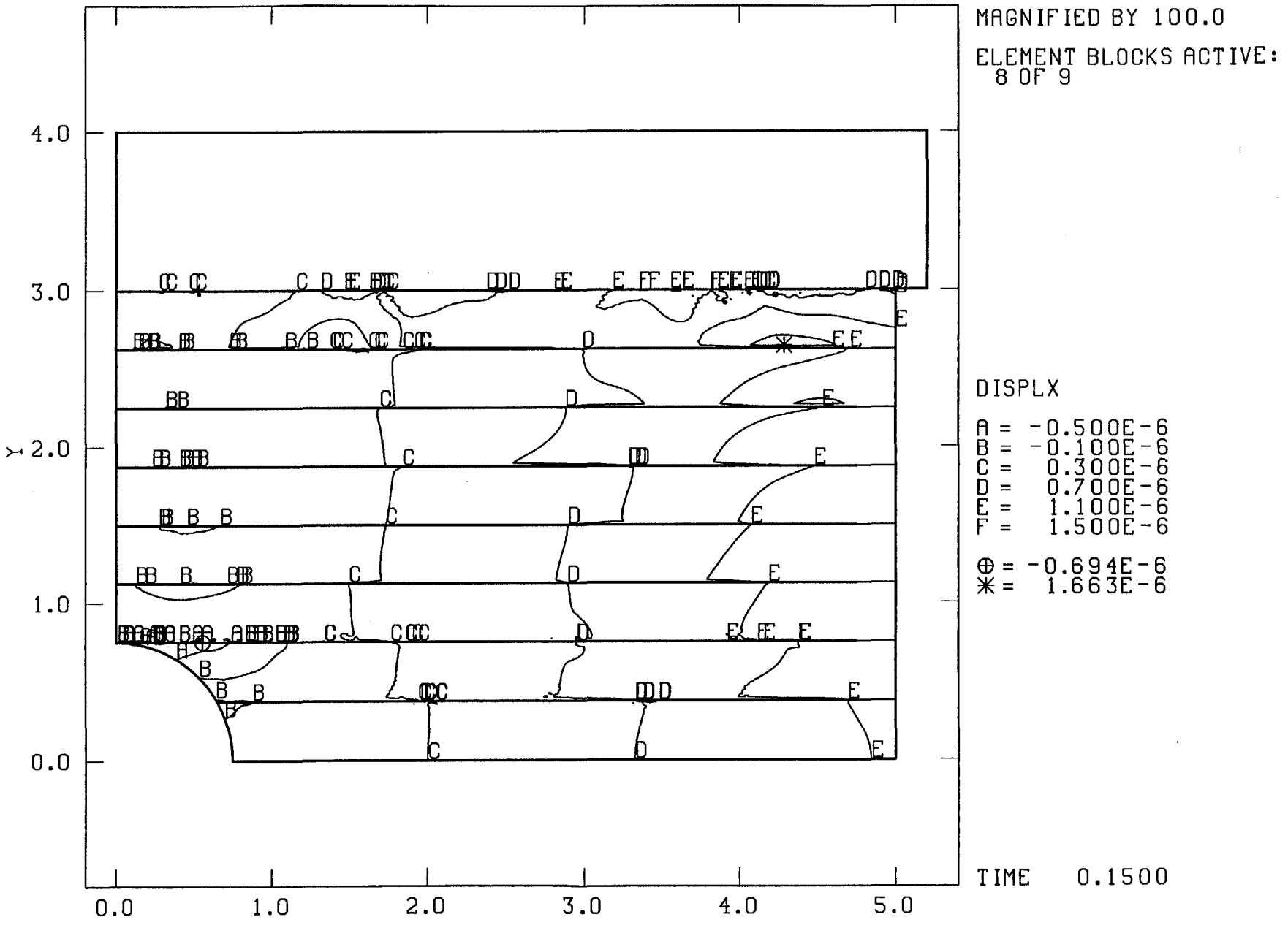

Figure 45: Horizontal Displacement Contours from the JAC2D Granite Plate Model at 0.15 MPa Load (all units in inches)

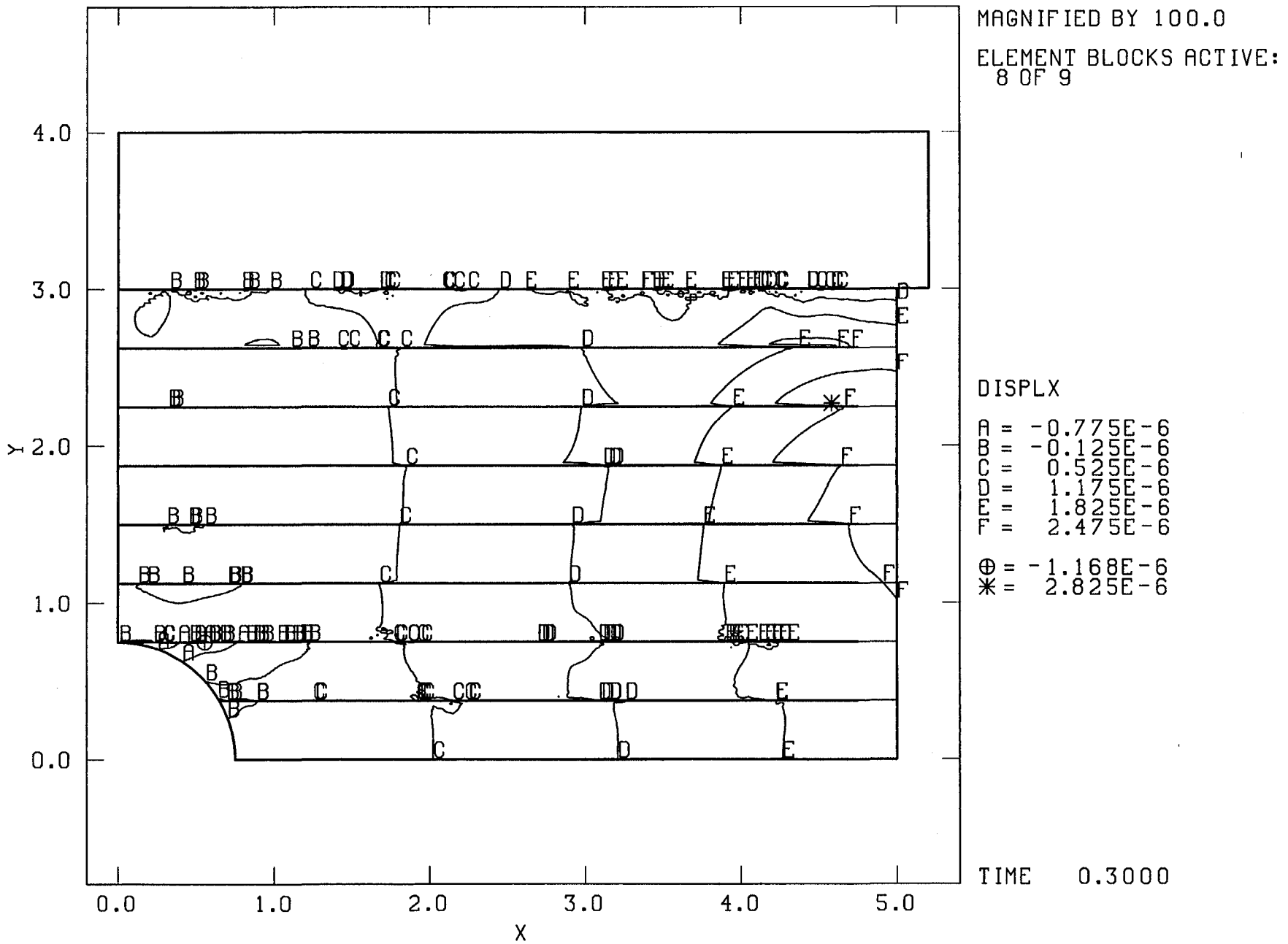

Figure 46: Horizontal Displacement Contours from the JAC2D Granite Plate Model at 0.30 MPa Load
(all units in inches)

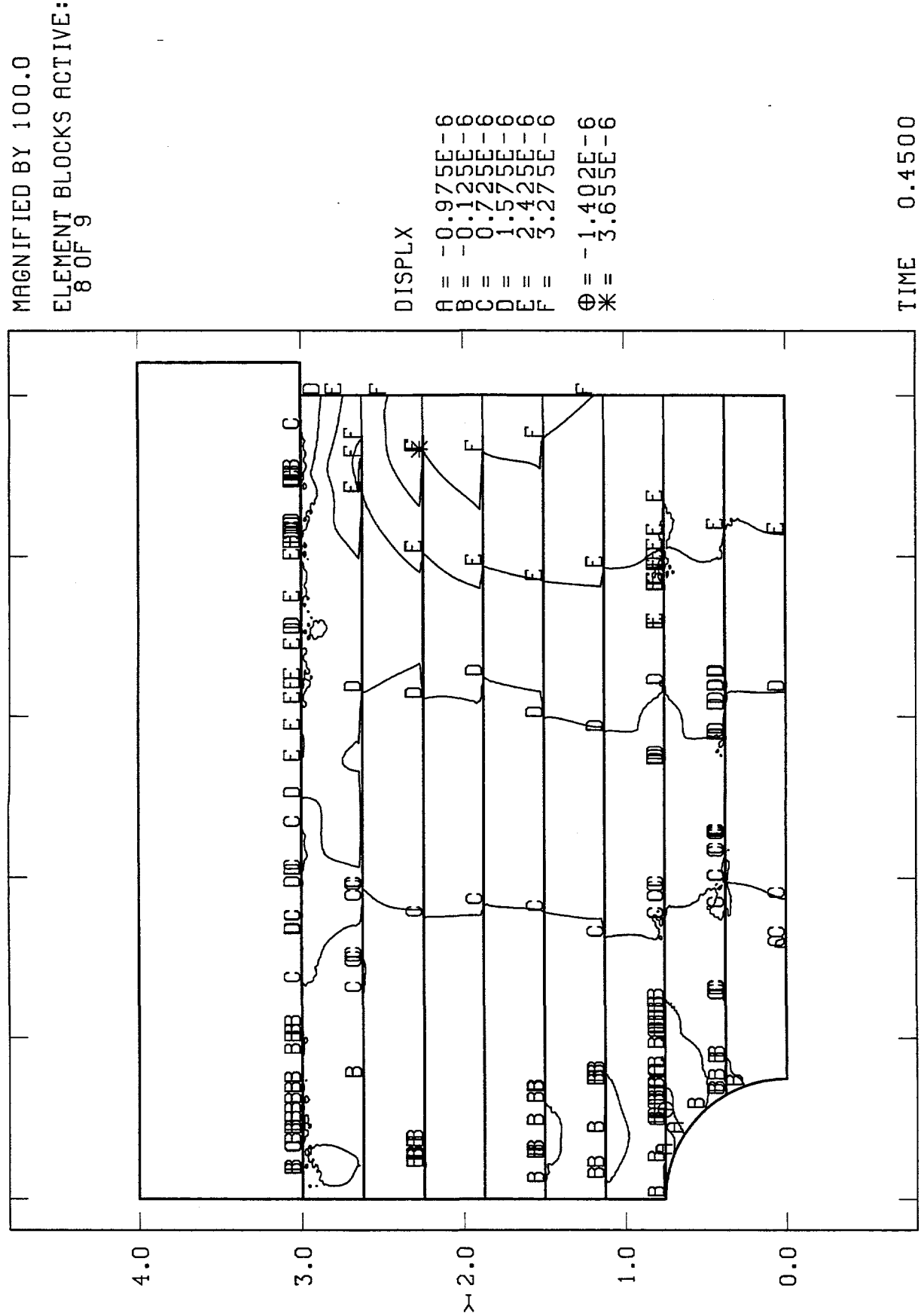

Figure 47: Horizontal Displacement Contours from the JAC2D Granite Plate Model at 0.45 MPa Load
(all units in inches)

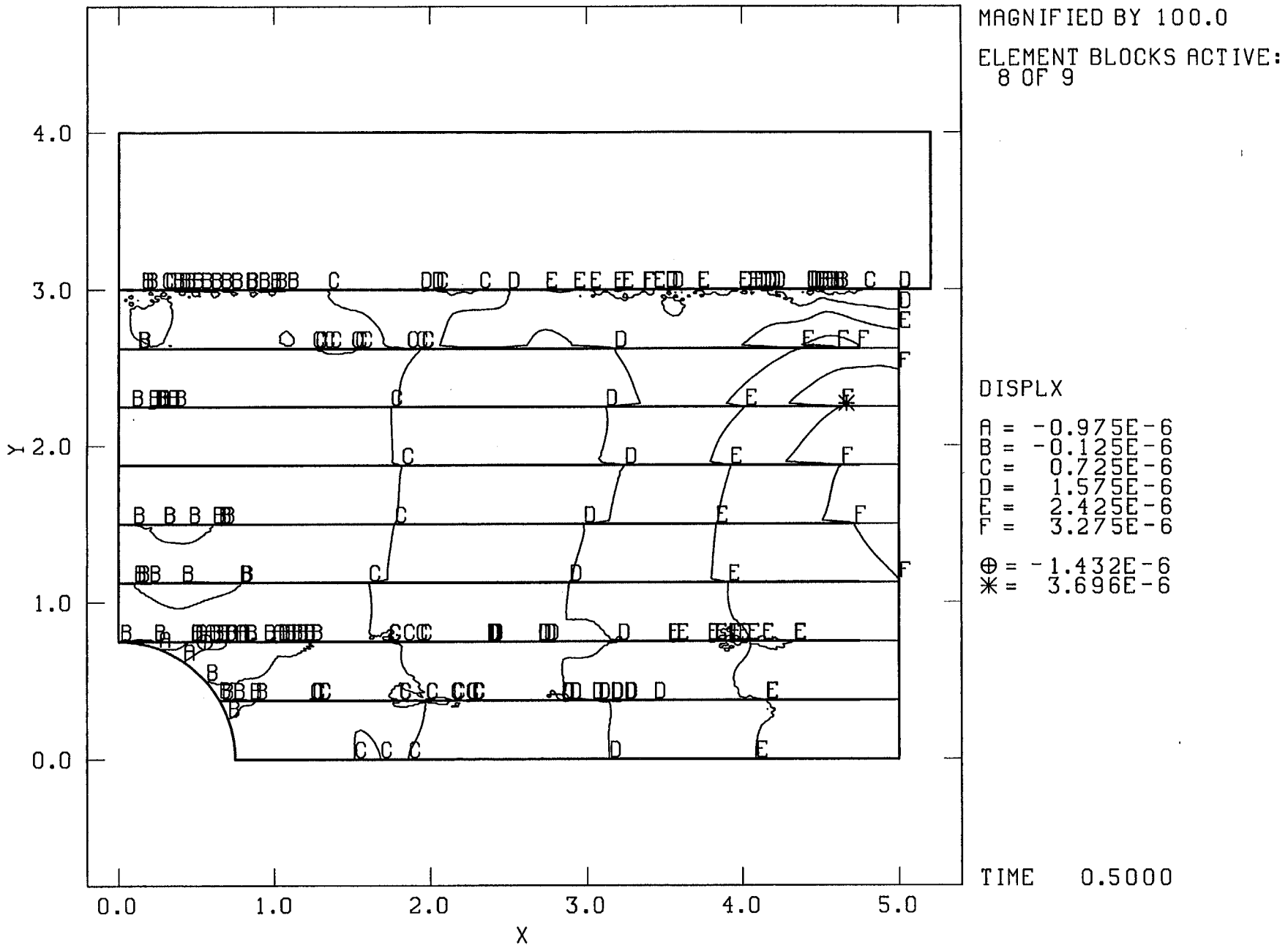

Figure 48: Horizontal Displacement Contours from the JAC2D Granite Plate Model at 0.50 MPa Load
(all units in inches)

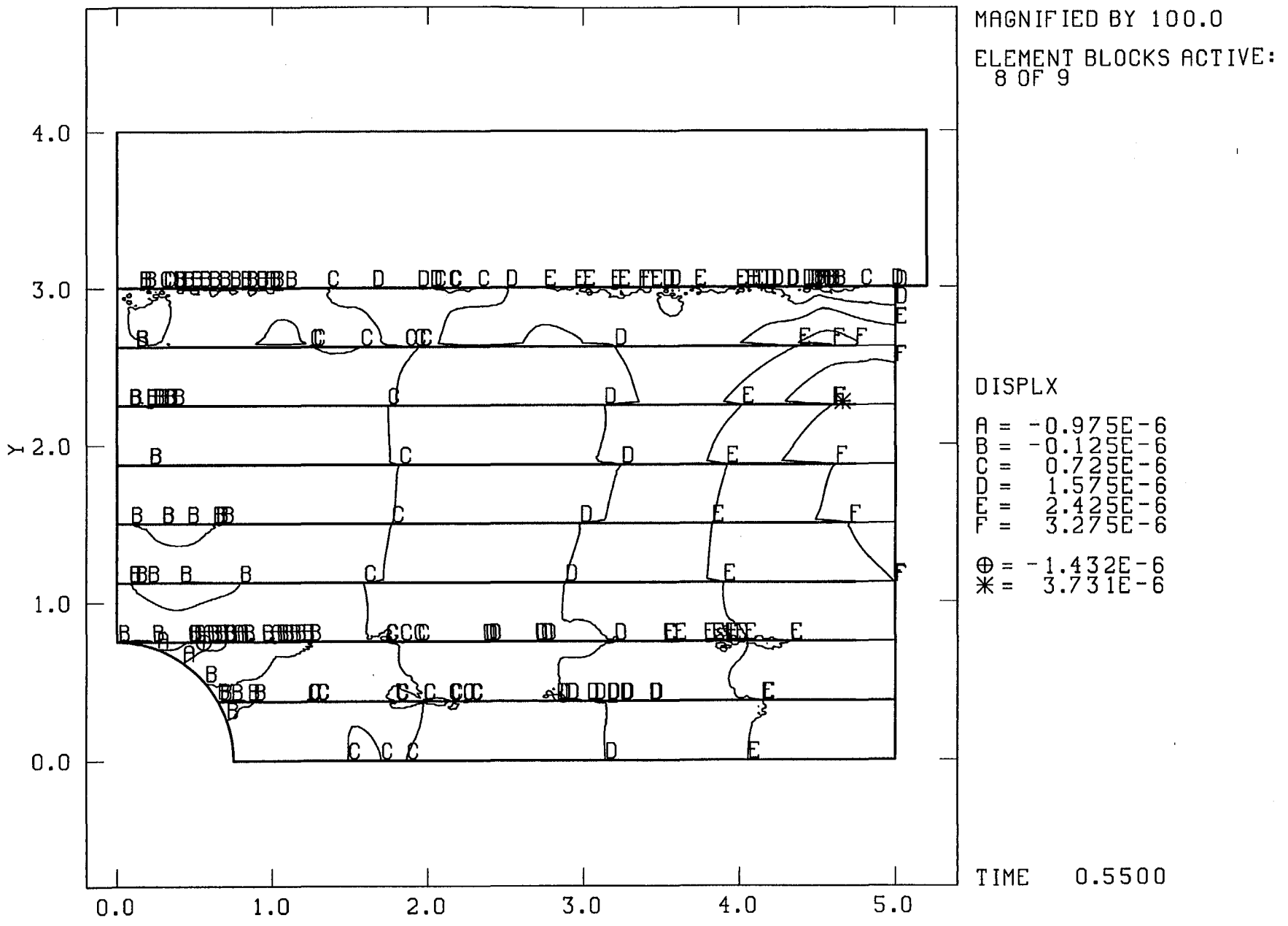

Figure 49: Horizontal Displacement Contours from the JAC2D Granite Plate Model at 0.55 MPa Load
(all units in inches)

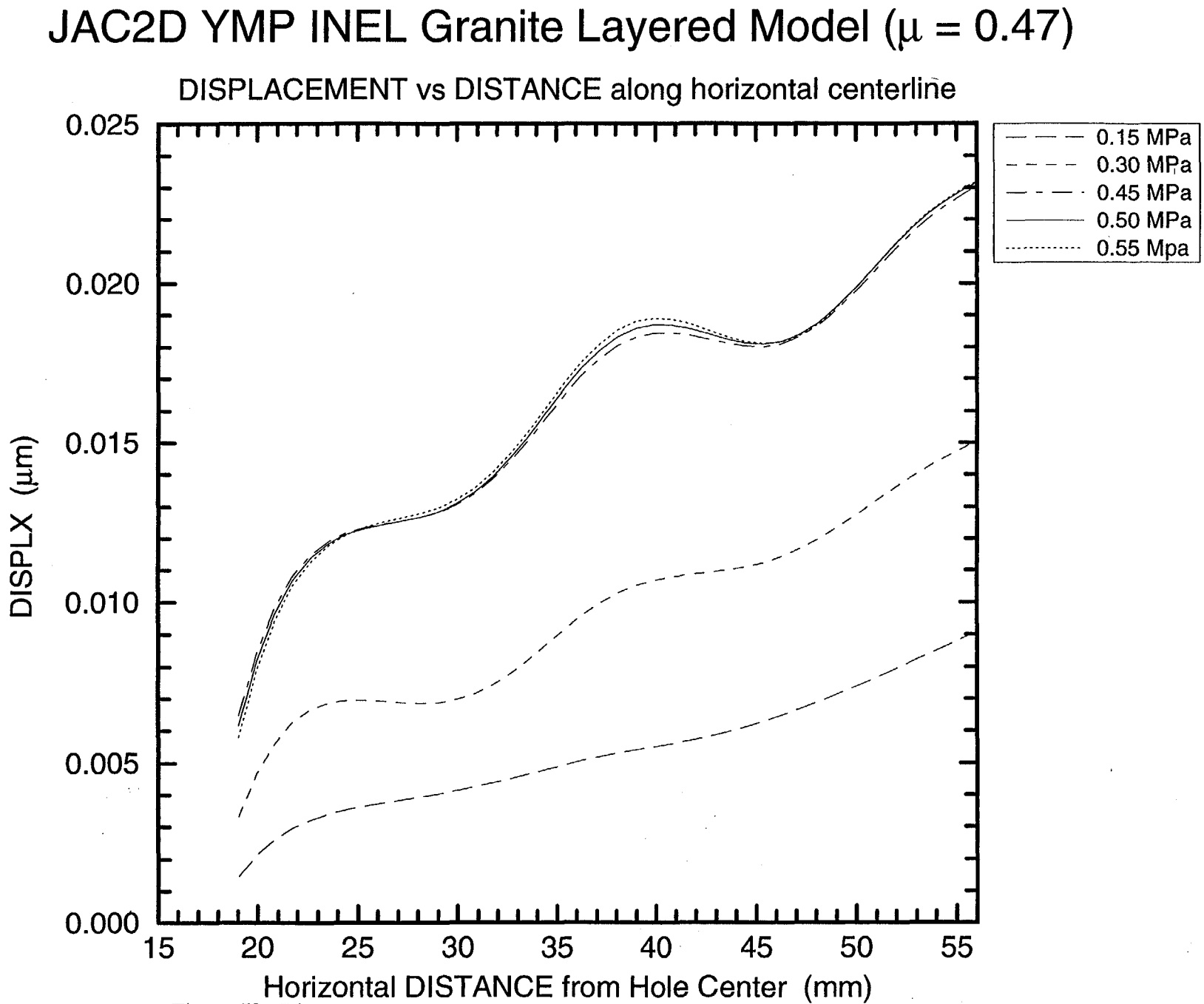

Figure 50: Displacements Along Horizontal Centerline of the JAC2D Granite Plate Model

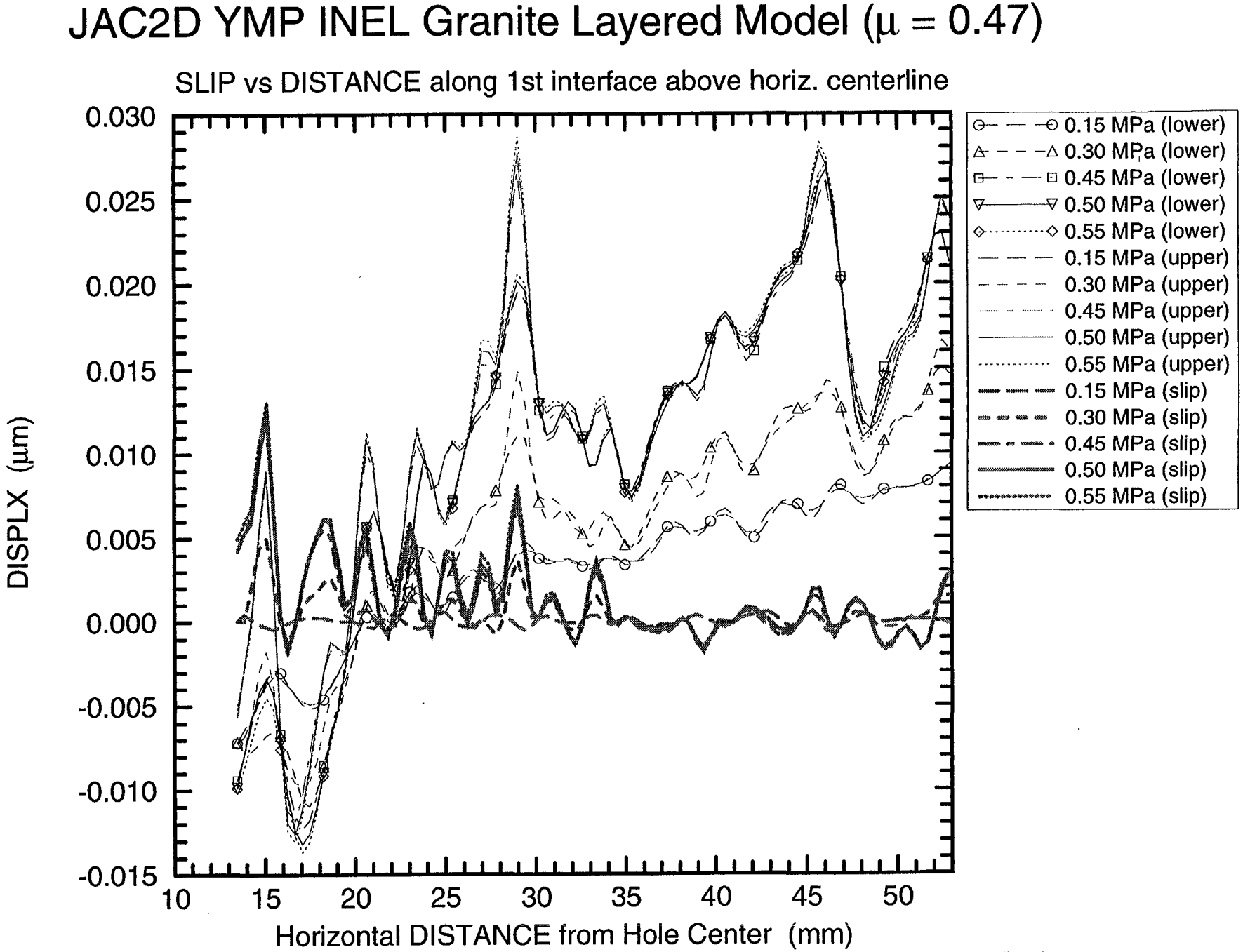

Figure 51: Displacements and Slip Along First Plate Interface above the Horizontal Centerline of the JAC2D Granite Plate Model

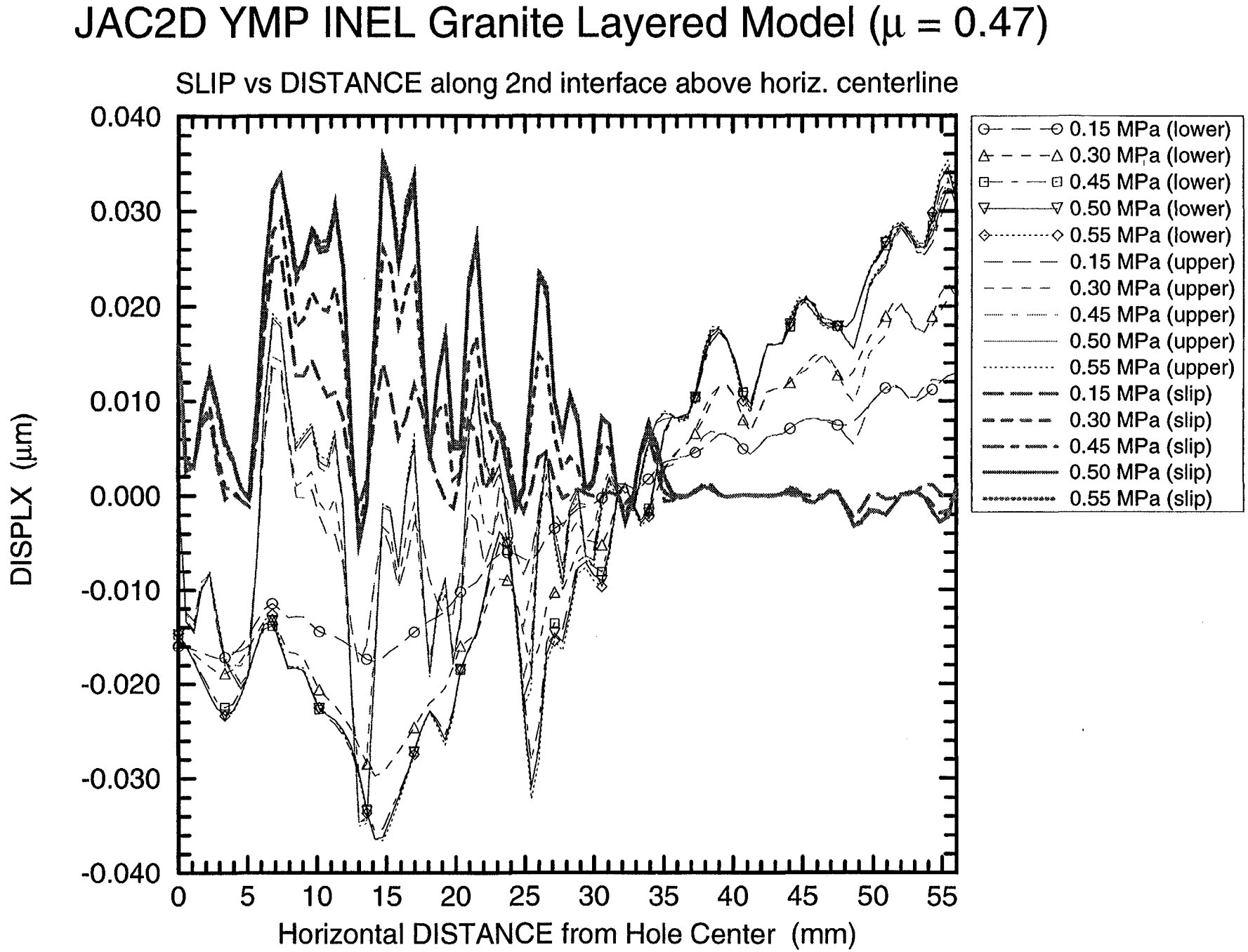

Figure 52: Displacements and Slip Along Second Plate Interface above the Horizontal Centerline of the JAC2D Granite Plate Model

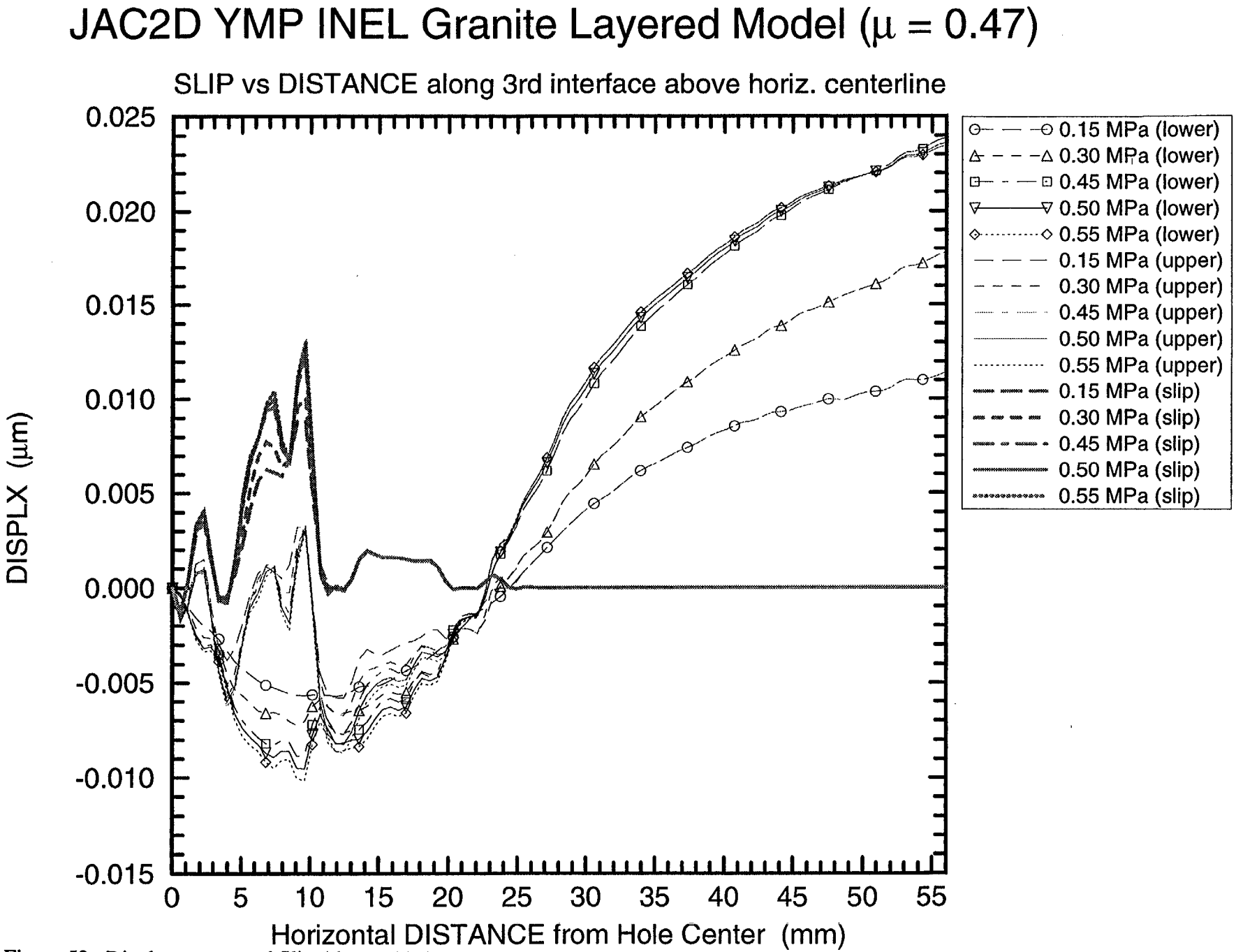

Figure 53: Displacements and Slip Along Third Plate Interface above the Horizontal Centerline of the JAC2D Granite Plate Model

5.0 Calculations Using JAS3D

A three-dimensional model of the Lexan plate experiment was created for use with the JAS3D code (Blanford, in preparation; see footnote 1). JAS3D is the algorithmic successor to the JAC2D and JAC3D codes and uses much of the same logic as the earlier codes, as well as incorporating new capabilities and enhancements. The initial validation calculations modeling the Lexan plate experiment were designed such that comparable results would be obtained with models as similar as possible for JAC2D and JAS3D. For the Lexan experiment calculations only the elastic material model in JAS3D was used; this is the same model which was implemented in JAC2D. The conjugate gradient solution method was used (also the same as for JAC2D). JAS3D is a code still under development and thus many of the capabilities of JAS3D were not exercised in these calculations. The dynamic relaxation method was not utilized because of indications that the run time for this sort of problem would be excessive. The compliant joint model was not appropriate for this work because there was no way to output joint slippage values versus distance results.

The three-dimensional Lexan plate model was deliberately created to be as similar as possible to the two-dimensional JAC2D model in order to compare directly the results from the two codes. The material properties used for Lexan in the JAC2D simulations were employed in the JAS3D simulations. The same contact surface representation of joint behavior used in JAC2D was used in JAS3D, as well as the same values for friction coefficient. The mesh for the JAS3D model is shown in Figure 54. As stated in Chapter 4, the mesh in Figure 54 and the JAS3D calculations were done in English units; the displacements and slips were then converted to SI units for comparison with the other experiment and numerical results.

The three-dimensional model was defined as tri-symmetric, representing one-eighth of the actual geometry. Symmetry planes were assumed to exist passing both horizontally and vertically across the center of the hole, as well as on one of the two model surfaces which the hole passes through (which will be referred to as the "back" surface; the "front" surface was unconstrained). As before, the outer one-quarter inch (6.35 mm) of the plate surfaces were generated with uninterrupted connectivity in order to simulate the glue holding the plates together. The mesh was somewhat coarser than the equivalent two-dimensional one due to the necessity of adding layers of elements to create depth in the third dimension, and consisted of 59,425 elements, 75,689 nodes, 13 material blocks, and 12 sliding interfaces. There were 7,428 eight-node, six-sided (brick) elements in each of the eight equally-sized element layers across the depth of the model.

Horizontal displacement contour plots at load levels of 0.15, 0.30, 0.45, 0.50, and 0.55 MPa, respectively, are shown in Figures 55 through 59, for the front (visible) face of the model. Comparable plots for the (hidden) back face of the model, which was constrained to in-plane displacements only due to the symmetry assumption and represents physically the middle vertical surface of each plate, are shown in Figures 65 through 69. The back face results are shown because they include the least influence from unconstrained edge effects and thus should provide the closest comparison to results from the plane strain assumption-based two-dimensional calculations. The overall magnitude of horizontal displacement achieved in the JAS3D Lexan model was about the same as for the JAC2D model, although with somewhat

different characteristics. At the higher load increments, for instance, the contour lines of equal displacement magnitude are oriented at an angle running diagonally from the hole upwards toward the outside end of the platen, whereas in the two-dimensional model the plotted contours are much more vertical in orientation. (Although at lower load levels, 0.30 MPa or less, the 3-D and 2-D plots are much more alike, with both showing the more vertical contour lines.) The area of inward horizontal displacement extends outward farther from the hole than it did in the JAC2D model, especially in the uppermost plates closest to the platen.

Slippage between plates of the JAS3D Lexan model is illustrated in Figures 60 through 64 for the front face plate edges and in Figures 70 through 74 for the back face. At first glance there appears to be widespread albeit small magnitude slippage occurring along each of the four plate interfaces above the horizontal midplane. However, this may be mostly a result of numerical "noise" due to the mesh coarseness and insufficient tightening of the code tolerance (residual force imbalance) values. In all but one case, slippage of less than a micron is indicated from this calculation. The most consistently indicated slippage occurs at the front face in the second plate interface above the horizontal midplane. The largest amount of slippage, almost two microns, occurs near the hole at the back face edge of the plate interface one plate above the horizontal midplane (the bottom of the model).

JAS3D required approximately 2.8 CPU-hours on SNL's Cray Y-MP computer running under Unicos 7.0. A comparison with the run times reported in Chapter 4 shows that JAC2D took a lot longer than JAS3D (20-35 CPU-hours for JAC2D versus 2.8 CPU-hours for JAS3D). This significant difference in run time occurred primarily because the Cray is a much faster machine than the HP9000 by over an order of magnitude. JAS3D could not be run on the HP9000 due to insufficient memory the number of elements used for these calculations. To do a valid comparison of run times for different codes, one must compare the number of equations that each code is solving, which is roughly equal to the number of degrees of freedom in each mesh. A two-dimensional model has three degrees of freedom at unconstrained nodes (x-displacement, y-displacement, and rotation about the z-axis), whereas a three-dimensional model has six degrees of freedom (x-, y-, and z-displacements plus rotations about each axis) for each node without constraining boundary conditions. There are additional equations to solve for any contact conditions at the nodes. The three-dimensional Lexan model had about 75,700 nodes (nearly four times as many nodes as the JAC2D Lexan simulation) and 12 contact surfaces (the same as the JAC2D Lexan simulation but with more nodes on each contact surface even with coarser node spacing because of the third dimension). Therefore, with twice the degrees of freedom and four times the number of nodes, the Lexan calculations performed with JAS3D with the conjugate gradient solver would be expected to run at least eight times longer on the same computer than the JAC2D calculations reported in Chapter 4.

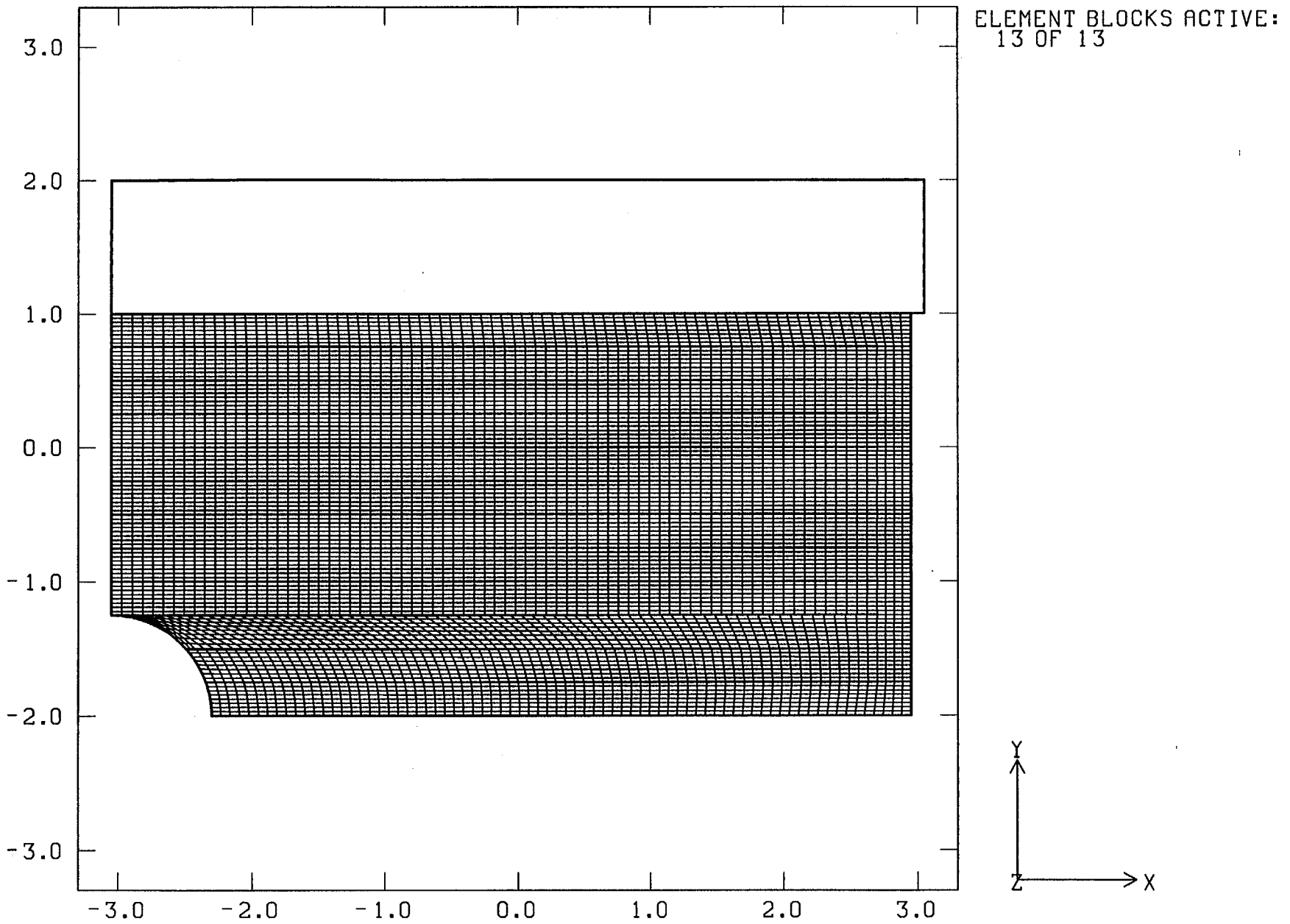

Figure 54: Undeformed Mesh for the JAS3D Lexan Plate Model (front surface of model)

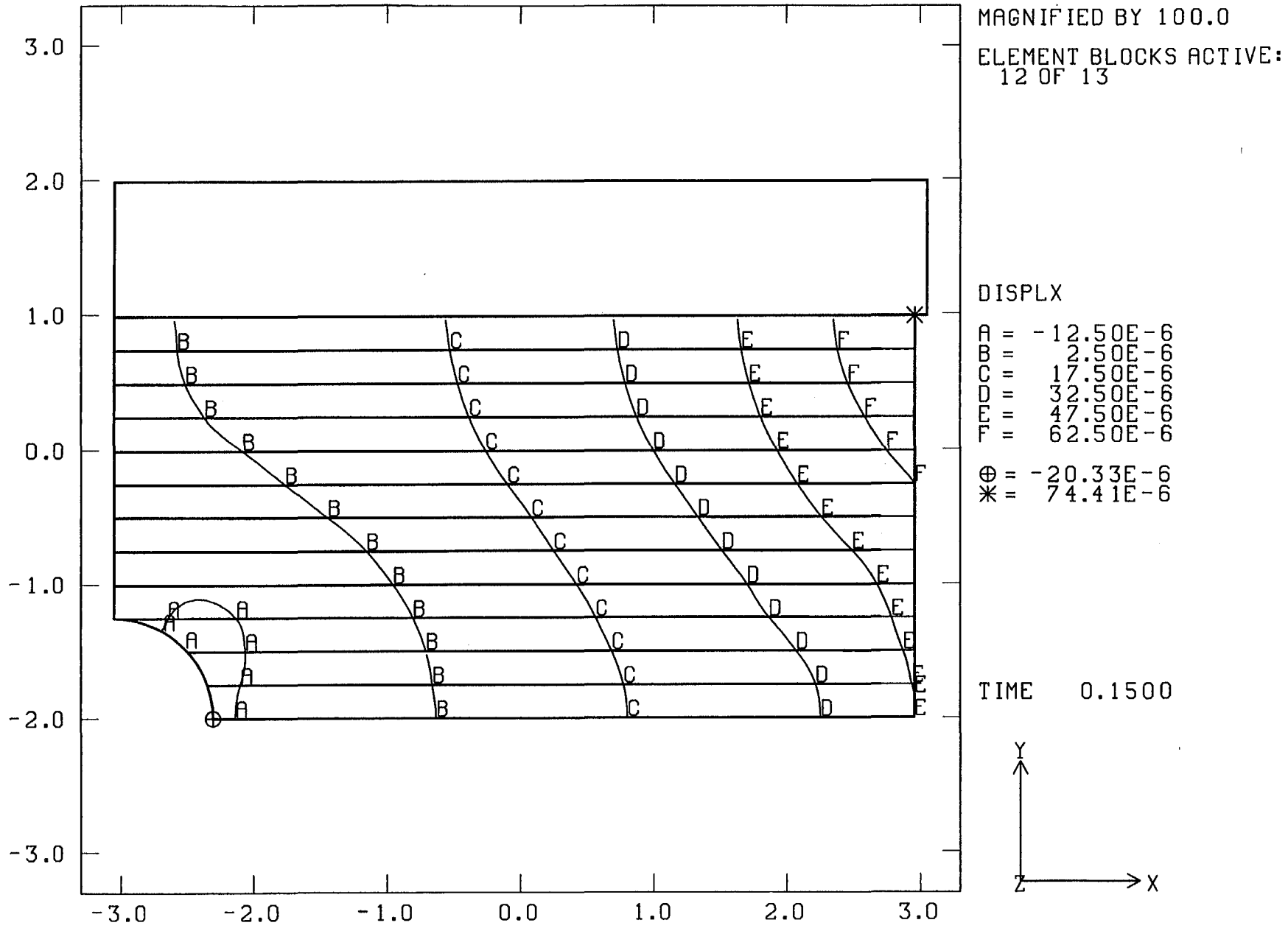

Figure 55: Horizontal Displacement Contours from the JAS3D Lexan Plate Model at 0.15 MPa Load (front surface)

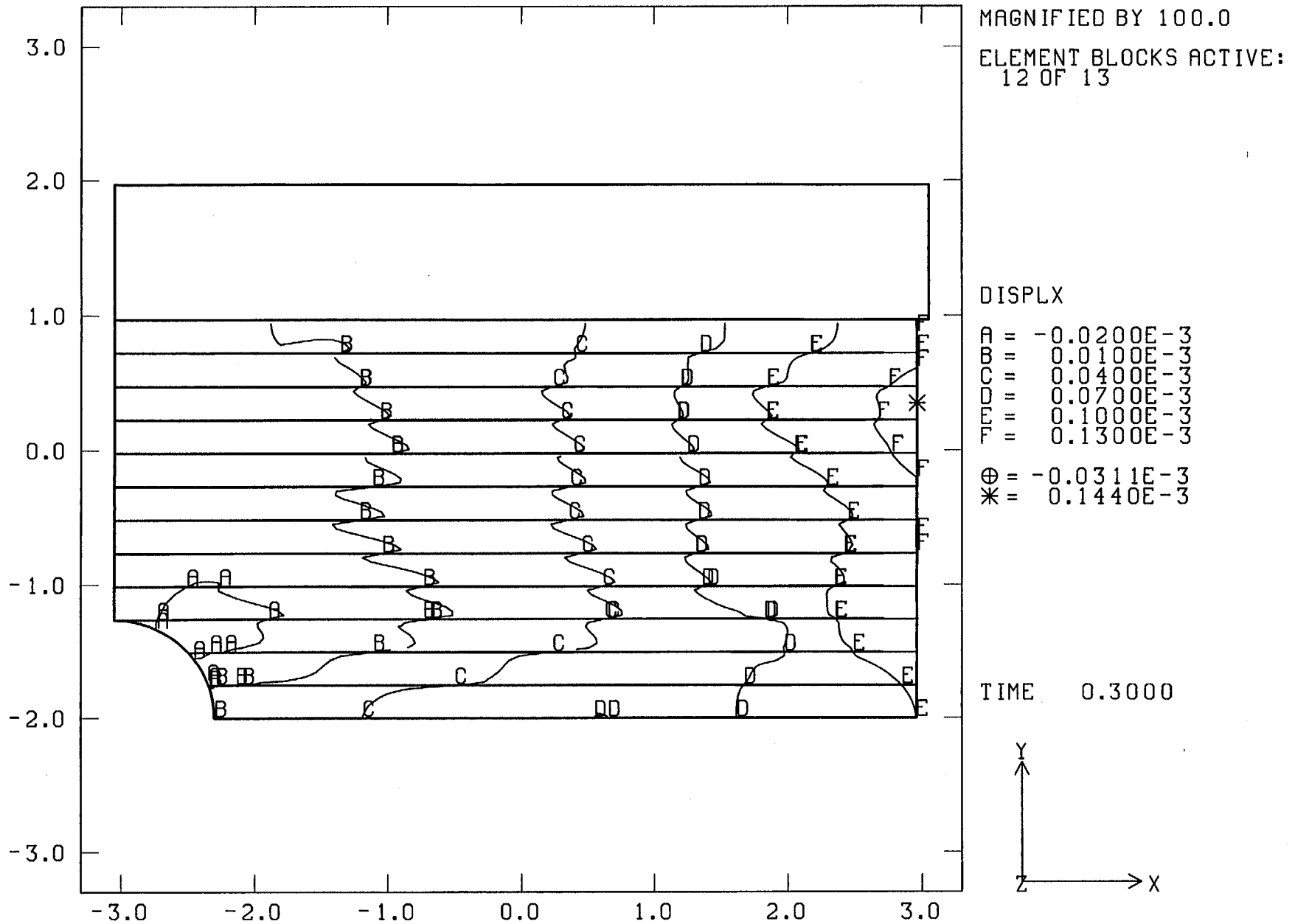

Figure 56: Horizontal Displacement Contours from the JAS3D Lexan Plate Model at 0.30 MPa Load (front surface)

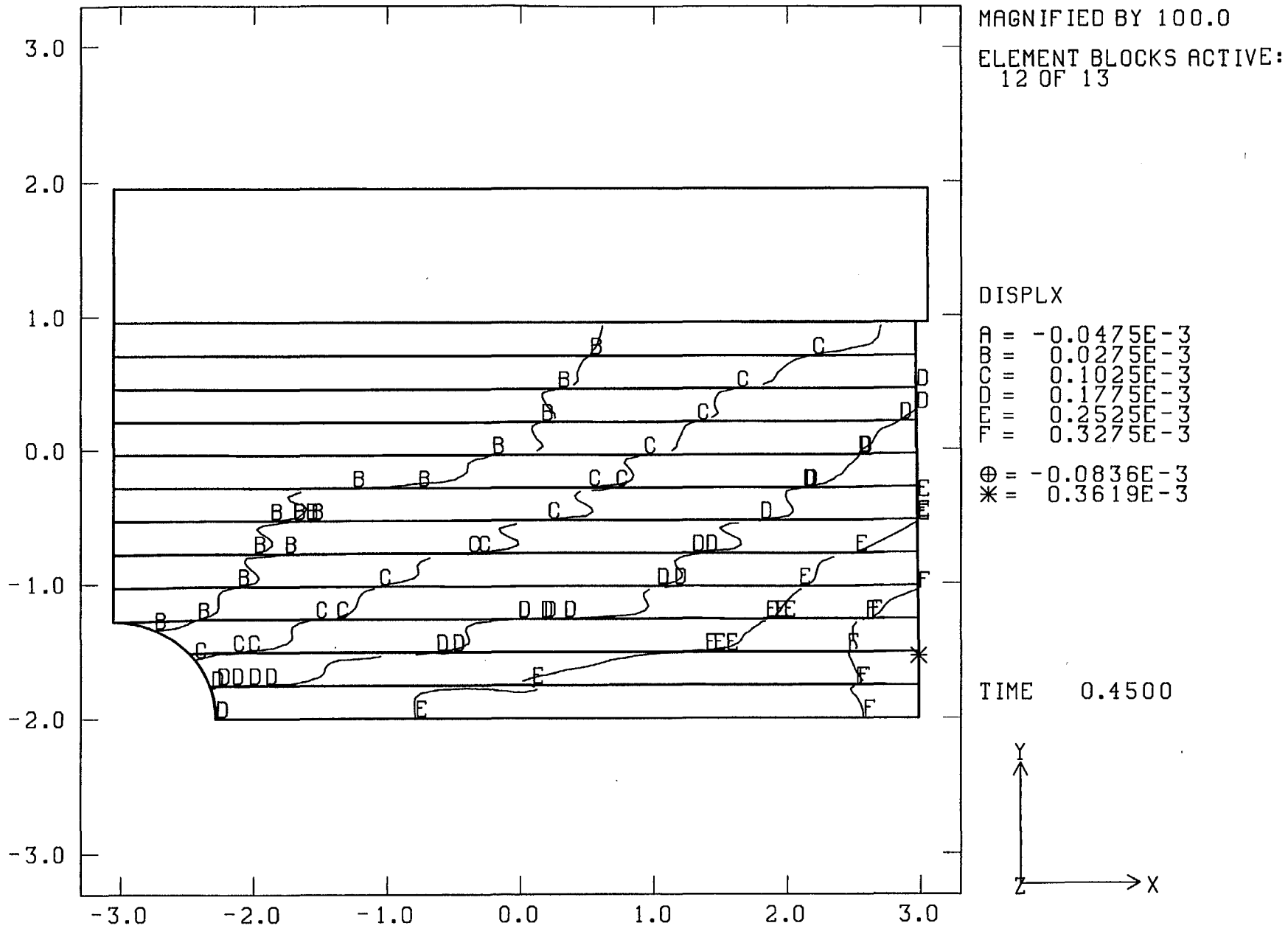

Figure 57: Horizontal Displacement Contours from the JAS3D Lexan Plate Model at 0.45 MPa Load (front surface)

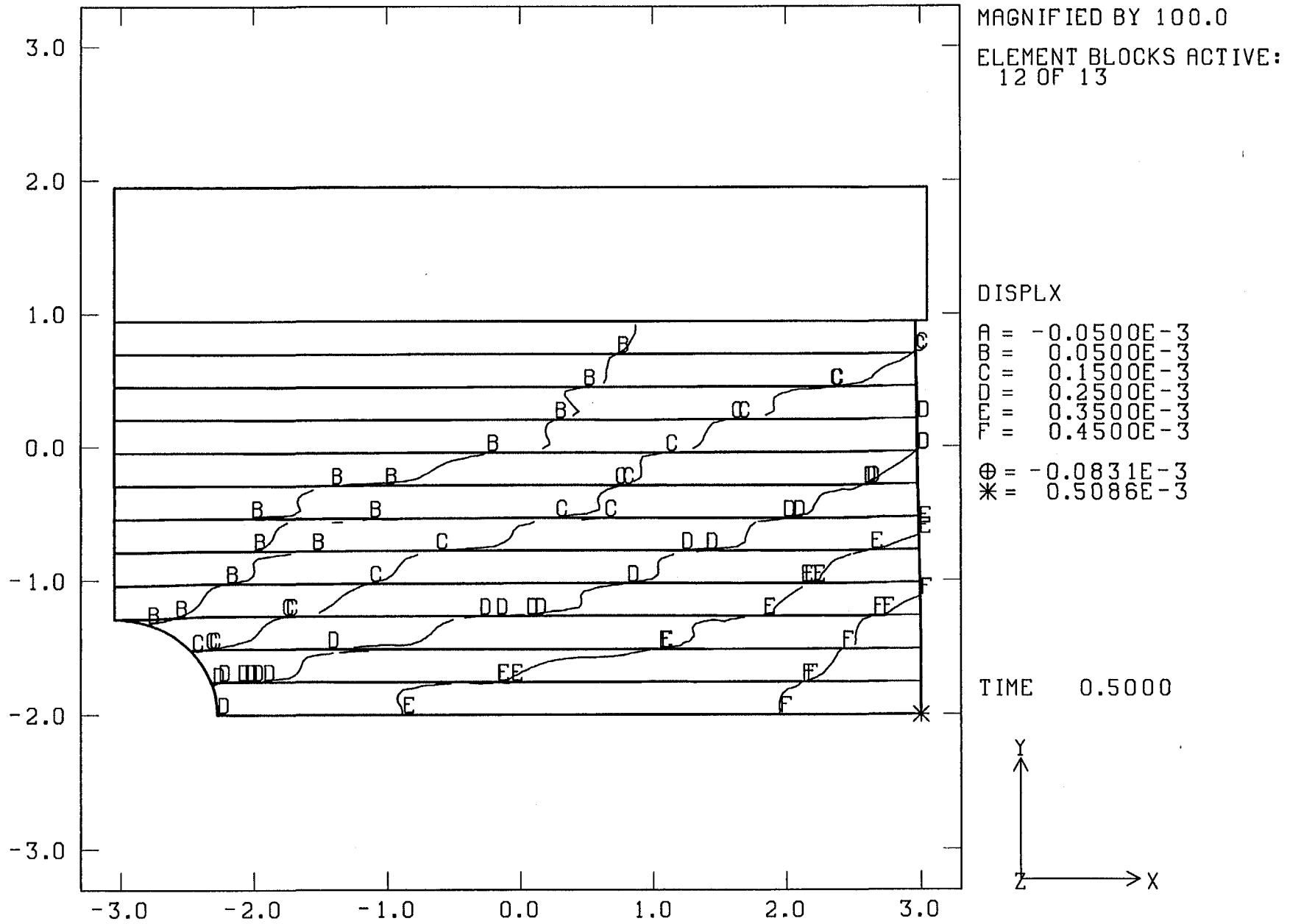

Figure 58: Horizontal Displacement Contours from the JAS3D Lexan Plate Model at 0.50 MPa Load (front surface)

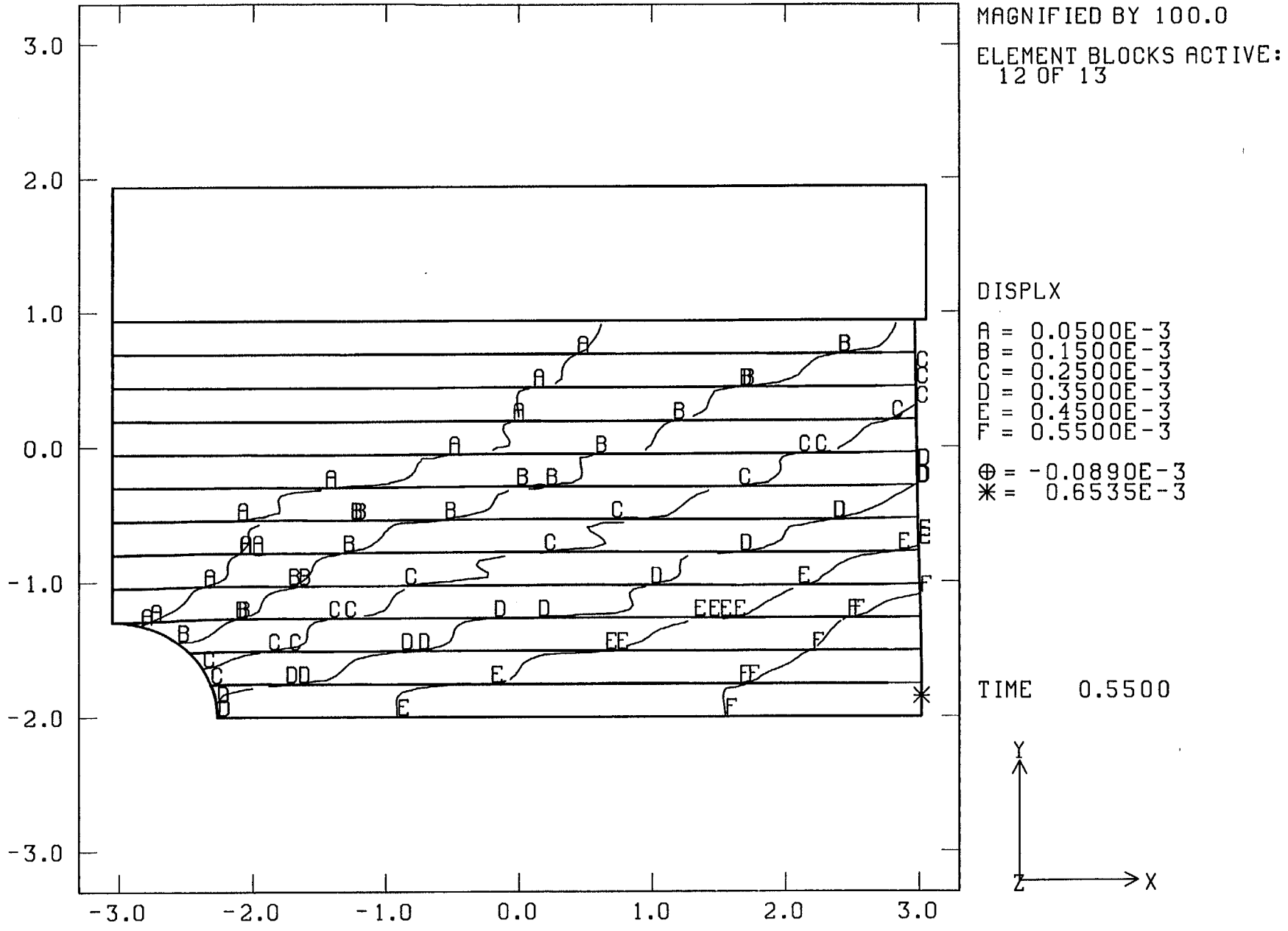

Figure 59: Horizontal Displacement Contours from the JAS3D Lexan Plate Model at 0.55 MPa Load (front surface)

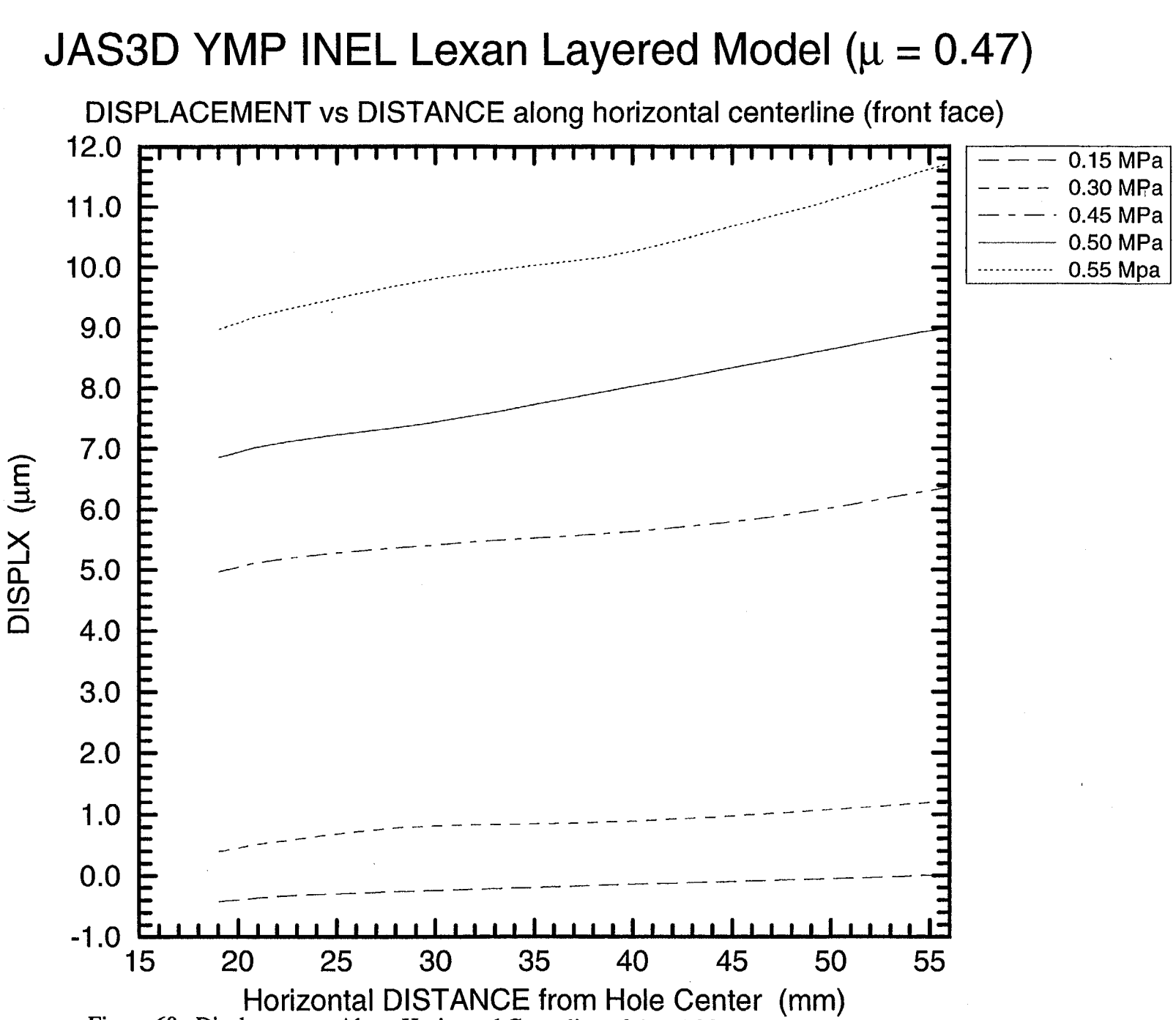

Figure 60: Displacements Along Horizontal Centerline of the JAS3D Lexan Plate Model (front surface)

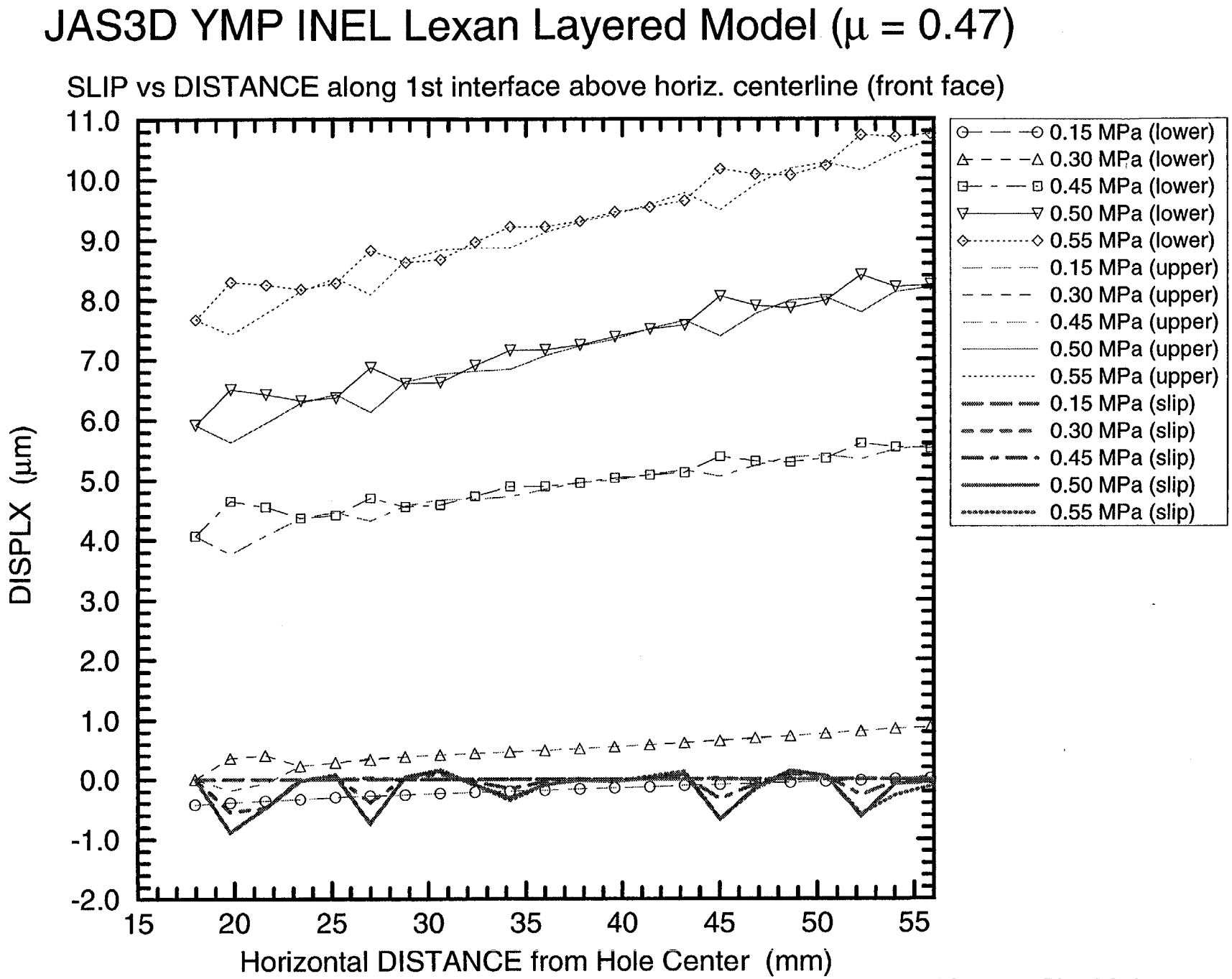

Figure 61: Displacements and Slip Along First Plate Interface above the Horizontal Centerline of the JAS3D Lexan Plate Model (front surface)

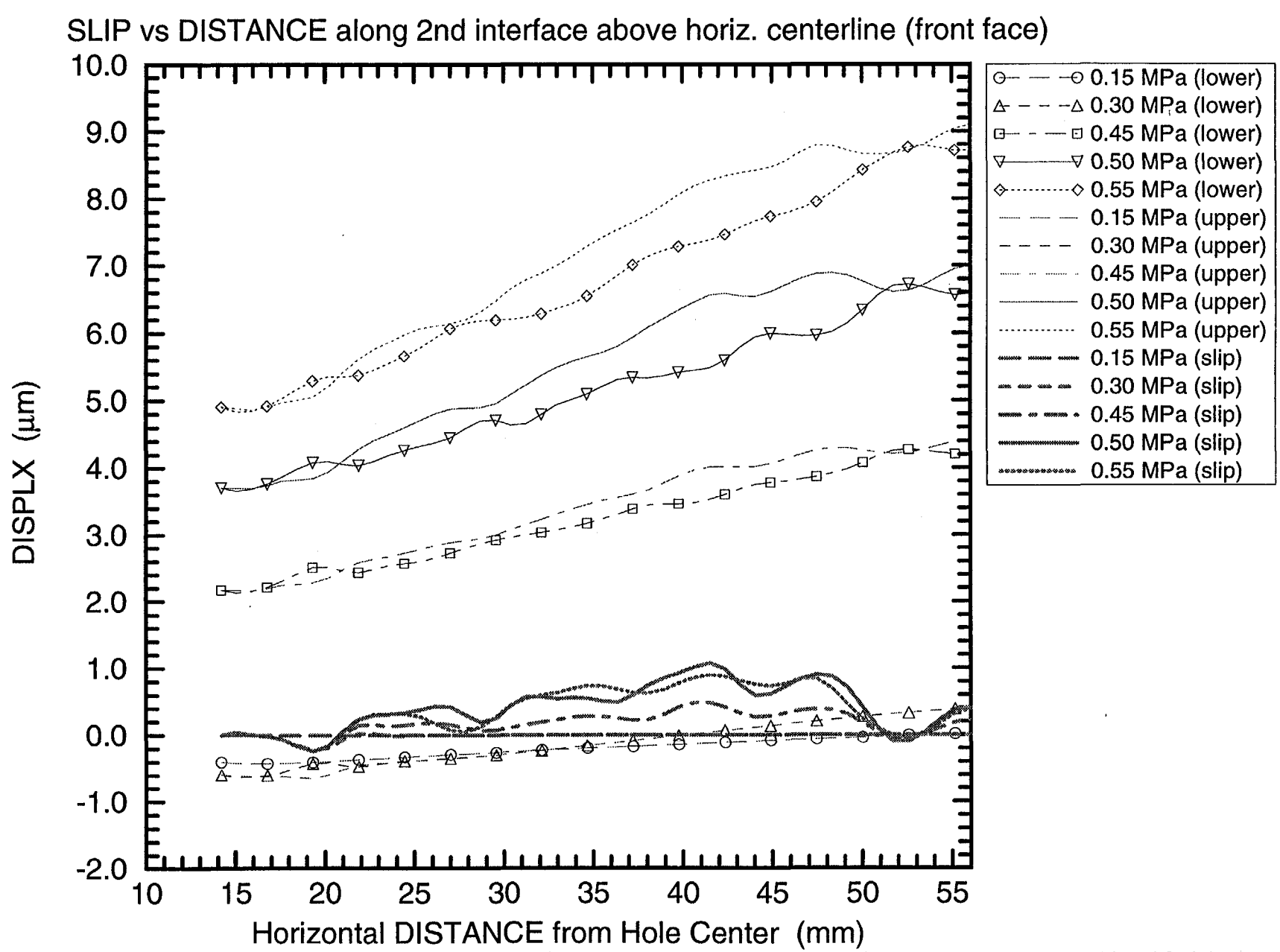

Figure 62: Displacements and Slip Along Second Plate Interface above the Horizontal Centerline of the JAS3D Lexan Plate Model (front surface)

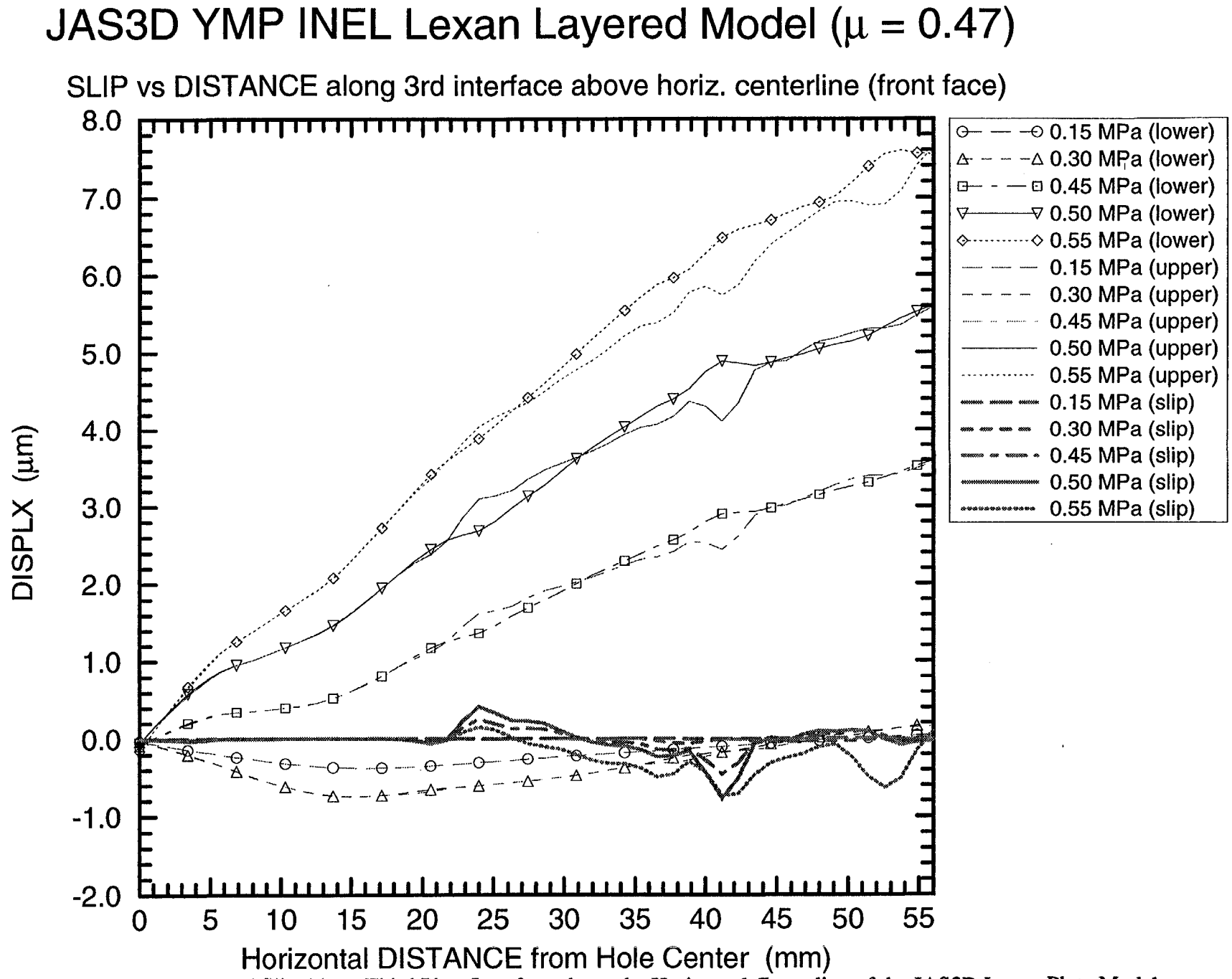

Figure 63: Displacements and Slip Along Third Plate Interface above the Horizontal Centerline of the JAS3D Lexan Plate Model (front surface)

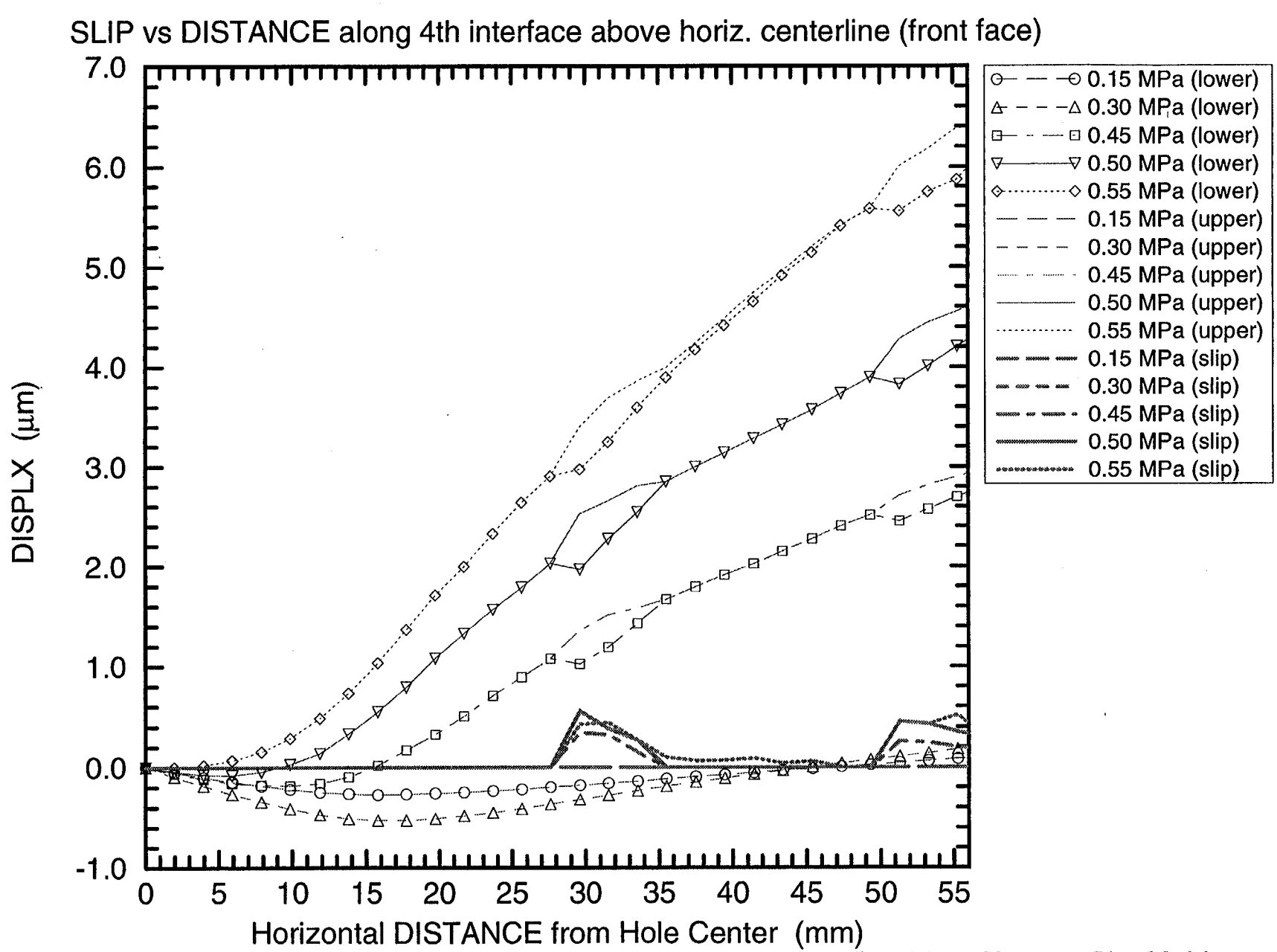

Figure 64: Displacements and Slip Along Fourth Plate Interface above the Horizontal Centerline of the JAS3D Lexan Plate Model (front surface)

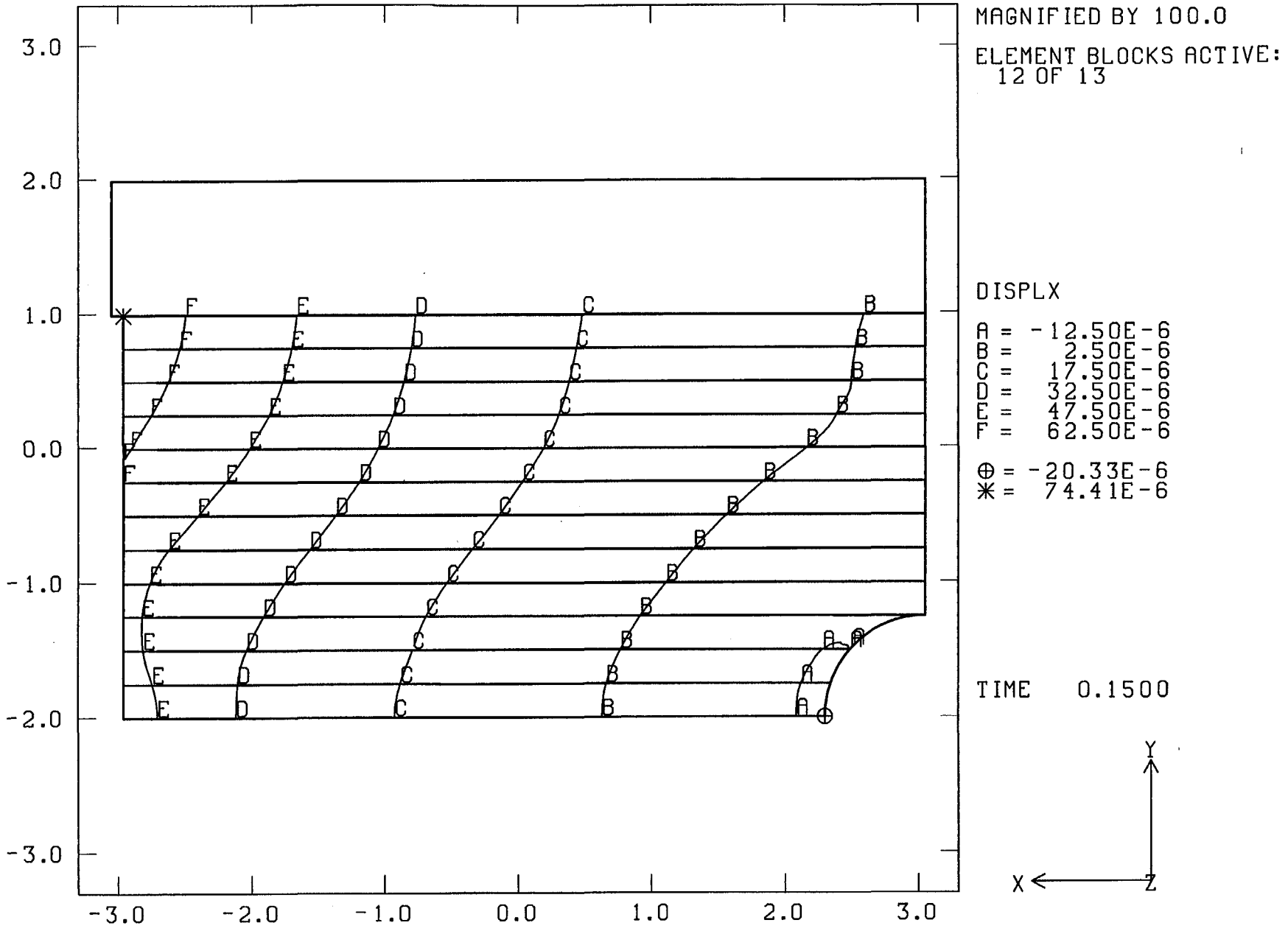

Figure 65: Horizontal Displacement Contours from the JAS3D Lexan Plate Model at 0.15 MPa Load (back surface)

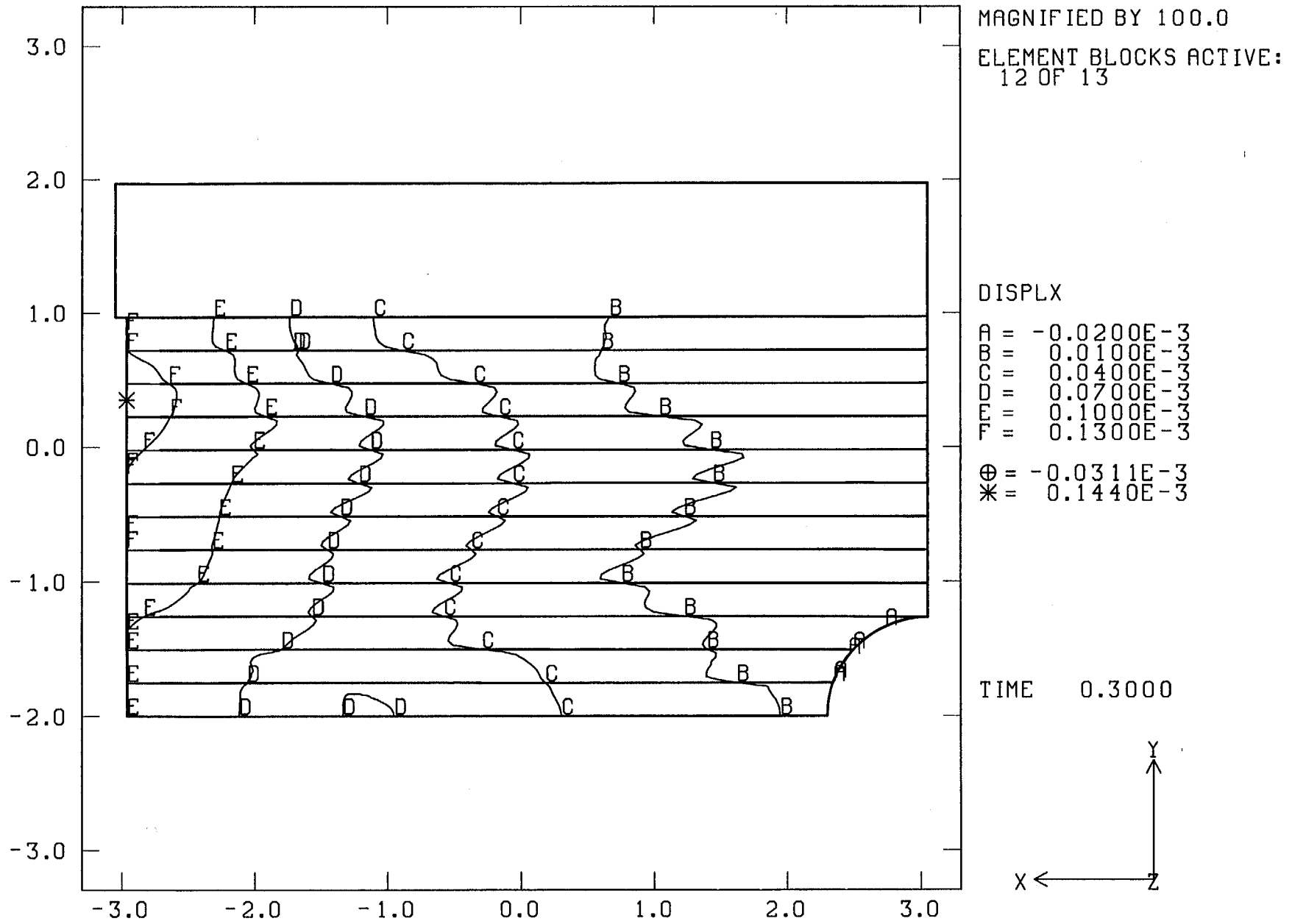

Figure 66: Horizontal Displacement Contours from the JAS3D Lexan Plate Model at 0.30 MPa Load (back surface)

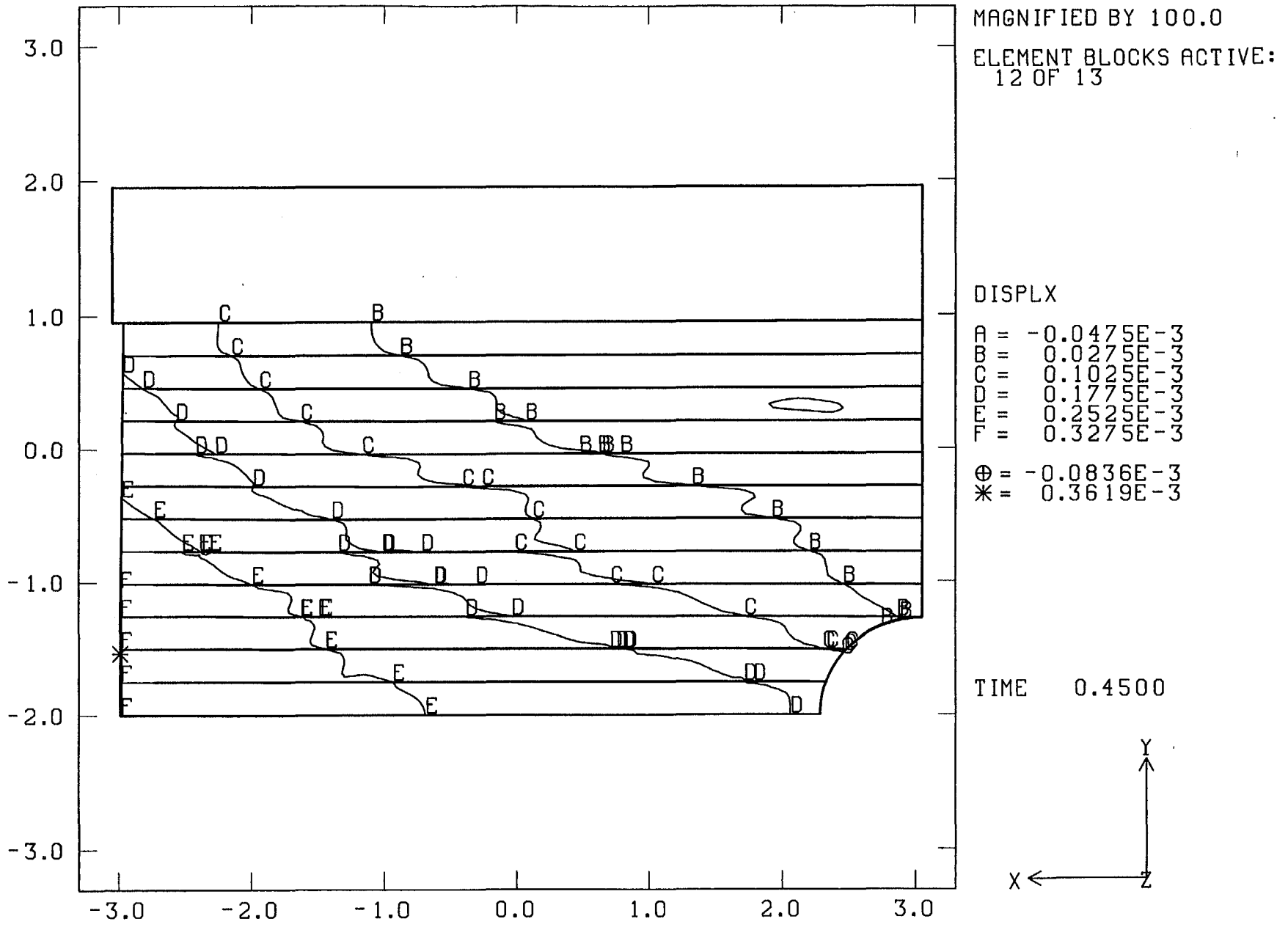

Figure 67: Horizontal Displacement Contours from the JAS3D Lexan Plate Model at 0.45 MPa Load (back surface)

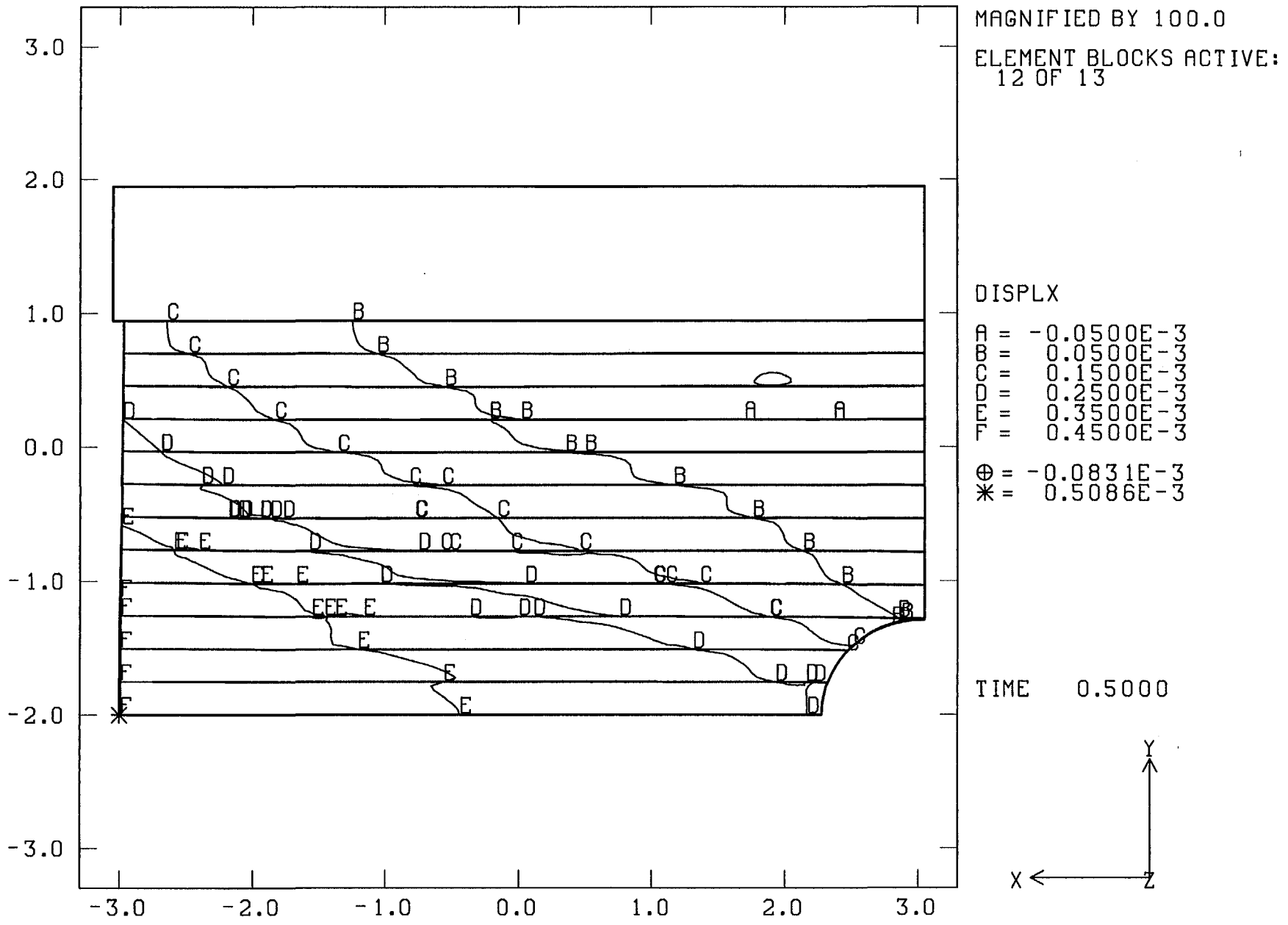

Figure 68: Horizontal Displacement Contours from the JAS3D Lexan Plate Model at 0.50 MPa Load (back surface)

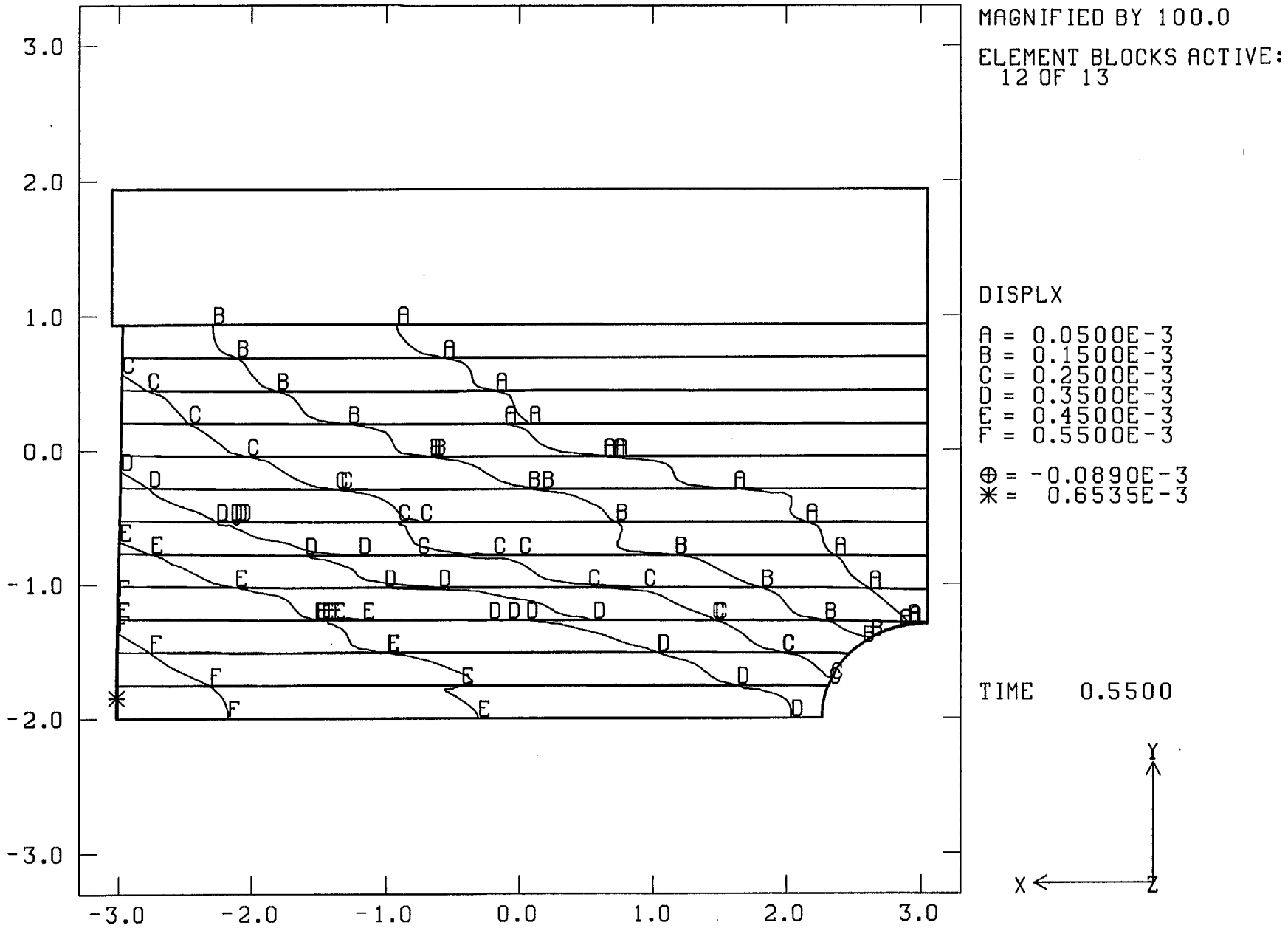

Figure 69: Horizontal Displacement Contours from the JAS3D Lexan Plate Model at 0.55 MPa Load (back surface)

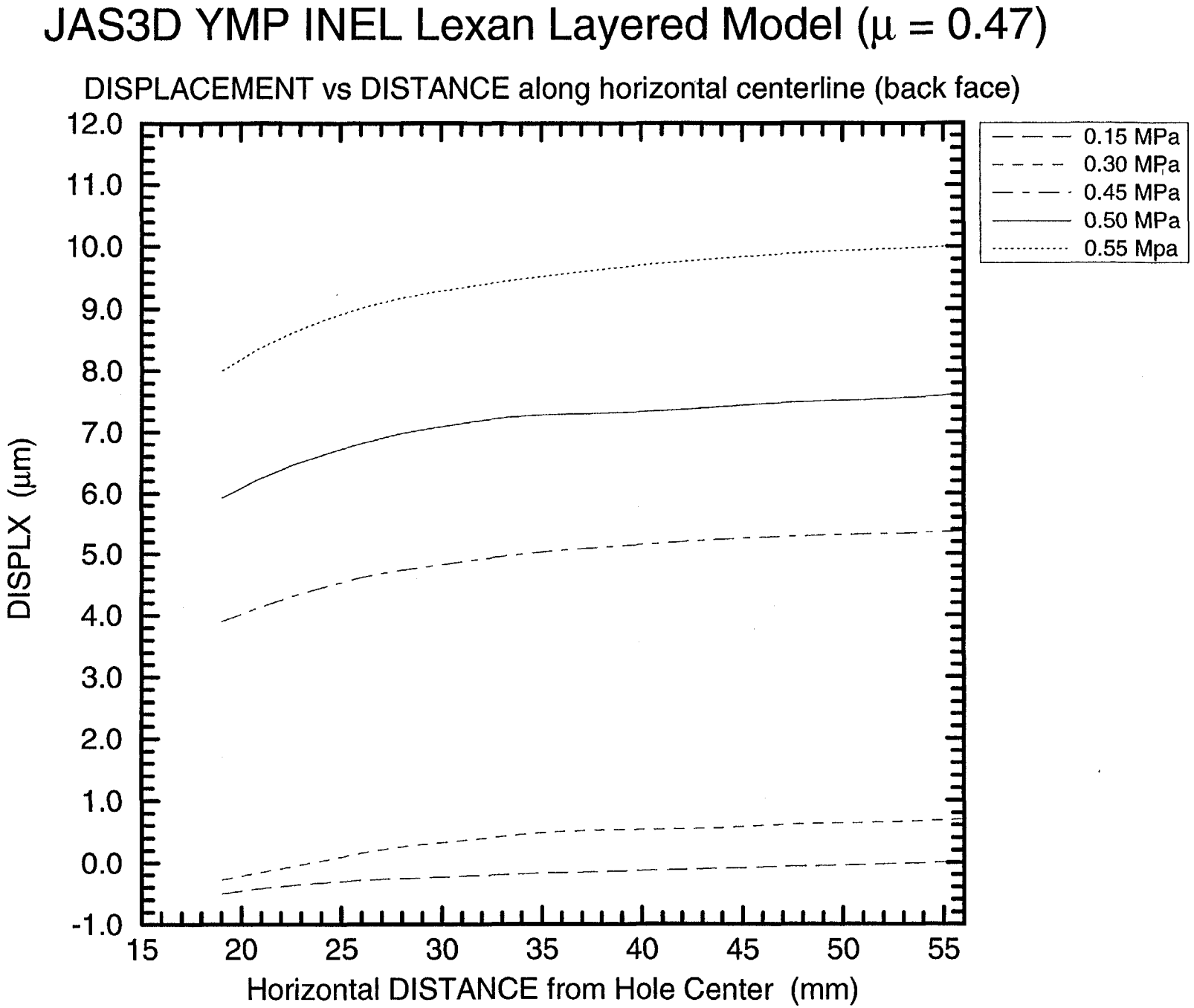

Figure 70: Displacements Along Horizontal Centerline of the JAS3D Lexan Plate Model (back surface)

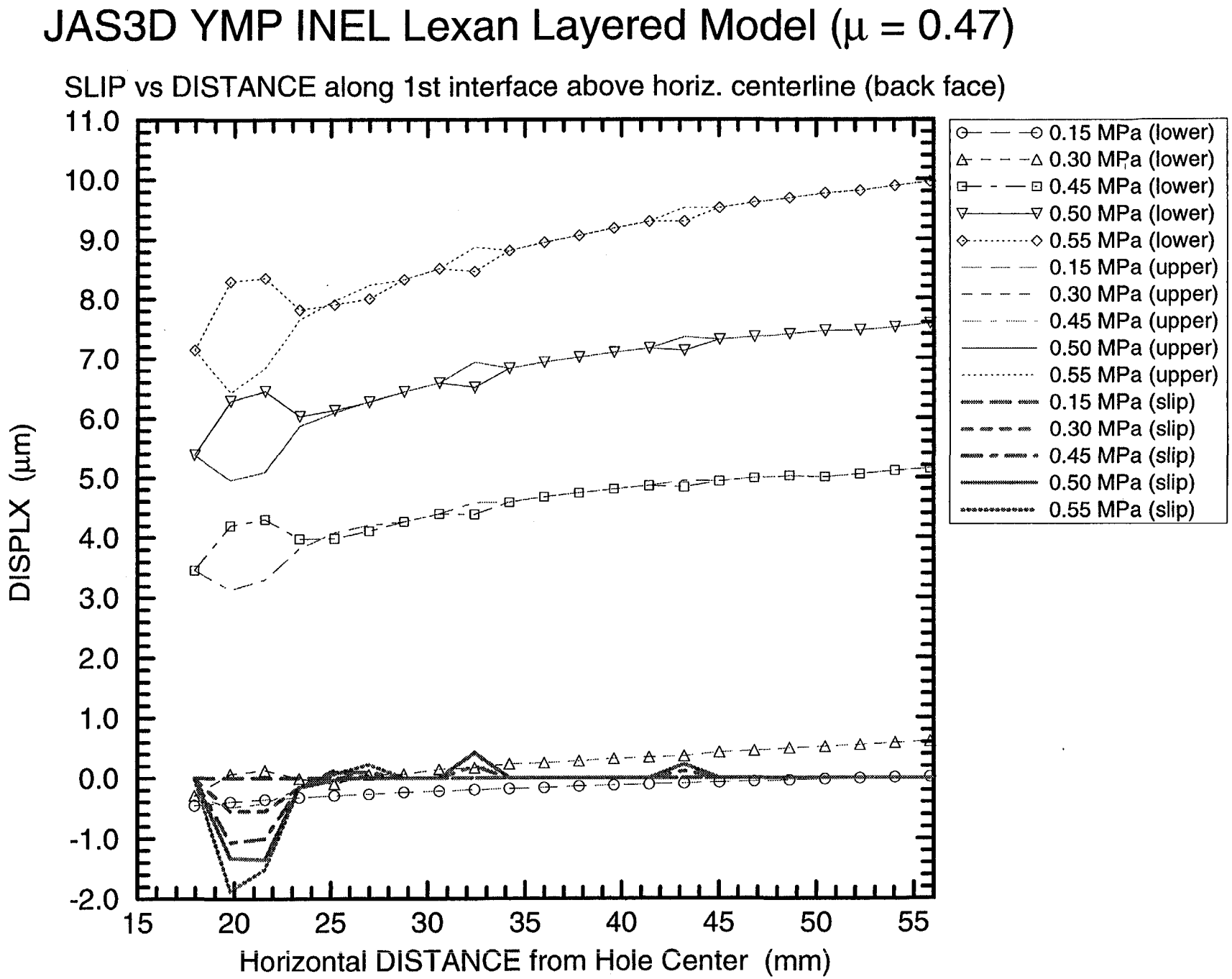

Figure 71: Displacements and Slip Along First Plate Interface above the Horizontal Centerline of the JAS3D Lexan Plate Model (back surface)

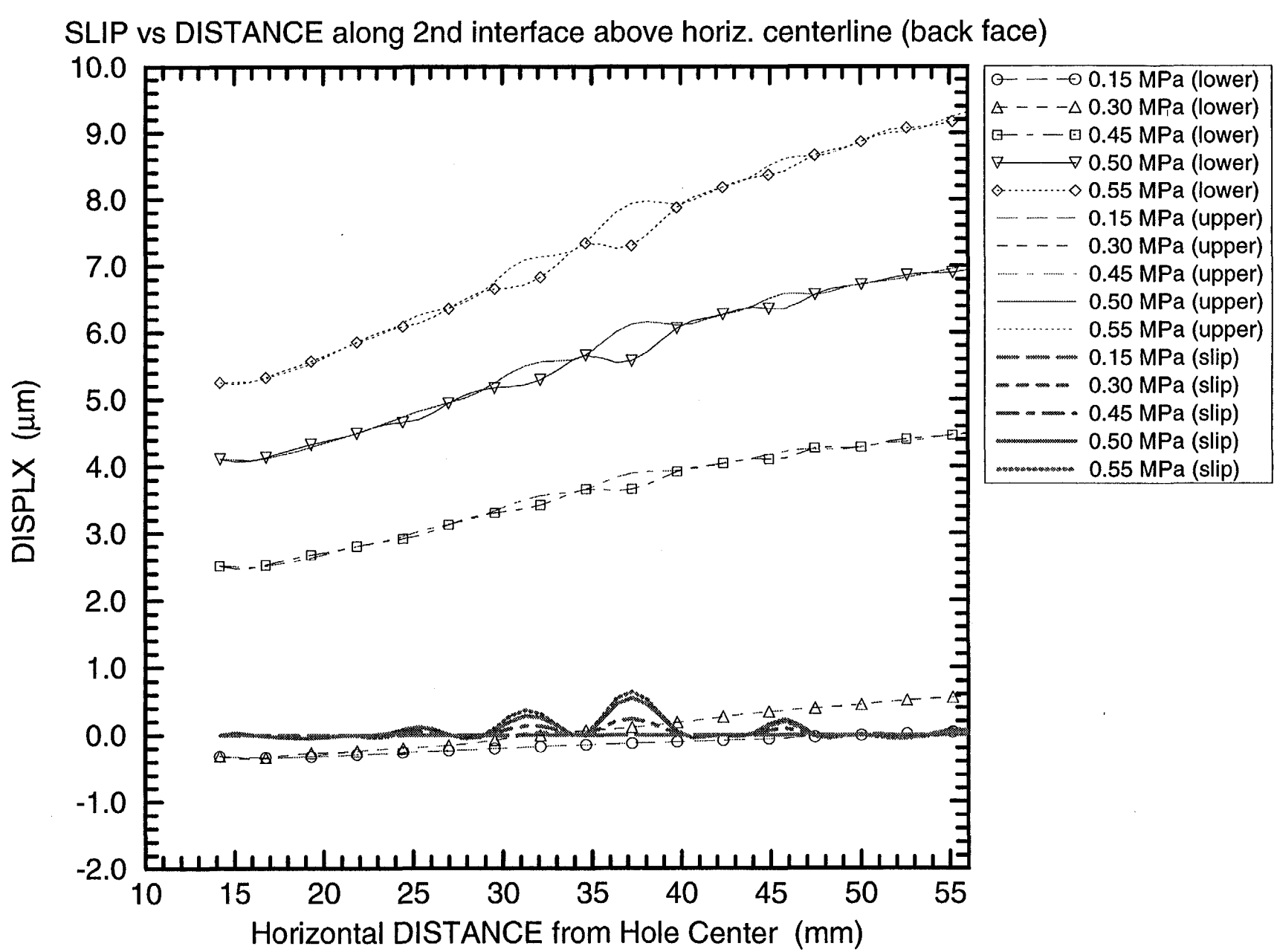

Figure 72: Displacements and Slip Along Second Plate Interface above the Horizontal Centerline of the JAS3D Lexan Plate Model (back surface)

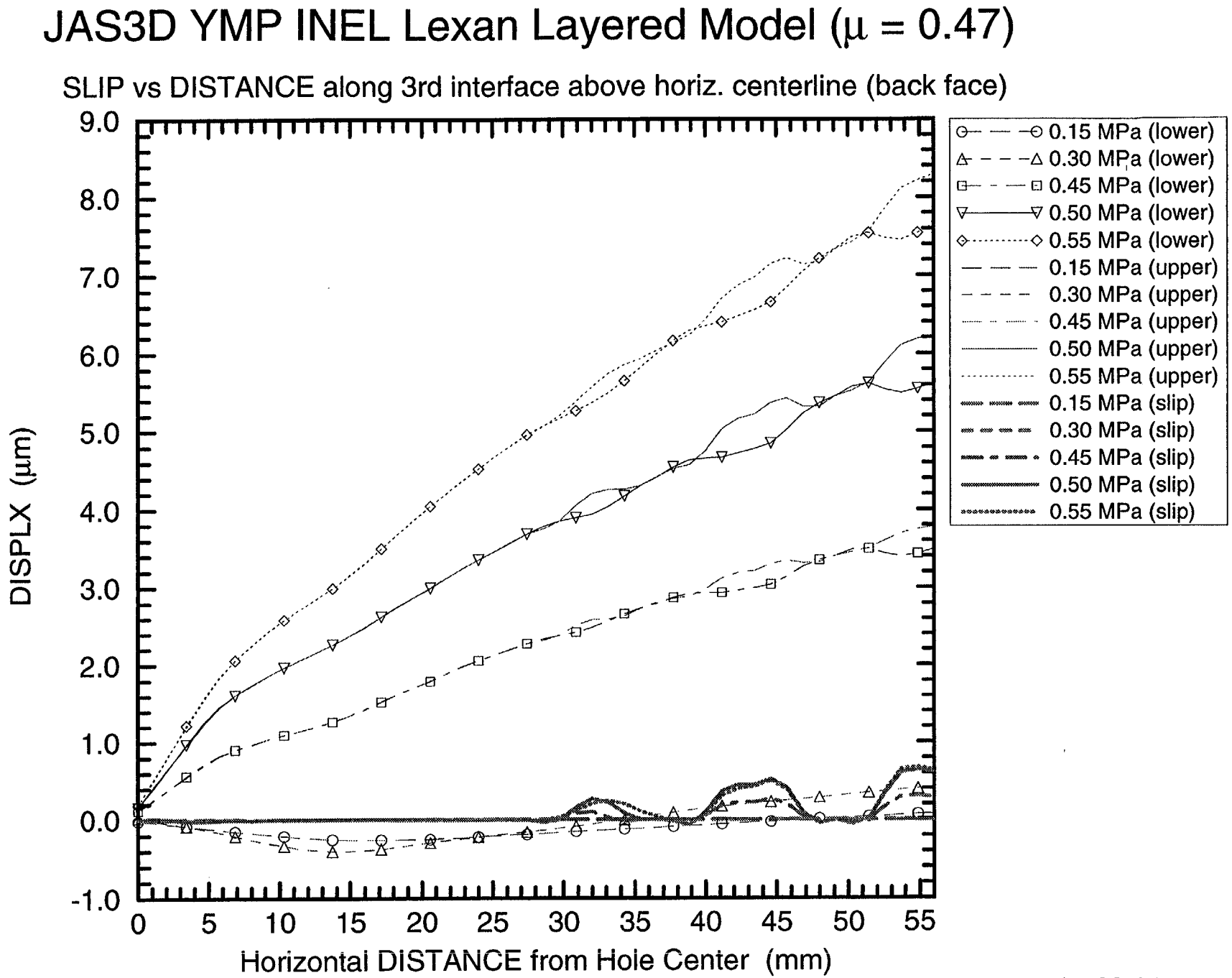

Figure 73: Displacements and Slip Along Third Plate Interface above the Horizontal Centerline of the JAS3D Lexan Plate Model (back surface)

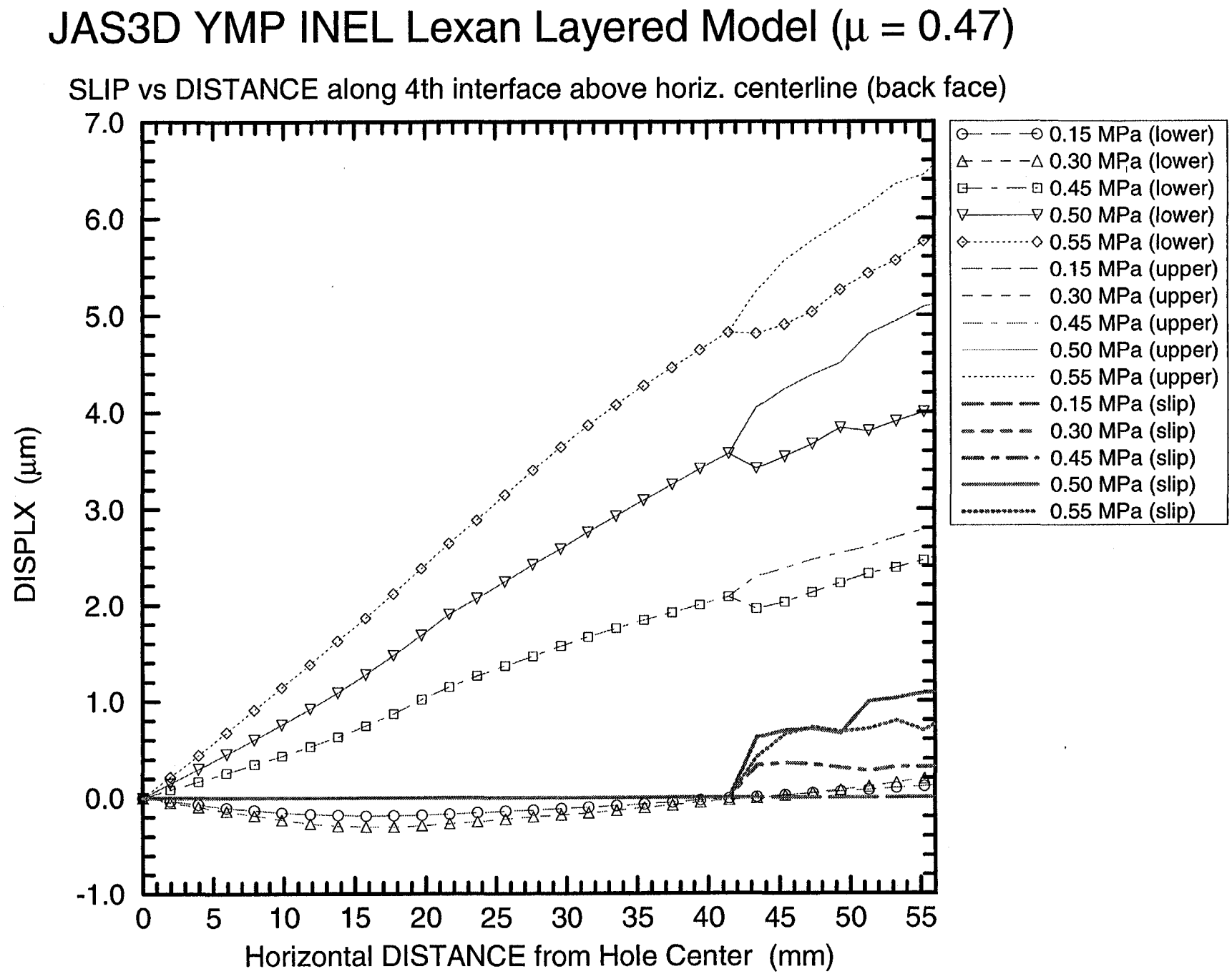

Figure 74: Displacements and Slip Along Fourth Plate Interface above the Horizontal Centerline of the JAS3D Lexan Plate Model (back surface)

6.0 Conclusions

This report describes the results of computational analyses modeling a series of uniaxial loading experiments designed to produce frictional slip in a stack of plates. The results of these analyses will be compared with each other as well as with the data from the uniaxial loading of Lexan plates.

There are several significant observations that can be made from a comparison of the UDEC, JAC2D, and JAS3D calculations for the Lexan experiments. The horizontal displacement contours from the three codes show significant differences in their prediction of the general displacement patterns. The UDEC predictions (Figures 8-12, 22-24) predict similar patterns to the JAS3D predictions at the higher loadings (≥0.45 MPa; Figures 57-59, 67-69); the contours run diagonally from the hole toward the corners of the stack of plates. These predictions indicate that the highest amounts of horizontal displacement are occurring in the plates through which the hole has been cut. On the other hand, the JAC2D calculations (Figures 34-38), and the JAS3D calculations at the lower loadings (Figures 55-56, 65-66), predict horizontal displacement contours which are roughly vertical and indicate the greatest amount of displacement at the corner of the stack of plates. The magnitude of horizontal displacements predicted by the UDEC runs with higher joint normal and joint shear stiffnesses are approximately the same as the JAC2D and JAS3D (with contact surface model, i.e. no assigned joint stiffnesses) runs, whereas the UDEC runs with lower joint stiffnesses predict displacement as much as three times greater.

The predictions of frictional slip of the Lexan plates are more dissimilar. The slip predictions from UDEC for the cases where k_n=k_s=10 GPa/m (Figures 14-16) are much higher than all the JAC2D and JAS3D predictions because of the relatively small joint stiffness values. The UDEC predictions for the cases of 0.45 MPa loading and k_n=k_s=100 GPa/m and 5660 GPa/m (Figures 26 and 27, respectively) are best used for comparison with the same loadings for JAC2D (Figures 40-43) and JAS3D (Figures 60-64, 70-74). For the sake of comparison, the predicted slips for each of the first four interfaces above the centerline for five sets of calculations at a loading of 0.45 MPa are shown in Figures 75-78, respectively. The magnitudes of slip for the UDEC and JAS3D plots were all on the order of 0.3-2 microns, although the slip gradient as shown by UDEC tended to occur directly next to the hole, whereas for JAS3D the changes in slip were more oscillatory and not necessarily next to the hole. The JAC2D calculations predicted the greatest slip would occur at the third interface, about 4 microns for the 0.45 MPa load. There was no apparent correlation between the three codes in terms of the predicted slip patterns (i.e., location of positive or negative changes in slip). When comparing all of the predicted results to the experimental results (Figures 3-5), it is apparent that the actual system of plates probably had a joint shear stiffness value toward the lower end of the range of values studied here. These calculations point to the necessity of quantifying the joint normal and shear stiffnesses for a given system in order to better estimate frictional slip.

The predictions of the frictional slip in the granite plates by UDEC and JAC2D displayed many of the same characteristics as the Lexan predictions. The horizontal displacement contours from the UDEC predictions (Figures 18, 19, and 29) showed the maximum displacement occurring in the plates through which the hole had been drilled, whereas those from the JAC2D predictions

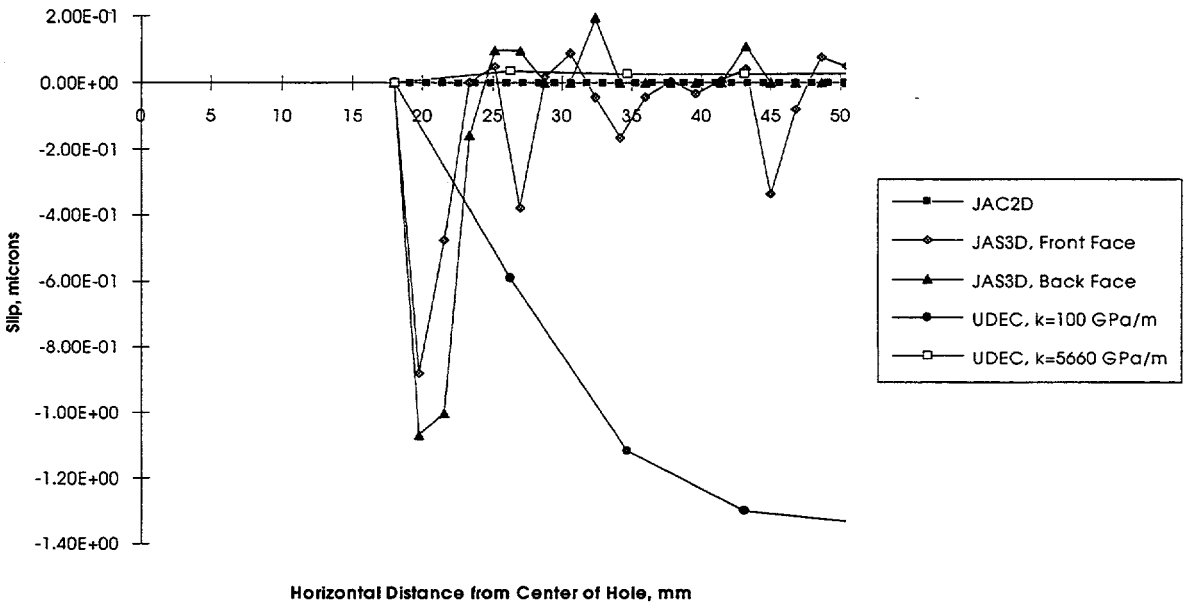

Figure 75: Slip vs. Distance at the First Interface Above the Horizontal Centerline, Lexan Plates, Load=0.45 MPa

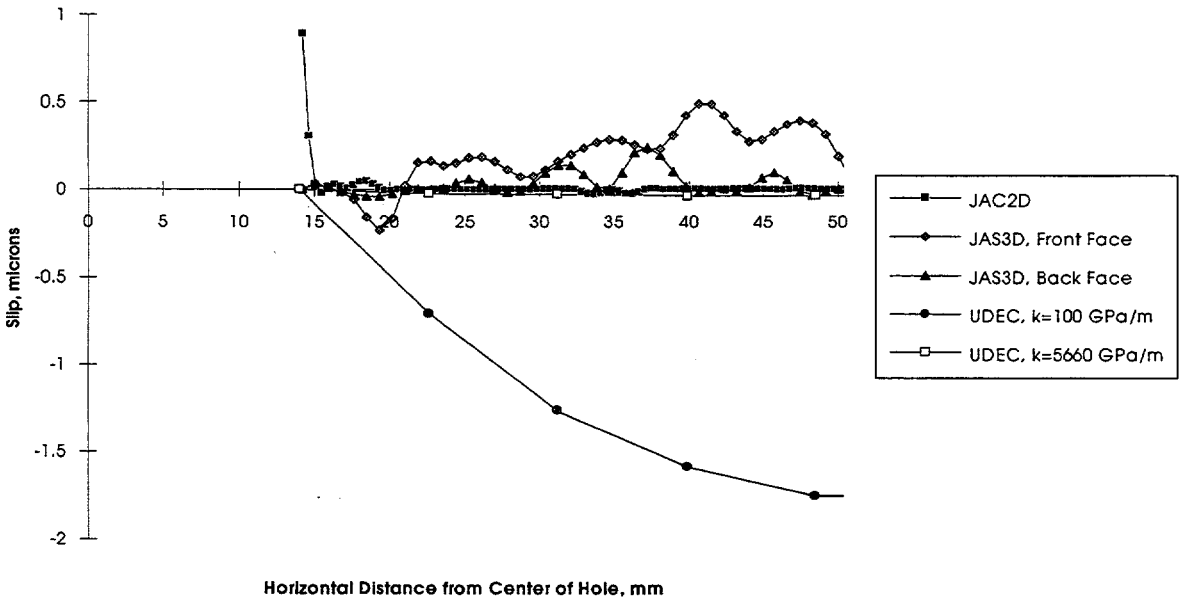

Figure 76: Slip vs. Distance at the Second Interface Above the Horizontal Centerline, Lexan Plates, Load=0.45 MPa

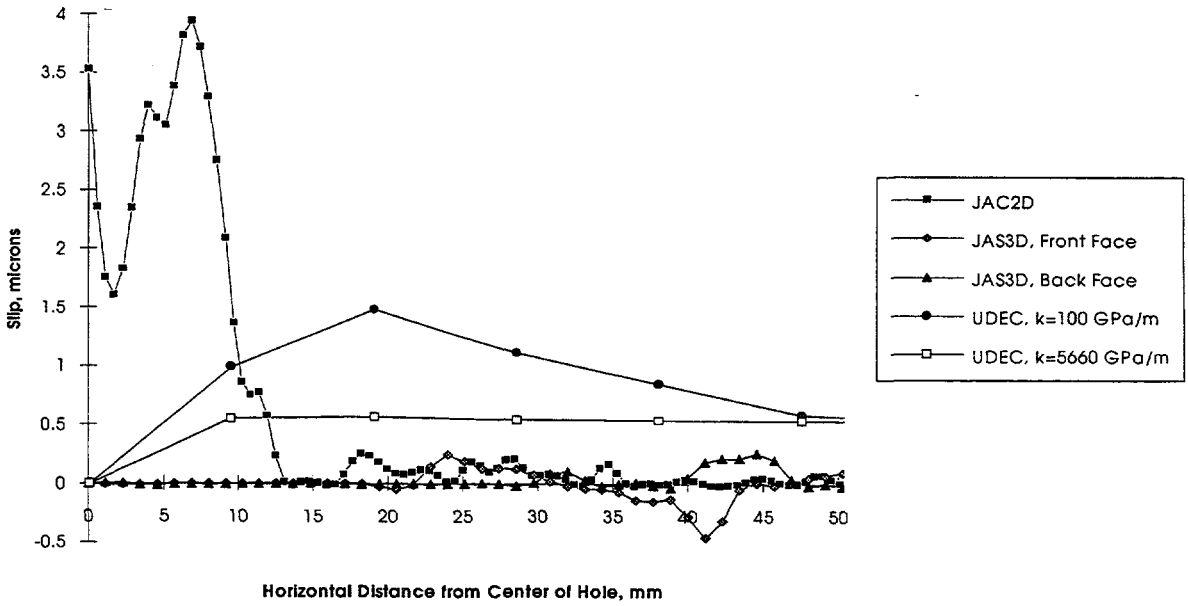

Figure 77: Slip vs. Distance at the Third Interface Above the Horizontal Centerline, Lexan Plates, Load=0.45 MPa

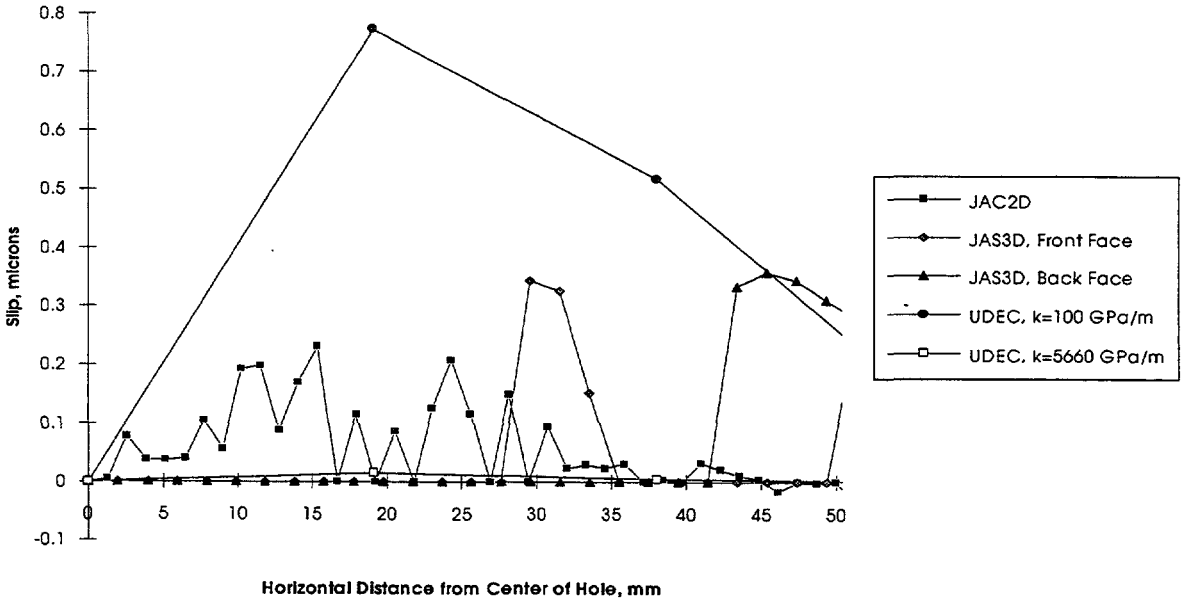

Figure 78: Slip vs. Distance at the Fourth Interface Above the Horizontal Centerline, Lexan Plates, Load=0.45 MPa

(Figures 45-49) indicated the maximum displacement to occur in plates between the hole and the steel platen. The slip predicted by UDEC for k_n=k_s=10 GPa/m was on the order of a few microns; the slip predicted by UDEC for k_n=k_s=100,000 GPa/m and by JAC2D was on the order of hundredths of microns. Again, the codes indicate that a better quantitative and qualitative understanding of joint normal and shear stiffness is required for their continued validation for design and performance assessment calculations.

Each of the models implemented in this preliminary validation effort has certain strengths and weaknesses which were exercised by these calculations. One of the conclusions from the work described in Chapter 3, 4, and 5 is that because of the non-linear nature of the models, code users as well as the codes themselves may require some sort of validation. The discrete block code UDEC probably did the best overall job in predicting slip along the interfaces. However, the difficulties in knowing when a "steady-state" solution to a static problem is achieved make the results obtained using UDEC dependent upon the skill of the UDEC user. Additionally, because UDEC is a discrete block code, its use for problems with large domains (e.g., several tunnel diameters) of highly fractured tuff may be limited to problems involving well-defined features, such as faults. For the cases involving JAC2D and JAS3D, slide lines were used to model the joints; the primary strength of these codes, the continuum joint model, was not exercised. The continuum joint models in the codes JAC2D and JAS3D are well-suited to evaluating stress fields in large domains of fractured rock. However, the behavior of discrete fractures is averaged over each element, so a validation exercise such as the uniaxial loading experiments does not adequately exercise the capabilities of these codes. Furthermore, it was demonstrated in the UDEC calculations that the magnitude of slip was highly dependent on the joint normal and shear stiffness values; therefore, the impact of the choice of joint model and joint stiffness values as input to JAC2D and JAS3D on prediction of in situ rock mass behavior requires further investigation.

The next natural steps in this rock mass model validation effort would be to predict slip for similar sets of plates undergoing biaxial loading, followed by the prediction of the frictional slip of blocky model consisting of evenly-spaced, orthogonal, discontinuous fractures. These experiments would be conducted using the same granite material used previously, as well as plates made from welded tuff obtained from the Yucca Mountain area.

7.0 References

Biffle, J.H., and M.L. Blanford, 1994. JAC2D--A Two-Dimensional Finite Element Computer Program for the Nonlinear Quasi-Static Response of Solids with the Conjugate Gradient Method, SAND93-1891, Sandia National Laboratories, Albuquerque, New Mexico.

DOE/YMP, 1989. Yucca Mountain Project Reference Information Base, Version 4, YMP/CC-0002, U.S. Department of Energy, Nevada Operations Office/Yucca Mountain Project Office, Las Vegas, Nevada.

Itasca, 1993. UDEC Universal Distinct Element Code, Version 1.8, Volume I: User's Manual, Itasca Consulting Group, Minneapolis, Minnesota.

Mills-Curran, W.C., A.P. Gilkey, and D.P. Flanagan, 1988. EXODUS: A Finite Element File Format for Pre- and Postprocessing, SAND87-2997, Sandia National Laboratories, Albuquerque, New Mexico.

Perry, K.E., Jr., B.J. Buescher, D. Anderson, and J.S. Epstein, 1995. Frictional Sliding in Layered Rock Model: Preliminary Experiments, SAND94-2384, Sandia National Laboratories, Albuquerque, New Mexico.

SNL (Sandia National Laboratories), 1987. Site Characterization Plan Conceptual Design Report, SAND84-2641, complied by MacDougall, Hugh R., Leo W. Scully, and Joe R. Tillerson, Albuquerque, New Mexico.

YUCCA MOUNTAIN SITE CHARACTERIZATION PROJECT
SAND95-2001 - DISTRIBUTION LIST
8/15/96

1 D. A. Dreyfus (RW-1)
Director
OCRWM
US Department of Energy
1000 Independence Avenue SW
Washington, DC 20585

1 L. H. Barrett (RW-2)
Acting Deputy Director
OCRWM
US Department of Energy
1000 Independence Avenue SW
Washington, DC 20585

1 S. Rousso (RW-40)
Office of Storage and Transportation
OCRWM
US Department of Energy
1000 Independence Avenue SW
Washington, DC 20585

1 R. A. Milner (RW-30)
Office of Program Management
and Integration
OCRWM
US Department of Energy
1000 Independence Avenue SW
Washington, DC 20585

1 D. R. Elle, Director
Environmental Protection Division
DOE Nevada Field Office
US Department of Energy
P.O. Box 98518
Las Vegas, NV 89193-8518

1 T. Wood (RW-14)
Contract Management Division
OCRWM
US Department of Energy
1000 Independence Avenue SW
Washington, DC 20585

4 Victoria F. Reich, Librarian
Nuclear Waste Technical Review Board
1100 Wilson Blvd., Suite 910
Arlington, VA 22209

1 Wesley Barnes, Project Manager
Yucca Mountain Site Characterization
Office
US Department of Energy
P.O. Box 98608–MS 523
Las Vegas, NV 89193-8608

1 Director, Public Affairs Office
c/o Technical Information Resource Center
DOE Nevada Operations Office
US Department of Energy
P.O. Box 98518
Las Vegas, NV 89193-8518

8 Technical Information Officer
DOE Nevada Operations Office
US Department of Energy
P.O. Box 98518
Las Vegas, NV 89193-8518

1 J. R. Dyer, Deputy Project Manager
Yucca Mountain Site Characterization Office
US Department of Energy
P.O. Box 98608 – MS 523
Las Vegas, NV 89193-88608

1 M. C. Brady
Laboratory Lead for YMP
M&O/Sandia National Laboratories
1261 Town Center Drive
Bldg. 4, Room 421A
Las Vegas, NV 89134

1 J. A. Canepa
Laboratory Lead for YMP
EES-13, Mail Stop J521
M&O/Los Alamos National Laboratory
P.O. Box 1663
Los Alamos, NM 87545

1 Repository Licensing & Quality
Assurance
Project Directorate
Division of Waste Management, MS T7J-9
US NRC
Washington, DC 20555

1 Senior Project Manager for Yucca
Mountain
Repository Project Branch
Division of Waste Management, MS T7J-9
US NRC
Washington, DC 20555

1 NRC Document Control Desk
Division of Waste Management, MS T7J-9
US NRC
Washington, DC 20555

1 Chad Glenn
NRC Site Representative
301 E Stewart Avenue, Room 203
Las Vegas, NV 89101

1 Center for Nuclear Waste
Regulatory Analyses
Southwest Research Institute
6220 Culebra Road
Drawer 28510
San Antonio, TX 78284

2 W. L. Clarke
Laboratory Lead for YMP
M&O/ Lawrence Livermore Nat'l Lab
P.O. Box 808 (L-51)
Livermore, CA 94550

1 Robert W. Craig
Acting Technical Project Officer/YMP
US Geological Survey
101 Convention Center Drive, Suite P-110
Las Vegas, NV 89109

1 J. S. Stuckless, Chief
Geologic Studies Program
MS 425
Yucca Mountain Project Branch
US Geological Survey
P.O. Box 25046
Denver, CO 80225

1 L. D. Foust
Technical Project Officer for YMP
TRW Environmental Safety Systems
101 Convention Center Drive
Suite P-110
Las Vegas, NV 89109

1 A. L. Flint
U. S. Geological Survey
MS 721
P. O. Box 327
Mercury, NV 89023

1 Robert L. Strickler
Vice President & General Manager
TRW Environmental Safety Systems, Inc.
2650 Park Tower Dr.
Vienna, VA 22180

1 Jim Krulik, Geology Manager
US Bureau of Reclamation
Code D-8322
P.O. Box 25007
Denver, CO 80225-0007

1 B. T. Brady
Records Specialist
US Geological Survey
MS 421
P.O. Box 25046
Denver, CO 80225

1 M. D. Voegele
Deputy of Technical Operations
M&O/SAIC
101 Convention Center Drive
Suite P-110
Las Vegas, NV 89109

2 A. T. Tamura
Science and Technology Division
OSTI
US Department of Energy
P.O. Box 62
Oak Ridge, TN 37831

1 P. J. Weeden, Acting Director
Nuclear Radiation Assessment Div.
US EPA
Environmental Monitoring Sys. Lab
P.O. Box 93478
Las Vegas, NV 89193-3478

1 John Fordham, Deputy Director
Water Resources Center
Desert Research Institute
P.O. Box 60220
Reno, NV 89506

1 The Honorable Jim Regan
Chairman
Churchill County Board of
Commissioners
10 W. Williams Avenue
Fallon, NV 89406

1 R. R. Loux
Executive Director
Agency for Nuclear Projects
State of Nevada
Evergreen Center, Suite 252
1802 N. Carson Street
Carson City, NV 89710

1 Brad R. Mettam
Inyo County Yucca Mountain
Repository Assessment Office
P. O. Drawer L
Independence, CA 93526

1 Vernon E. Poe
Office of Nuclear Projects
Mineral County
P.O. Box 1600
Hawthorne, NV 89415

1 Les W. Bradshaw
Program Manager
Nye County Nuclear Waste Repository
Project Office
P.O. Box 1767
Tonopah, NV 89049

1 Florindo Mariani
White Pine County Coordinator
P. O. Box 135
Ely, NV 89301

1 Tammy Manzini
Lander County Yucca Mountain
Information Officer
P.O. Box 10
Austin, NV 89310

1 Jason Pitts
Lincoln County Nuclear Waste
Program Manager
P. O. Box 158
Pioche, NV 89043

1 Dennis Bechtel, Coordinator
Nuclear Waste Division
Clark County Dept. of Comprehensive
Planning
P.O. Box 55171
Las Vegas, NV 89155-1751

1 Juanita D. Hoffman
Nuclear Waste Repository
Oversight Program
Esmeralda County
P.O. Box 490
Goldfield, NV 89013

1 Sandy Green
Yucca Mountain Information Office
Eureka County
P.O. Box 714
Eureka, NV 89316

1 Economic Development Dept.
City of Las Vegas
400 E. Stewart Avenue
Las Vegas, NV 89101

1 Community Planning & Development
City of North Las Vegas
P.O. Box 4086
North Las Vegas, NV 89030

2 Librarian
YMP Research & Study Center
101 Convention Center Drive, Suite P-110
Las Vegas, NV 89109

1 Library Acquisitions
Argonne National Laboratory
Building 203, Room CE-111
9700 S. Cass Avenue
Argonne, IL 60439

1 Glenn Van Roekel
Manager, City of Caliente
P.O. Box 158
Caliente, NV 89008

1 G. S. Bodvarsson
Head, Nuclear Waste Department
Lawrence Berkeley National Laboratory
1 Cyclotron Road, MS 50E
Berkeley, CA 94720

1 Steve Hanauer (RW-2)
OCRWM
U. S. Department of Energy
1000 Independence Ave.
Washington, DC 20585

	MS	
1	0443	B. J. Thorne
5	1146	J. D. Miller
1	1146	T. Luera
1	1325	L. S. Costin
1	1325	N. S. Brodsky
1	1325	R. E. Finley
1	1325	R. H. Price
1	1325	E. E. Ryder
5	1325	S. R. Sobolik
2	1330	B. Pierson, 6811 100/123274/SAND95-2001/NQ
20	1330	WMT Library, 6752
1	9018	Central Technical Files, 8523-2
5	0899	Technical Library, 4414
2	0619	Review and Approval Desk, 12630, For DOE/OSTI